Supramolecular Polymeric Networks via Hydrogen Bonding in Ionic Liquids

A DISSERTATION
SUBMITTED TO THE FACULTY OF THE GRADUATE SCHOOL
OF THE UNIVERSITY OF MINNESOTA
BY

Yu Lei

IN PARTIAL FULFILLMENT OF THE REQUIREMENTS
FOR THE DEGREE OF
DOCTOR OF PHILOSOPHY

Adviser: Timothy P. Lodge

December 2012

© Yu Lei 2012

Acknowledgements

It has been a little more than five years since I entered graduate school at Minnesota. I was definitely fortunate to get this wonderful opportunity. I would not have been able to accomplish this thesis without the help and support of many people. Foremost, I would like to express my sincere gratitude to my adviser, Prof. Tim Lodge, for his invaluable guidance, continuous support and encouragement throughout my graduate education, especially tremendous patience during difficult times.

I am also grateful to many individuals who have contributed to my thesis research. In particular, I thank Prof. Atsushi Noro at Nagoya University for his efforts on the molecular design and preliminary work of this project; Dr. David Giles in the polymer rheology lab for providing initial rheometer training service and sharing many useful tips of rheological measurements; Dr. Zhifeng Bai and Dr. Chun Liu for helping me in various aspects during the first couple of years. Furthermore, I have greatly benefited from helpful discussions and technical support from many past and present Lodge group members whom I have had a chance to interact with: Dr. Soo-Hyung Choi, Yuanyan Gu, Dr. Brad Jones, Dr. Hau-Nan Lee, Jie Lu, Dr. Keun Hyung Lee, Dr. Joseph Lott, Lucas McIntosh, Dr. Michelle Mok, Dr. Adam Moughton, Dr. Sehban Ozair, Dr. Peter Simone, Soonyong So, Dr. Takeshi Ueki, Dr. Sipei Zhang, Can Zhou.

Last but not least, I owe deep gratitude to my parents, for their love, sacrifice, encouragement, and support throughout my life, without which I would never reach where I am. I dedicate this thesis to them.

Dedicated to my parents

Abstract

Swelling a cross-linked polymeric network with an ionic liquid to produce an ion gel is a facile and promising strategy to supply ionic liquids with mechanical integrity and persistent structure without sacrificing their fascinating properties. This thesis examines a special system from supramacromolecular assembly via hydrogen bonding, consisting of a poly(2-vinylpyridine-*b*-ethylene oxide-*b*-2-vinylpyridine) (P2VP–PEO–P2VP) triblock copolymer, a poly(4-vinylphenol) (PVPh) linear homopolymer, and an ionic liquid, 1-ethyl-3-methylimidazolium bis(trifluoromethylsulfonyl)amide ([EMIM][TFSA]), where hydrogen bonding between the P2VP blocks and PVPh cross-linkers generates a transient polymer network. This thesis aims to systematically study the structure and dynamics of this versatile hydrogen-bonded supramolecular ion gel system.

The substantially wide liquidus temperature range of the ionic liquid affords access to interesting and unprecedented rheological response of the resulting gels. For example, the terminal relaxation time varies by 15 decades from the gel temperature down to room temperature; extremely wide temperature- and frequency-independent rubbery plateaus are pronounced, indicating the formation of a well-defined polymer network structure; the applicability of time–temperature superposition is striking, suggesting the invariance of the underlying relaxation mechanism.

In order to elucidate the underlying molecular mechanisms that control the structure and dynamics, viscoelastic properties and morphologies were investigated over wide composition and temperature ranges. In terms of the relaxation mechanism, the macroscopic rheology was qualitatively correlated with the average lifetime of a

P2VP↔PVPh association, which is determined by the number of hydrogen bonds involved. This establishes the plausibility of the interpretation that stress relaxation occurs through simultaneous breaking of all hydrogen bonds involved. In terms of mechanical properties, it was demonstrated that the extent of cross-linking, and therefore ultimate mechanical strength, can be modulated through variation in the concentration of the cross-linker added. In terms of morphology, a long-range ordered hexagonal morphology was observed after annealing at elevated temperatures for a sufficient period of time.

Overall, this thesis highlights that the utilization of hydrogen bonding to achieve ion gels is an advantageous approach to impart tunability in terms of viscoelastic and mechanical properties. Our strategy should be potentially useful in designing tailor-made smart materials.

Table of Contents

List of Tables

List of Figures

Chapter 1

Background

1.1 Supramolecular Polymers

Conventional synthetic polymers are long-chain molecules consisting of many repeating structural units connected by covalent bonds. Thanks to a wealth of fascinating properties, they have been used extensively in everyday life and sophisticated technologies for more than a half century. Over the last twenty-five years, the ubiquity of reversible supramolecular interactions has been recognized with the development of supramolecular chemistry, defined by Lehn as the chemistry beyond molecules,[1] which has stimulated scientists to construct reversible alternatives for covalent polymers. However, it was not straightforward at the beginning as to how to incorporate highly directional, sufficiently strong, but still reversible interactions to direct small molecules to assemble into polymeric arrays with significant degrees of polymerization. Impressive progress was not made until the pioneering work by Sijbesma *et al.* in 1997,[2] in which 2-ureido-4[1*H*]-pyrimidinone (UPy) units were shown to assemble into long chains through quadruple cooperative hydrogen bonds in an array, yielding products with mechanical properties that until then were exclusively associated with covalent polymers. Furthermore, it was demonstrated that their behavior can be described by well-established theories of polymer physics. These novel functional materials are termed "supramolecular polymers", which are defined as polymeric arrays of monomer units which are held together by reversible and highly directional non-covalent interactions.[3–5]

This pioneering work represents a landmark in this realm, and have led to a recent surge in attention for this promising class of materials.

The long-chain character of supramolecular polymers gives rise to many of the well-known properties that have made conventional polymers highly successful. Concurrently, owing to the intrinsic reversibility of non-covalent interactions, supramolecular polymers are endowed with unprecedented features in comparison to their covalent counterparts. Because of the built-in reversible interactions, supramolecular polymers are often under thermodynamic equilibrium, and the architectural and dynamic parameters that determine their properties, such as degree of polymerization, chain conformation, and bond lifetime, can be reversibly adjusted by external stimuli. One undesirable disadvantage of conventional polymers is their high melt viscosities originating from chain entanglements, which render them difficult to process. In contrast, supramolecular polymers generally exhibit a strongly temperature-dependent melt viscosity, which enhances their processability in a less viscous state at temperatures only moderately higher than their melting or glass transition temperatures. The molecular origin of this interesting phenomenon is attributed to a stress relaxation mechanism exclusive to supramolecular polymers. Besides moving like a snake (reptation) as conceived by de Gennes,[6] which is the predominant mechanism in covalent polymers, supramolecular polymers also break and reform their chains with other strain-free ends. The latter process is accelerated at elevated temperatures where bond lifetimes shorten considerably, resulting in strongly temperature-dependent behavior. Furthermore, self-healable supramolecular systems have been reported.[7–11] Leibler and coworkers demonstrated that

a cross-linked supramolecular rubber showed fully recoverable extensibility and little creep under load but, in striking contrast to conventional covalent rubbers, exhibited unique self-healing behavior toward their original strength and elasticity after two fractured surfaces were simply brought into contact at ambient temperature for a given period of time.[10] In a recent work by Burnworth *et al.*,[11] ultraviolet light absorption was utilized to induce mechanical healing behavior in a metallosupramolecular polymer based on a light–heat conversion step. Upon exposure to ultraviolet light, the metal–ion bonds are electronically excited and the absorbed energy is converted into heat.

The non-covalent interactions in supramolecular polymers typically encompass hydrogen bonding,[2,10,12–27] metal–ligand coordination,[11,28–33] ionic interactions,[34–36] and hydrophobic interactions.[37,38] For example, Sijbesma *et al.* synthesized polymeric materials using well-defined dimerization of UPy units with quadruple cooperative hydrogen bonds.[2] Schubert and coworkers described functional supramolecular polymers based on 2,2′:6′,2″-terpyridine–metal complexes.[29–31] Two oppositely charged dyes, a perylenediimide and a copper–phthalocyanine derivative, were shown by Guan *et al.* to assemble into supramolecular polymers, in which a stacked structure with fiber-like subunits is stabilized by ionic interactions.[35] Bis-urea monomers with coexistent hydrogen-bonding and hydrophobic groups were shown by Obert *et al.* to assemble into long rigid filaments in a variety of solvents with significantly tunable polarity.[37]

One of the key challenges of supramolecular polymer chemistry is to modulate the strength and specificity of the interactions among structural units in a precisely controlled fashion, in order to create a robust macromolecular architecture yet with dynamic

flexibility. Hydrogen bonding is the most versatile non-covalent interaction to fabricate supramolecular polymers, primarily because of the unprecedented tunability window of the association strength. The association strength of hydrogen bonds depends on the nature of the donor and acceptor moieties, as well as on the polarity of the solvent, and therefore, subtle modifications in the chemistry can result in significant changes in the association strength.[39] Furthermore, when stronger interactions are required than achievable with single hydrogen bonds, functional units which involve multiple hydrogen bonding sites have been designed based on the cooperativity of hydrogen bonds, whereby the specificity of the interactions is enhanced as well. The strength and specificity of multiple hydrogen bonding systems vary widely, from weakly complementary pyridine–phenol pairs to extraordinarily strong sextuple hydrogen bonding motifs,[26,27] with association constants ranging from 1 M^{-1} to as high as 10^9 M^{-1}. Alternatively, employing additional stabilization factors, for example, liquid crystallinity[40] and phase separation,[41,42] prove to be effective approaches to enhance hydrogen bonding interactions. For example, Rowan and coworkers have demonstrated that weakly hydrogen-bonded complexes from telechelic polymers based on adenine and cytosine can be stabilized through a combination of weak hydrogen bonding with phase segregation.[41]

Polymeric networks are superior to their uncross-linked precursors in the sense that they typically exhibit mechanical rigidity and enhanced stability when exposed to extreme conditions. In contrast to traditional covalent approaches employed for the cross-linking step, supramolecular strategies give rise to reversible polymeric networks without extensive side reactions, thus exerting a greater degree of control over the final network

structure. Impressive attempts have been focused on developing general theories to describe the equilibrium and dynamic properties of transient polymer networks.[43–48] Their bulk properties are directly related to the association strength and kinetics of the cross-links as well as the network microstructure. Supramolecular polymer gels,[49–51] in which a supramolecular polymeric network is dispersed within a significant amount of mobile solvent molecules, are potentially useful in a variety of high-tech applications including tissue engineering,[51] would healing,[52] drug delivery,[53] and nanoscale electronics.[54]

Supramolecular polymers are already beginning to reach the commercial market, taking advantages of the reversibility and responsiveness of the non-covalent interactions. Based on the attractive properties such as enhanced processability in the melt or solution, excellent mechanical properties in the solid state, and facile removability, supramolecular polymers are foreseen to give even superior performances than their covalent analogues in everyday applications, ranging from printing, coatings, adhesives, to cosmetics. For example, consider ink-jet printing, in which images are created on a piece of paper by the ejection of ink droplets via a small orifice. While reasonable mobility is a prerequisite for the ink to be ejected in small droplets, it must become highly viscous, close to a solid, once the droplets hit the paper; otherwise, the ink will spread on the paper, resulting in a blurry image. Here, supramolecular polymers are additives which function as viscosity modifiers to induce the dramatic changes over a relatively narrow temperature window.

Through bringing together supramolecular chemistry and polymer science, an unparalleled platform is generated for designing smart materials that integrate macromolecular architecture and dynamic flexibility to achieve functions such as

responsiveness to stimuli, environmental adaptability, self-healing ability, and enhanced processability. The most challenging task is to design appropriate building block functionalities with synthetic accessibility and high stability. Supramolecular polymers have already been demonstrated to be scientifically interesting and technologically relevant, and thus a bright future of this field can be foreseen.

1.2 Polymer/Ionic Liquid Composites

Ionic liquids are ambient temperature molten salts. The discovery of ionic liquids traces back to the early 20th century. The molten salt ethyl ammonium nitrate ($[EtNH_3][NO_3]$), with a melting point of 13–14 ℃ reported by Walden in 1914,[55] is generally acknowledged as the first ionic liquid described in the literature. However, it was not until the discovery of dialkylimidazolium chloroaluminate ionic liquids made from mixtures of aluminum chloride and 1,3-dialkylimidazolium chloride in 1982[56] that ionic liquids received much attention from scientists. Since the first synthesis of moisture-stable ionic liquids in 1992[57] with alkylimidazolium-based cations and anions, such as tetrafluoroborate and nitrate, scientific interest in ionic liquids has been increasing very rapidly.[58,59] Ionic liquids are composed entirely of cations and anions. For example, 1,3-dialkylimidazolium, *N*-alkylpyridinium, tetraalkylphosphonium, and tetraalkylammonium are common cations, while tetrafluoroborate, hexafluorophosphate, bis(trifluoromethylsulfonyl)amide, and triflate are common anions. In comparison with traditional inorganic salts, such as sodium chloride, the component ions of ionic liquids

are typically bulky, irregularly shaped, and with delocalized charge. These features suppress their tendency to pack into tight and well-ordered crystal lattices, leading to much lower melting points than traditional inorganic salts.

One of the primary factors behind the worldwide interest in ionic liquids is their fascinating set of physicochemical properties. One distinct feature is their negligible vapor pressure (as low as 10^{-10} Pa at 25 ℃), which enables their straightforward introduction in analytical instruments requiring high vacuum conditions,[60] such as X-ray photospectroscopy (XPS), matrix-assisted laser desorption/ionization (MALDI) mass spectroscopy, scanning electron microscopy (SEM), and transmission electron microscopy (TEM). For example, it has been demonstrated the viability of using room temperature conventional TEM to visualize polymeric nanostructures in ionic liquid solutions,[61] as opposed to cryogenic TEM, which involves a delicate controlled environment vitrification system for sample preparation and can result in artifacts.[62] Nevertheless, it has been recently reported that certain families of ionic liquids can be distilled at reduced pressure without decomposition, yielding products of high purity levels.[63] Furthermore, ionic liquids are known as "designer solvents" because the availability of numerous component ions provides virtually unlimited tunability in their properties. For example, Watanabe and coworkers characterized a series of 1,3-dialkylimidazolium-based ionic liquids to determine how their physical properties, such as thermal behavior, density, viscosity, self-diffusion coefficient, and ionic conductivity, are affected by variation in cationic[64]/anionic[65] species and imidazolium alkyl chain length.[66] Additional remarkable properties of ionic liquids include high ionic conductivity

(up to 100 mS/cm), a wide liquidus temperature range (*ca.* 173–523 K), wide electrochemical windows (typically 4–6 V), exceptional chemical and thermal stability, fire resistance, and preferential permeability of certain gases. Although the number of commercially available ionic liquids has been expanding, most of them are currently too expensive for extensive applications in large scale industrial processes. Furthermore, their toxicity and biodegradability have rarely been addressed thus far,[67] which needs to be carefully considered as the usage of ionic liquids grows.

The attractive properties of ionic liquids have enabled their applications in many technologies. One primary example is to utilize them as the solvation media for synthesis and catalysis,[68–72] where several advantages can be envisioned. First, their negligible volatility enables their straightforward containment at elevated temperatures and ultrahigh vacuum, and eliminates the concern of their environmental emission and contamination. Second, unlimited opportunities of component ion substitutions enable fine tailoring of solvation properties to optimize yield, selectivity, substrate solubility, and separation performance. Third, unlike traditional molecular solvents, they are ionic and highly structured solvents and usually display highly polar and weakly coordinating chemistry, which may lead to favorable reaction mechanisms. Fourth, ionic liquids dissolve a wide variety of materials due to the possibility of multiple solvent–solute interactions. Fifth, biphasic systems of ionic liquids with organic solvents and water are ideal systems for biphasic catalysis, in which catalysts are immobilized in one phase while products are readily separated from the other phase, whereby both the advantages of homogeneous catalysis (high catalytic performance) and heterogeneous catalysis

(facile product separation and catalyst recycling) can be married.[70] Ionic liquids have also been widely employed in separation technology, such as stationary phases in gas chromatography, liquid–liquid extractions, and supported liquid membranes.[73] Furthermore, the remarkable electrochemical properties of ionic liquids, such as high ionic conductivity and wide electrochemical windows, render them key components in electronic double layer capacitors, fuel cells, lithium ion batteries, and solar cells.[74]

Over the last twenty years, polymer/ionic liquid composites have become a subject of extensive research.[75–77] One of the earliest activities in these systems was using ionic liquids as solvents in polymerization processes.[78] This was triggered by the observation that the propagation rate constant (k_p) of methyl methacrylate increases considerably when polymerization is carried out in an ionic liquid, 1-butyl-3-methylimidazolium hexafluorophosphate ([BMIM][PF_6]).[79] Further investigation of this system revealed a decrease in the termination rate constant (k_t).[80] The enhancement in k_p was attributed to the increased polarity of the medium, which favors the transition state involving charge transfer, while the decrease in k_t was related to the slower diffusion hindered by the high viscosity of ionic liquids.[80] Controlled radical polymerizations conducted in ionic liquids have also been reported. Since ionic liquids dissolve certain inorganic or organometallic compounds that are employed as catalysts in atom transfer radical polymerization (ATRP), polymerization proceeds under homogeneous conditions and products can be conveniently separated from catalysts using solvents which dissolve the polymer but not the ionic liquid.[81] Other polymerization protocols documented in the literature include reverse ATRP,[82] reversible addition–fragmentation chain transfer (RAFT)

polymerization,[83] nitroxide-mediated polymerization (NMP),[84] ionic polymerization,[85] group transfer polymerization,[86] polycondensation,[87] and ring-opening polymerization.[88]

Polymer solubilization in ionic liquids is complicated and not readily predicted.[89] Solubilization of a solute in a solvent is generally governed by thermodynamic factors. However, the higher viscosities of ionic liquids compared with molecular solvents could afford a serious barrier to mass and phase transfer, and therefore result in significantly prolonged kinetics to reach thermodynamic equilibrium. Winterton and coworkers reported a comprehensive, but still empirical, study on the solubility of 17 polymers in three common ionic liquids.[90] Excitingly, ionic liquids have enabled direct dissolution of biopolymers such as cellulose,[91] which is insoluble in water and most common organic solvents, due to the presence of extensive hydrogen-bonded supramolecular network structure. Rogers and coworkers[92] found that ionic liquids incorporating anions which are strong hydrogen bonding acceptors were highly effective to dissolve cellulose, presumably solubilizing cellulose through hydrogen bonding between cellulose hydroxyl groups and anions of the solvent. This phenomenon may establish an approach for "green processing" of the most abundant natural polymer.

Stimuli-responsive polymer/ionic liquid systems are of particular interest. Ueki and Watanabe reported the upper critical solution temperature (UCST) phase behavior, *i.e.*, a critical temperature above which different components of a mixture are miscible for all compositions, of poly(*N*-isopropylacrylamide) (PNIPAm) in a common ionic liquid, 1-ethyl-3-methylimidazolium bis(trifluoromethylsulfonyl)amide ([EMIM][TFSA]).[93] Interestingly, PNIPAm exhibits lower critical solution temperature (LCST) phase

behavior, *i.e.*, a critical temperature below which different components of a mixture are miscible for all compositions, in aqueous solutions.[94] Ueki and Watanabe also reported the LCST phase behavior of poly(benzyl methacrylate) (PBzMA) and its derivatives in [EMIM][TFSA].[95–97] Lee and Lodge described LCST phase behavior of poly(ethylene oxide) (PEO) in 1,3-dialkylimidazolium tetrafluoroborate ionic liquids.[98] One unusual feature of this system is that the cloud point curves in the temperature–composition phase diagrams are strongly asymmetric, with the critical composition shifted to high concentrations of PEO. A PEO derivative, poly(ethyl glycidyl ether) (PEGE), also displays LCST phase behavior in [EMIM][TFSA].[99] Photo-responsive polymers in ionic liquids have also been reported. Ueki *et al.* discovered that the *cis*-state (excited) of poly(4-phenylazophenyl methacrylate) (PAzoMA) is soluble in [EMIM][TFSA] while the *trans*-state (ground) is not. Consequently, a random copolymer of P(AzoMA-*r*-BzMA) exhibits an LCST which differs by 22 ℃ between the *trans*- and *cis*-state.[100] Similarly, the UCST of a random copolymer P(AzoMA-*r*-NIPAm) differs by 43 ℃ between the *trans*- and *cis*-state.[101]

Self-assembly of block copolymers in ionic liquids is an emerging field.[102] The ability of block copolymers to self-assemble into predictable nanostructures is well established. Lodge and coworkers have shown that two diblocks, poly((1,2-butadiene)-*b*-ethylene oxide) (PB–PEO)[103] and poly(styrene-*b*-methyl methacrylate) (PS–PMMA),[104] aggregate strongly and form micelles in [BMIM][PF_6]. Consistent with aqueous and organic systems, the micellar structure progresses from spheres to cylinders to vesicles upon decreasing the fraction of the solvatophilic blocks. Further investigation of these systems

resulted in the discovery of a micelle shuttle system: a reversible, quantitative, and intact transfer of micelles between water and a hydrophobic ionic liquid.[105–109] The most remarkable feature of this micelle shuttle system is the intact transfer of the micelles, as opposed to a dissolution–reassembly process. This facile phase transfer offers a route to transport non-polar substances into and out of the ionic liquids, without removal of the expensive ionic liquids from the reaction vessel. Thermo-responsive polymer/ionic liquid systems have been utilized to exert delicate control over the micellization processes. For example, doubly thermosensitive micellization–unimer–inverse micellization was demonstrated by a PBzMA–PNIPAm diblock in [EMIM][TFSA][110] and a PNIPAm–PEO diblock in [EMIM][BF_4]/[BMIM][BF_4] blends.[111] Meli *et al.* investigated the relaxation kinetics of nonergodic PB–PEO block copolymer micelles in [EMIM][TFSA],[112,113] taking advantage of the wide liquidus temperature range of the ionic liquid.

Poly(ionic liquid)s are a class of emerging materials, in which ionic liquid species are constrained to the repeating units in a polymer chain.[114] They combine the unique properties of ionic liquids with the flexibility and enhanced mechanical properties arising from the macromolecular architecture. Poly(ionic liquid)s can be synthesized either by direct polymerization of ionic liquid monomers or by chemical modification of polymeric precursors. Because the non-volatility limits the availability of high purity ionic liquid monomers, conventional free radical polymerizations have been the primary technique thus far,[115] where the propagating species are tolerant to impurities and moisture. Recently, impressive progress in the development of controlled radical polymerizations has provided an unparalleled platform to precisely design and control the macromolecular

architecture of ionic liquid species within a polymer matrix.[116,117] Poly(ionic liquid)s have been demonstrated to be useful in a variety of applications, including ionic conductors, dispersants, stabilizers, absorbents, porous polymers, and carbon precursors.

Currently, the research scope of ionic liquids in polymer science is under significant expansion from traditional solvents to functional additives with desired properties. Functional polymer/ionic liquid composites are only beginning to be investigated and relevant design principles remain to be elucidated. The outstanding challenges are to design composite materials with mechanical integrity, exquisite nanostructure, and tailored ionic liquid properties.

1.3 Ion Gels as Solid Polymer Electrolytes

Polymer electrolytes are currently a subject of extensive research for applications in electrochemical devices,[118–120] due to the potential to alleviate the shortcomings of organic solvent-based electrolytes, including leakage, flammability, and durability, while offering additional desirable properties, such as thin-film forming ability, flexibility, and transparency. The most common type of conventional polymer electrolytes is alkali metal salt complexes of PEO.[121] However, they typically possess rather low conductivity (on the order of 10^{-4} mS/cm at 25 ℃) due to the crystalline nature of PEO.[122] While this can be addressed through the addition of organic solvents as plasticizers,[119] additional issues regarding durability and safety concerns are raised. Ionic liquids possess negligible volatility, non-flammability, high ionic conductivity, and wide electrochemical windows,

which render them promising alternatives to replace organic solvents. Significant enhancement in conductivity has been observed upon incorporating room temperature ionic liquids into PEO-based electrolytes,[123] and lithium batteries utilizing polymer/ionic liquid composites as electrolytes have been documented.[124]

Recently, a novel class of polymer electrolytes was prepared by dispersing a cross-linked polymeric network in ionic liquids, termed "ion gels". In comparison to traditional polymer electrolytes obtained by simply doping polymers with ionic liquids,[125,126] ion gels require significantly less polymer and thus offer enhanced ionic conductivity (*e.g.*, on the order of 10 mS/cm at 25 ℃).

Chemically cross-linked ion gels can be prepared through polymerization of vinyl monomers in the presence of a cross-linker or direct polymerization of multifunctional monomers. For example, in the pioneering work on chemically cross-linked ion gels by Watanabe and coworkers, they successfully prepared self-standing, flexible, and transparent ion gel films via *in-situ* free radical polymerization of methyl methacrylate (MMA) in [EMIM][TFSA], in the presence of a small amount of cross-linker.[127] They found that the temperature dependence of the ionic conductivity of the resulting ion gels followed the Vogel–Fulcher–Tammann (VFT) equation over the whole composition range, and promisingly, the ionic conductivity at ambient temperature approached a value close to 10 mS/cm. Rogers and coworkers synthesized resilient, rubbery, and transparent ion gels through the cross-linking reaction of disuccinimidylpropyl poly(ethylene glycol) and four-arm tetraamine poly(ethylene glycol) oligomers in a hydrophobic ionic liquid, 1-hexyl-3-methylimidazolium bis(trifluoromethylsulfonyl)amide ([HMIM][TFSA]).[128]

In comparison to covalent approaches, physical cross-linking strategy provides greater flexibility in terms of tuning morphologies and properties through variations in monomer identity, block length, block sequence, and copolymer content. Over the last five years, our group has initiated systematic studies on the synthesis, electrical and viscoelastic properties, and applications of block copolymer-based ion gels.[129–140] Addition of as little as 4 wt% poly(styrene-*b*-ethylene oxide-*b*-styrene) (PS–PEO–PS) triblock copolymer into a midblock-selective ionic liquid [BMIM][PF_6], was found to form a soft but highly elastic solid.[129] Because thermoreversibility is a desirable feature from a processing perspective, a thermoreversible ion gel was then developed by replacing the PS block with PNIPAm and the [BMIM][PF_6] ionic liquid with [EMIM][TFSA],[130] where PNIPAm exhibits UCST phase behavior in [EMIM][TFSA].[93] The gelation temperature was further adjusted over the range of 17–48 ℃ by incorporating short solvophobic PS blocks to produce well-defined PNIPAm–PS–PEO–PS–PNIPAm pentablock copolymers, depending on the PS block length.[131] Very recently, Kitazawa *et al.* developed an ion gel that melts on cooling by dissolving a poly(benzyl methacrylate-*b*-methyl methacrylate-*b*-benzyl methacrylate) (PBzMA–PMMA–PBzMA) triblock copolymer in [EMIM][TFSA],[132] where PBzMA exhibits LCST phase behavior in [EMIM][TFSA] around 105 ℃.[95]

In addition to their employment as polymer electrolytes, these ion gels have also been explored as high-performance membranes for gas separation technology, high-capacitance dielectric materials for organic thin-film transistors, and electroresponsive materials in electromechanical actuators. Gu and Lodge found that by incorporating a

poly(ionic liquid) midblock into a triblock copolymer ion gel, both high permeability and high real selectivity for CO_2/N_2 and CO_2/CH_4 gas pairs were achieved.[136] Ion gels have shown superior performance as gate dielectrics in organic thin-film transistors.[137–140] Their extremely high specific capacitance (*ca.* 10 $\mu F/cm^2$) enables a very high carrier density in the organic semiconductor channel (*e.g.*, poly(3-hexylthiophene)). Furthermore, the high ionic mobility contributes to switching speeds that are over three orders of magnitude faster than achievable with conventional polymer electrolytes (*e.g.*, $PEO/LiClO_4$), allowing the device to operate at higher frequencies. In electromechanical actuators, an applied electric field results in differential ion migration, which further leads to asymmetric swelling and thus to bending.[141,142] With the demonstrated device performances greatly enhanced, research interest in the synthesis and characterization of ion gels will continue to grow and more applications will be envisioned in the future.

1.4 Supramolecular Ion Gels via Hydrogen Bonding

In 2008, Noro *et al.* developed a thermoreversible supramolecular ion gel system by adding a poly(4-vinylphenol) (PVPh) cross-linker to a poly(2-vinylpyridine-*b*-ethyl acrylate-*b*-2-vinylpyridine) (P2VP–PEA–P2VP) triblock solution in a hydrophobic ionic liquid [EMIM][TFSA], a good solvent for the entire triblock chain, where hydrogen bonding between the P2VP blocks and PVPh cross-linkers generates a transient polymer network.[22,23] The component polymers were synthesized by RAFT polymerization. The substantially wide liquidus temperature range of the ionic liquid affords access to interesting and unprecedented rheological response, as demonstrated by the preliminary

results from a representative mixture comprised of 10 wt% triblock and 4 wt% cross-linker. Figure 1.1 shows the temperature dependence of the dynamic shear storage modulus (G') and loss modulus (G''). The material undergoes a sharp transition from viscous liquid-like behavior at elevated temperatures to elastic gel-like behavior at low temperatures, with a well-defined transition temperature around 140 ℃ termed gel temperature (T_{gel}) where $G' = G''$. A wide temperature-independent rubbery plateau is pronounced below T_{gel}, suggesting the formation of a well-defined polymer network structure, which does not evolve appreciably with temperature. One important assumption is that the number of hydrogen bonds per P2VP↔PVPh association increases upon cooling, while no substantial rearrangement of network connectivity takes place due to very high activation energy required to break multiple hydrogen bonds simultaneously. Therefore, the strength of a given P2VP↔PVPh association is greatly enhanced as temperature decreases, while the network structure is essentially locked in place at T_{gel}.

Figure 1.2 shows a time–temperature superposition (tTS) master curve of G' and G'', constructed by shifting the isothermal dynamic frequency sweep data collected every 10 ℃ over the temperature range of 160–30 ℃ along the frequency axis. The appearance of an extremely wide frequency-independent rubbery plateau extending almost 10 orders of magnitude was particularly remarkable. The applicability of tTS suggests that the underlying origin of viscoelastic relaxation does not evolve with temperature, while wide frequency-independent rubbery plateau suggests the formation of a well-defined polymer network structure. The longest relaxation time (τ_1) varied by a factor of 10^{12} from the gel point (*ca.* 140 ℃) down to room temperature, as suggested by the shift factors. This

striking temperature sensitivity was attributed to the formation of multiple hydrogen bonds on a single P2VP↔PVPh association. It was further hypothesized that τ_1 is determined by the average lifetime of a P2VP↔PVPh association, which is directly related to the number of hydrogen bonds involved. On the basis of this hypothesis, the many orders of magnitude variation in τ_1 was interpreted in terms of the variation in the number of hydrogen bonds on a P2VP↔PVPh association, and therefore, the activation energy barrier to junction dissociation, as temperature changes.

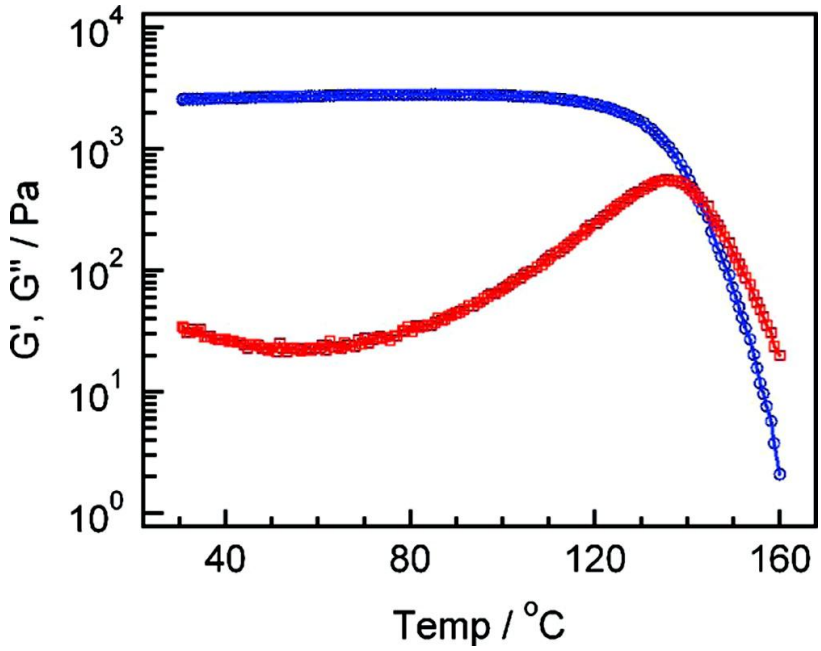

Figure 1.1 Temperature dependence of G' (○) and G'' (□) collected at an angular frequency of 0.3 rad/s, a cooling rate of 1 ℃/min, and a strain amplitude of 3%. Reprinted with permission from Noro, A.; Matsushita, Y.; Lodge, T. P. *Macromolecules* **2008,** *41*, 5839–5844. Copyright 2008 American Chemical Society.

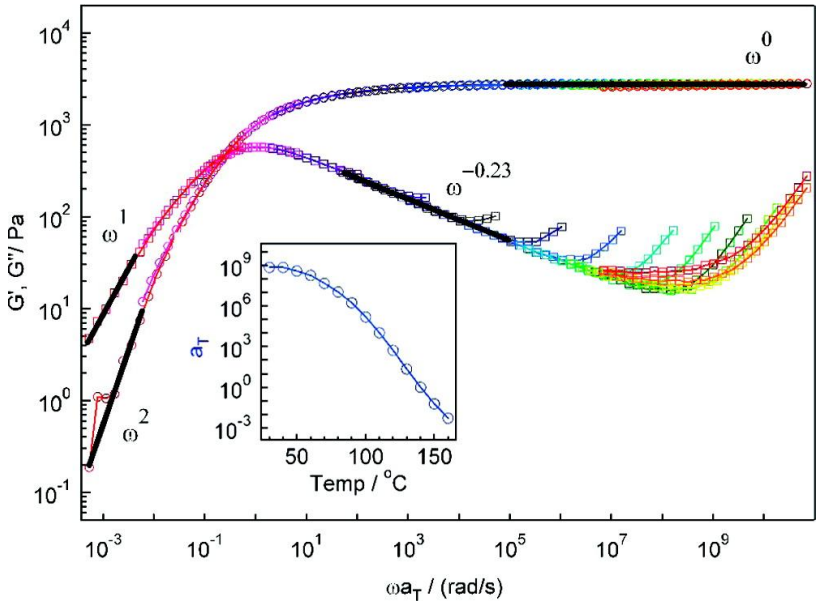

Figure 1.2 Time–temperature superposition master curve of G' (○) and G'' (□) collected every 10 ℃ over the temperature range of 160–30 ℃, with a reference temperature of 140 ℃. The shift factors are plotted against temperature in the inset. Reprinted with permission from Noro, A.; Matsushita, Y.; Lodge, T. P. *Macromolecules* **2008,** *41*, 5839–5844. Copyright 2008 American Chemical Society.

It was further demonstrated that the gel quality was strongly influenced by the stoichiometry between the hydrogen bonding donor and acceptor units, where the gel quality was assessed in terms of the magnitude of the modulus (G_N), the sharpness of the gel–liquid transition, and the minimum value of tan δ in the gel regime. By these criteria, the gel quality is not monotonic with the cross-linker content, but goes through a maximum where the molar ratio of phenol to pyridine units is *ca.* 1/1. At low molar ratios

of phenol/pyridine units, a significant amount of P2VP blocks are dangling ends due to the exhaustion of PVPh cross-linkers, whereas at the opposite extreme, the mechanism responsible for the deterioration in the gel quality was attributed to the formation of monofunctional and difunctional cross-links, neither of which contributes to the elasticity of the polymer network.

1.5 Thesis Overview

The overall objective of this thesis research is to elucidate the underlying mechanisms that control the structure and dynamics in this hydrogen-bonded supramolecular ion gel system. This dissertation is outlined as follows.

Chapter 2 describes the experimental details of the materials synthesis and characterization, and theoretical background for the experimental techniques, including size exclusion chromatography, rheology and small-angle scattering.

Chapter 3 investigates the rheological consequences of varying the lengths of the P2VP block and PVPh cross-linker. Key parameters such as the longest relaxation time (τ_1), gel temperature (T_{gel}), and plateau modulus (G_N) are extracted and discussed. It was found that while the terminal relaxation dynamics is dramatically retarded upon increasing the P2VP block length, it is relatively insensitive to the PVPh cross-linker length. The macroscopic rheology is qualitatively correlated with the number of hydrogen bonds on a given P2VP↔PVPh association.

Chapter 4 demonstrates that the variation in the amount of the cross-linker added allows for fine-tuning of the degree of cross-linking and ultimately the mechanical properties through changes in the stoichiometry of the complementary hydrogen bonding units. Interestingly, the modulus does not increase monotonically with the amount of cross-linker, but goes through a maximum where the hydrogen bonding donors and acceptors are under a certain stoichiometric balance. This essentially reflects significant changes in the microstructure of the hydrogen-bonded polymer networks.

Chapter 5 describes a thermally induced morphological evolution into a hexagonal morphology with long-range ordering of the hydrogen-bonded network microdomains. This process usually reveals very slow kinetics on a time scale that is much longer than a typical cooling or heating experiment, which results in significant hysteresis at high temperatures in the rheological response during a cooling–heating cycle. It turns out that this hexagonally ordered phase can be developed only within a narrow temperature window, which is limited at low-temperature by chain exchange and at high-temperature by the eventual dissolution of the hydrogen-bonded network microdomains.

Chapter 6 addresses a fundamental and interesting question as to how many hydrogen bonds per P2VP↔PVPh association are required at the gel point. The lifetime of a single phenol–pyridine hydrogen bond in [EMIM][TFSA] is estimated based on an empirical relationship from the literature, which turns out to be on the order of sub-nanoseconds. The ultrafast exchange dynamics implies that multiple hydrogen bonds per P2VP↔PVPh association are required to generate a polymer network that is sufficiently stable over a

timescale of seconds. In particular, at least 6 hydrogen bonds per P2VP↔PVPh association are required at room temperature.

Chapter 7 summarizes the research presented in this thesis and recommends directions for future work.

1.6 References

(1) Lehn, J.-M. *Angew. Chem. Int. Ed. Engl.* **1990,** *29*, 1304–1319.

(2) Sijbesma, R. P.; Beijer, F. H.; Brunsveld, L.; Folmer, B. J. B.; Hirschberg, J. H. K. K.; Lange, R. F. M.; Lowe, J. K. L.; Meijer, E. W. *Science* **1997,** *278*, 1601–1604.

(3) Brunsveld, L.; Folmer, B. J. B.; Meijer, E. W.; Sijbesma, R. P. *Chem. Rev.* **2001,** *101*, 4071–4097.

(4) de Greef, T. F. A.; Meijer, E. W. *Nature* **2008,** *453*, 171–173.

(5) Aida, T.; Meijer, E. W.; Stupp, S. I. *Science* **2012,** *335*, 813–817.

(6) de Gennes, P. G. *J. Chem. Phys.* **1971,** *55*, 572–579.

(7) Wool, R. P. *Soft Matter* **2008,** *4*, 400–418.

(8) Blaiszik, B. J.; Kramer, S. L. B.; Olugebefola, S. C.; Moore, J. S.; Sottos, N. R.; White, S. R. *Annu. Rev. Mater. Res.* **2010,** *40*, 179–211.

(9) van Gemert, G. M. L.; Peeters, J. W.; Söntjens, S. H. M.; Janssen, H. M.; Bosman, A. W. *Macromol. Chem. Phys.* **2012,** *213*, 234–242.

(10) Cordier, P.; Tournilhac, F.; Souli é-Ziakovic, C.; Leibler, L. *Nature* **2008,** *451*, 977–980.

(11) Burnworth, M.; Tang, L.; Kumpfer, J. R.; Duncan, A. J.; Beyer, F. L.; Fiore, G. L.; Rowan, S. J.; Weder, C. *Nature* **2011,** *472*, 334–337.

(12) Beijer, F. H.; Sijbesma, R. P.; Kooijman, H.; Spek, A. L.; Meijer, E. W. *J. Am. Chem. Soc.* **1998,** *120*, 6761–6769.

(13) Beijer, F. H.; Kooijman, H.; Spek, A. L.; Sijbesma, R. P.; Meijer, E. W. *Angew. Chem. Int. Ed.* **1998,** *37*, 75–78.

(14) Hirschberg, J. H. K. K.; Beijer, F. H.; van Aert, H. A.; Magusin, P. C. M. M.; Sijbesma, R. P.; Meijer, E. W. *Macromolecules* **1999,** *32*, 2696–2705.

(15) Lange, R. F. M.; van Gurp, M.; Meijer, E. W. *J. Polym. Sci., Part A: Polym. Chem.* **1999,** *37*, 3657−3670.

(16) Folmer, B. J. B.; Sijbesma, R. P.; Versteegen, R. M.; van der Rijt, J. A. J.; Meijer, E. W. *Adv. Mater.* **2000,** *12*, 874–878.

(17) Feldman, K. E.; Kade, M. J.; de Greef, T. F. A.; Meijer, E. W.; Kramer, E. J.; Hawker, C. J. *Macromolecules* **2008,** *41*, 4694–4700.

(18) Feldman, K. E.; Kade, M. J.; Meijer, E. W.; Hawker, C. J.; Kramer, E. J. *Macromolecules* **2009,** *42*, 9072–9081.

(19) Nair, K. P.; Breedveld, V.; Weck, M. *Macromolecules* **2008,** *41*, 3429–3438.

(20) Nair, K. P.; Breedveld, V.; Weck, M. *Soft Matter* **2011,** *7*, 553–559.

(21) Yamauchi, K.; Lizotte, J. R.; Long, T. E. *Macromolecules* **2003,** *36*, 1083−1088.

(22) Noro, A.; Matsushita, Y.; Lodge, T. P. *Macromolecules* **2008,** *41*, 5839–5844.

(23) Noro, A.; Matsushita, Y.; Lodge, T. P. *Macromolecules* **2009,** *42*, 5802–5810.

(24) Noro, A.; Yamagishi, H.; Matsushita, Y. *Macromolecules* **2009,** *42*, 6335–6338.

(25) Noro, A.; Hayashi, M.; Ohshika, A.; Matsushita, Y. *Soft Matter* **2011,** *7*, 1667–1670.

(26) Berl, V.; Schmutz, M.; Krische, M. J.; Khoury, R. G.; Lehn, J.-M. *Chem. Eur. J.* **2002,** *8*, 1227–1244.

(27) Kolomiets, E.; Buhler, E.; Candau, S. J.; Lehn, J.-M. *Macromolecules* **2006,** *39*, 1173–1181.

(28) Beck, J. B.; Rowan, S. J. *J. Am. Chem. Soc.* **2003,** *125*, 13922–13923.

(29) Hofmeier, H.; Schubert, U. S. *Chem. Soc. Rev.* **2004,** *33*, 373–399.

(30) Andres, P. R.; Schubert, U. S. *Adv. Mater.* **2004,** *16*, 1043–1068.

(31) Fustin, C.-A.; Guillet, P.; Schubert, U. S.; Gohy, J.-F. *Adv. Mater.* **2007,** *19*, 1665–1673.

(32) Yount, W. C.; Loveless, D. M.; Craig, S. L. *J. Am. Chem. Soc.* **2005,** *127*, 14488–14496.

(33) Piepenbrock, M.-O. M.; Lloyd, G. O.; Clarke, N.; Steed, J. W. *Chem. Rev.* **2010,** *110*, 1960–2004.

(34) Faul, C. F. J.; Antonietti, M. *Adv. Mater.* **2003,** *15*, 673–683.

(35) Guan, Y.; Yu, S.-H.; Antonietti, M.; Böttcher, C.; Faul, C. F. J. *Chem. Eur. J.* **2005,** *11*, 1305–1311.

(36) Wathier, M.; Grinstaff, M. W. *Macromolecules* **2010,** *43*, 9529–9533.

(37) Obert, E.; Bellot, M.; Bouteiller, L.; Andrioletti, F.; Lehen-Ferrenbach, C.; Boué, F. *J. Am. Chem. Soc.* **2007,** *129*, 15601–15605.

(38) Ustinov, A.; Weissman, H.; Shirman, E.; Pinkas, I.; Zuo, X.; Rybtchinski, B. *J. Am. Chem. Soc.* **2011,** *133*, 16201–16211.

(39) Cooke, G.; Rotello, V. M. *Chem. Soc. Rev.* **2002,** *31*, 275–286.

(40) Ambrožič, G.; Žigon, M. *Macromol. Rapid Commun.* **2000,** *21*, 53–56.

(41) Sivakova, S.; Bohnsack, D. A.; Mackay, M. E.; Suwanmala, P.; Rowan, S. J. *J. Am. Chem. Soc.* **2005,** *127*, 18202–18211.

(42) Tang, C.; Lennon, E. M.; Fredrickson, G. H.; Kramer, E. J.; Hawker, C. J. *Science* **2008,** *322*, 429–432.

(43) Green, M. S.; Tobolsky, A. V. *J. Chem. Phys.* **1946,** *14*, 80–92.

(44) Lodge, A. S. *Trans. Faraday Soc.* **1956,** *52*, 120–130.

(45) Leibler, L.; Rubinstein, M.; Colby, R. H. *Macromolecules* **1991,** *24*, 4701–4707.

(46) Tanaka, F.; Edwards, S. F. *Macromolecules* **1992,** *25*, 1516–1523.

(47) Semenov, A. N.; Rubinstein, M. *Macromolecules* **1998,** *31*, 1373–1385.

(48) Rubinstein, M.; Semenov, A. N. *Macromolecules* **1998,** *31*, 1386–1397.

(49) Smith, D. K. *Nat. Chem.* **2010,** *2*, 162–163.

(50) Noro, A.; Hayashi, M.; Matsushita, Y. *Soft Matter* **2012,** *8*, 2416–2429.

(51) Hirst, A. R.; Escuder, B.; Miravet, J. F.; Smith, D. K. *Angew. Chem. Int. Ed.* **2008,** *47*, 8002–8018.

(52) Yang, Z.; Xu, K.; Wang, L.; Gu, H.; Wei, H.; Zhang, M.; Xu, B. *Chem. Commun.* **2005,** 4414−4416.

(53) Rodríguez-Llansola, F.; Miravet, J. F.; Escuder, B. *Chem. Commun.* **2011,** *47*, 4706−4708.

(54) Puigmartí-Luis, J.; Laukhin, V.; Pérez del Pino, Á.; Vidal-Gancedo, J.; Rovira, C.; Laukhina, E.; Amabilino, D. B. *Angew. Chem. Int. Ed.* **2007,** *46*, 238−241.

(55) Walden, P. *Bull. Acad. Impér. Sci. St. Pétersbourg* **1914,** *8*, 405–422.

(56) Wilkes, J. S.; Levisky, J. A.; Wilson, R. A.; Hussey, C. L. *Inorg. Chem.* **1982,** *21*, 1263–1264.

(57) Wilkes, J. S.; Zaworotko, M. J. *J. Chem. Soc., Chem. Commun.* **1992,** 965–967.

(58) Wilkes, J. S. *Green Chem.* **2002,** *4*, 73–80.

(59) Rogers, R. D.; Seddon, K. R. *Science* **2003,** *302*, 792–793.

(60) Kuwabata, S.; Tsuda, T.; Torimoto, T. *J. Phys. Chem. Lett.* **2010,** *1*, 3177–3188.

(61) Maddikeri, R. R.; Colak, S.; Gido, S. P.; Tew, G. N. *Biomacromolecules* **2011,** *12*, 3412–3417.

(62) Zhong, S.; Pochan, D. J. *Polym. Rev.* **2010,** *50*, 287–320.

(63) Earle, M. J.; Esperança, J. M. S. S.; Gilea, M. A.; Canongia Lopes, J. N.; Rebelo, L. P. N.; Magee, J. W.; Seddon, K. R.; Widegren, J. A. *Nature* **2006,** *439*, 831–834.

(64) Tokuda, H.; Ishii, K.; Susan, M. A. B. H.; Tsuzuki, S.; Hayamizu, K.; Watanabe, M. *J. Phys. Chem. B* **2006,** *110*, 2833–2839.

(65) Tokuda, H.; Hayamizu, K.; Ishii, K.; Susan, M. A. B. H.; Watanabe, M. *J. Phys. Chem. B* **2004,** *108*, 16593–16600.

(66) Tokuda, H.; Hayamizu, K.; Ishii, K.; Susan, M. A. B. H.; Watanabe, M. *J. Phys. Chem. B* **2005,** *109*, 6103–6110.

(67) Pham, T. P. T.; Cho, C.-W.; Yun, Y.-S. *Water Res.* **2010,** *44*, 352–372.

(68) Welton, T. *Chem. Rev.* **1999,** *99*, 2071–2083.

(69) Hallett, J. P.; Welton, T. *Chem. Rev.* **2011,** *111*, 3508–3576.

(70) Dupont, J.; de Souza, R. F.; Suarez, P. A. Z. *Chem. Rev.* **2002,** *102*, 3667–3692.

(71) Pârvulescu, V. I.; Hardacre, C. *Chem. Rev.* **2007,** *107*, 2615–2665.

(72) van Rantwijk, F.; Sheldon, R. A. *Chem. Rev.* **2007,** *107*, 2757–2785.

(73) Han, X.; Armstrong, D. W. *Acc. Chem. Res.* **2007,** *40*, 1079–1086.

(74) Armand, M.; Endres, F.; MarFarlane, D. R.; Ohno, H.; Scrosati, B. *Nat. Mater.* **2009,** *8*, 621–629.

(75) Lodge, T. P. *Science* **2008,** *321*, 50–51.

(76) Ueki, T.; Watanabe, M. *Macromolecules* **2008,** *41*, 3739–3749.

(77) Lu, J.; Yan, F.; Texter, J. *Prog. Polym. Sci.* **2009,** *34*, 431–448.

(78) Kubisa, P. *Prog. Polym. Sci.* **2009,** *34*, 1333–1347.

(79) Harrisson, S.; Mackenzie, S. R.; Haddleton, D. M. *Chem. Commun.* **2002,** 2850–2851.

(80) Harrisson, S.; Mackenzie, S. R.; Haddleton, D. M. *Macromolecules* **2003,** *36*, 5072–5075.

(81) Carmichael, A. J.; Haddleton, D. M.; Bon, S. A. F.; Seddon, K. R. *Chem. Commun.* **2000,** 1237–1238.

(82) Ma, H.; Wan, X.; Chen, X.; Zhou, Q.-F. *J. Polym. Sci., Part A: Polym. Chem.* **2003,** *41*, 143–151.

(83) Perrier, S.; Davis, T. P.; Carmichael, A. J.; Haddleton, D. M. *Chem. Commun.* **2002,** 2226–2227.

(84) Ryan, J.; Aldabbagh, F.; Zetterlund, P. B.; Yamada, B. *Macromol. Rapid Commun.* **2004,** *25*, 930–934.

(85) Vijayaraghavan, R.; MacFarlane, D. R. *Chem. Commun.* **2004,** 700–701.

(86) Vijayaraghavan, R.; MacFarlane, D. R. *Chem. Commun.* **2005,** 1149–1151.

(87) Vygodskii, Y. S.; Lozinskaya, E. I.; Shaplov, A. S. *Macromol. Rapid Commun.* **2002,** *23*, 676–680.

(88) Biedroń, T.; Bednarek, M.; Kubisa, P. *Macromol. Rapid Commun.* **2004,** *25*, 878–881.

(89) Winterton, N. *J. Mater. Chem.* **2006,** *16*, 4281–4293.

(90) Snedden, P.; Cooper, A. I.; Scott, K.; Winterton, N. *Macromolecules* **2003,** *36*, 4549–4556.

(91) Pinkert, A.; Marsh, K. N.; Pang, S.; Staiger, M. P. *Chem. Rev.* **2009,** *109*, 6712–6728.

(92) Swatloski, R. P.; Spear, S. K.; Holbrey, J. D.; Rogers, R. D. *J. Am. Chem. Soc* **2002,** *124*, 4974–4975.

(93) Ueki, T.; Watanabe, M. *Chem. Lett.* **2006,** *35*, 964–965.

(94) Schild, H. G. *Prog. Polym. Sci.* **1992,** *17*, 163–249.

(95) Ueki, T.; Watanabe, M. *Langmuir* **2007,** *23*, 988–990.

(96) Kodama, K.; Nanashima, H.; Ueki, T.; Kokubo, H.; Watanabe, M. *Langmuir* **2009,** *25*, 3820–3824.

(97) Ueki, T.; Arai, A. A.; Kodama, K.; Kaino, S.; Takada, N.; Morita, T.; Nishikawa, K.; Watanabe, M. *Pure Appl. Chem.* **2009,** *81*, 1829–1841.

(98) Lee, H.-N.; Lodge, T. P. *J. Phys. Chem. Lett.* **2010,** *1*, 1962–1966.

(99) Tsuda, R.; Kodama, K.; Ueki, T.; Kokubo, H.; Imabayashi, S.; Watanabe, M. *Chem. Commun.* **2008,** 4939–4941.

(100) Ueki, T.; Yamaguchi, A.; Ito, N.; Kodama, K.; Sakamoto, J.; Ueno, K.; Kokubo, H.; Watanabe, M. *Langmuir* **2009,** *25*, 8845–8848.

(101) Ueki, T.; Nakamura, Y.; Yamaguchi, A.; Niitsuma, K.; Lodge, T. P.; Watanabe, M. *Macromolecules* **2011,** *44*, 6908–6914.

(102) Greaves, T. L.; Drummond, C. J. *Chem. Soc. Rev.* **2008,** *37*, 1709–1726.

(103) He, Y.; Li, Z.; Simone, P.; Lodge, T. P. *J. Am. Chem. Soc* **2006,** *128*, 2745–2750.

(104) Simone, P. M.; Lodge, T. P. *Macromol. Chem. Phys.* **2007,** *208*, 339–348.

(105) He, Y.; Lodge, T. P. *J. Am. Chem. Soc* **2006,** *128*, 12666–12667.

(106) Bai, Z.; He, Y.; Lodge, T. P. *Langmuir* **2008,** *24*, 5284–5290.

(107) Bai, Z.; He, Y.; Young, N. P.; Lodge, T. P. *Macromolecules* **2008,** *41*, 6615–6617.

(108) Bai, Z.; Lodge, T. P. *J. Phys. Chem. B* **2009,** *113*, 14151–14157.

(109) Bai, Z.; Lodge, T. P. *Langmuir* **2010,** *26*, 8887–8892.

(110) Ueki, T.; Watanabe, M.; Lodge, T. P. *Macromolecules* **2009,** *42*, 1315–1320.

(111) Lee, H.-N.; Bai, Z.; Newell, N.; Lodge, T. P. *Macromolecules* **2010,** *43*, 9522–9528.

(112) Meli, L.; Lodge, T. P. *Macromolecules* **2009,** *42*, 580–583.

(113) Meli, L.; Santiago, J. M.; Lodge, T. P. *Macromolecules* **2010,** *43*, 2018–2027.

(114) Yuan, J.; Antonietti, M. *Polymer* **2011,** *52*, 1469–1482.

(115) Ohno, H.; Yoshizawa, M.; Ogihara, W. *Electrochim. Acta* **2004,** *50*, 255–261.

(116) Tang, H.; Tang, J.; Ding, S.; Radosz, M.; Shen, Y. *J. Polym. Sci., Part A: Polym. Chem.* **2005,** *43*, 1432–1443.

(117) Vijayakrishna, K.; Jewrajka, S. K.; Ruiz, A.; Marcilla, R.; Pomposo, J. A.; Mecerreyes, D.; Taton, D.; Gnanou, Y. *Macromolecules* **2008,** *41*, 6299–6308.

(118) Bruce, P. G.; Vincent, C. A. *J. Chem. Soc., Faraday Trans.* **1993,** *89*, 3187–3203.

(119) Meyer, W. H. *Adv. Mater.* **1998,** *10*, 439–448.

(120) Smitha, B.; Sridhar, S.; Khan, A. A. *J. Membr. Sci.* **2005,** *259*, 10–26.

(121) Fenton, D. E.; Parker, J. M.; Wright, P. V. *Polymer* **1973,** *14*, 589–589.

(122) Robitaille, C. D.; Fauteux, D. *J. Electrochem. Soc.* **1986,** *133*, 315–325.

(123) Shin, J.-H.; Henderson, W. A.; Passerini, S. *Electrochem. Commun.* **2003,** *5*, 1016–1020.

(124) Shin, J.-H.; Henderson, W. A.; Passerini, S. *J. Electrochem. Soc.* **2005,** *152*, A978–A983.

(125) Lewandowski, A.; Świderska, A. *Solid State Ionics* **2004,** *169*, 21–24.

(126) Singh, B.; Sekhon, S. S. *J. Phys. Chem. B* **2005,** *109*, 16539–16543.

(127) Susan, M. A. B. H.; Kaneko, T.; Noda, A.; Watanabe, M. *J. Am. Chem. Soc.* **2005,** *127*, 4976–4983.

(128) Klingshirn, M. A.; Spear, S. K.; Subramanian, R.; Holbrey, J. D. Huddleston, J. G.; Rogers, R. D. *Chem. Mater.* **2004,** *16*, 3091–3097.

(129) He, Y.; Boswell, P. G.; Bühlmann, P.; Lodge, T. P. *J. Phys. Chem. B* **2007,** *111*, 4645–4652.

(130) He, Y.; Lodge, T. P. *Chem. Commun.* **2007,** 2732–2734.

(131) He, Y.; Lodge, T. P. *Macromolecules* **2008,** *41*, 167–174.

(132) Kitazawa, Y.; Ueki, T.; Niitsuma, K.; Imaizumi, S.; Lodge, T. P.; Watanabe, M. *Soft Matter* **2012,** *8*, 8067–8074.

(133) Zhang, S.; Lee, K. H.; Frisbie, C. D.; Lodge, T. P. *Macromolecules* **2011,** *44*, 940–949.

(134) Zhang, S.; Lee, K. H.; Sun, J.; Frisbie, C. D.; Lodge, T. P. *Macromolecules* **2011,** *44*, 8981–8989.

(135) Lee, K. H.; Zhang, S.; Lodge, T. P.; Frisbie, C. D. *J. Phys. Chem. B* **2011,** *115*, 3315–3321.

(136) Gu, Y.; Lodge, T. P. *Macromolecules* **2011,** *44*, 1732–1736.

(137) Lee, J.; Panzer, M. J.; He, Y.; Lodge, T. P.; Frisbie, C. D. *J. Am. Chem. Soc.* **2007,** *129*, 4532–4533.

(138) Cho, J. H.; Lee, J.; He, Y.; Kim, B. S.; Lodge, T. P.; Frisbie, C. D. *Adv. Mater.* **2008,** *20*, 686–690.

(139) Cho, J. H.; Lee, J.; Xia, Y.; Kim, B.; He, Y.; Renn, M. J.; Lodge, T. P.; Frisbie, C. D. *Nat. Mater.* **2008,** *7*, 900–906.

(140) Lee, J.; Kaake, L. G.; Cho, J. H.; Zhu, X.-Y.; Lodge, T. P.; Frisbie, C. D. *J. Phys. Chem. C* **2009,** *113*, 8972–8981.

(141) Lu, W.; Fadeev, A. G.; Qi, B.; Smela, E.; Mattes, B. R.; Ding, J.; Spinks, G. M.; Mazurkiewicz, J.; Zhou, D.; Wallace, G. G.; MacFarlane, D. R.; Forsyth, S. A.; Forsyth, M. *Science* **2002,** *297,* 983−987.

(142) Ding, J.; Zhou, D.; Spinks, G.; Wallace, G.; Forsyth, S.; Forsyth, M.; MacFarlane, D. *Chem. Mater.* **2003,** *15,* 2392−2398.

Chapter 2

Materials Synthesis and Characterization

2.1 Polymer Synthesis and Characterization

2.1.1 Triblock Synthesis and Characterization

The triblock copolymer used in the previous system was poly(2-vinylpyridine-*b*-ethyl acrylate-*b*-2-vinylpyridine) (P2VP–PEA–P2VP).[1,2] However, the PEA midblock was relatively polydisperse, and therefore we switched to a PEO midblock, which can provide a narrower molecular weight distribution. Poly(2-vinylpyridine-*b*-ethylene oxide-*b*-2-vinylpyridine) (P2VP–PEO–P2VP) triblock copolymers were synthesized via reversible addition–fragmentation chain transfer (RAFT) polymerization (Figure 2.1).[3,4] A dihydroxy-terminated PEO precursor was purchased from Aldrich, and purified by dissolution in dichloromethane and precipitation in hexanes. It has a molecular weight of 35 kg/mol and a dispersity of 1.04, as determined by size exclusion chromatography (SEC) with light scattering detection, where tetrahydrofuran (THF) with 1% tetramethylethylenediamine (TMEDA) by volume was used as the mobile phase. 2-Vinylpyridine monomer was purchased from Aldrich and passed through a basic alumina column to remove inhibitors prior to use. 2,2′-Azobisisobutyronitrile (AIBN) was purchased from Aldrich and purified by recrystallization from methanol. A chain transfer agent (CTA), *S*-1-dodecyl-*S*'-(α, α'-dimethyl-α"-acetic acid) trithiocarbonate, was previously synthesized following a reported procedure.[5]

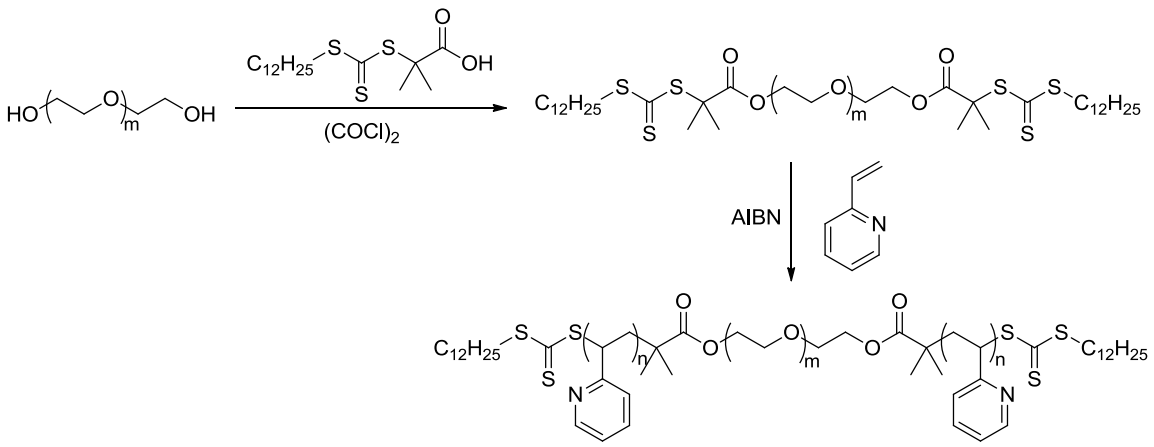

Figure 2.1 Synthetic scheme of P2VP–PEO–P2VP triblock copolymer.

A CTA end-capped PEO macroinitiator was first prepared by coupling a dihydroxy-terminated PEO precursor with the CTA via an acid chloride intermediate. CTA was mixed with excess oxalyl chloride in anhydrous CH_2Cl_2 under argon atmosphere and stirred at room temperature until gas evolution stopped (*ca.* 2 h). Residual reagents were removed under vacuum, and the residue was redissolved in anhydrous CH_2Cl_2 followed by the addition of PEO. The mixture was vigorously stirred at room temperature for 24 hours, after which the contents were precipitated four times in hexanes and dried in a vacuum oven overnight at 50 ℃. The PEO end-functionalization by the CTA was confirmed by the appearance of characteristic ^{1}H NMR signals of the dodecyl fragment in the difunctional macroinitiator (Figure 2.2). The quantitative degree of end-functionalization was 100%, as determined from the relative integration area of the PEO and CTA characteristic peaks in ^{1}H NMR spectrum, with the molecular weight of the PEO precursor (35 kg/mol) as a reference. The CTA end-capped PEO macroinitiator was

subsequently used to grow the P2VP blocks. In a typical polymerization, weighed amounts of CTA end-capped PEO macroinitiator, AIBN, 2-vinylpyridine monomer, and *N*,*N*-dimethylformamide (DMF) solvent were mixed in a dry round-bottom flask equipped with a magnetic stir bar and sealed with a rubber septum. The mixture was degassed by multiple freeze-pump-thaw cycles and the polymerization was then carried out at 60 ℃. The polymerization was quenched by liquid nitrogen. The contents was diluted with CH_2Cl_2 and precipitated in hexanes. The final product was dried in a vacuum oven at 50 ℃ for 24 hours. The high efficiency of chain extension was confirmed by the clear shift in the SEC traces of the difunctional macroinitiator and the resulting triblock, without any detectable signal from residual PEO precursor (Figure 2.3).

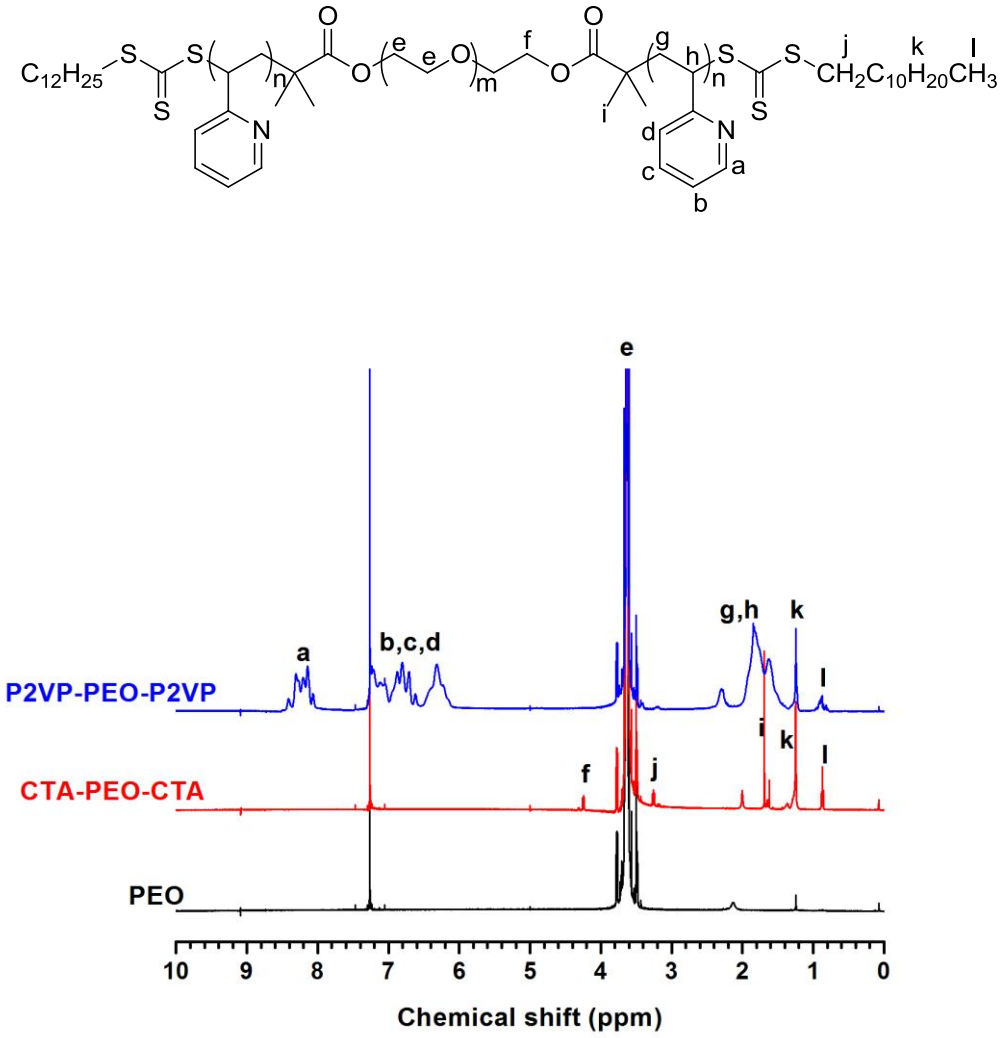

Figure 2.2 ^{1}H NMR spectra of the PEO precursor, CTA–PEO–CTA difunctional macroinitiator, and P2VP–PEO–P2VP triblock copolymer.

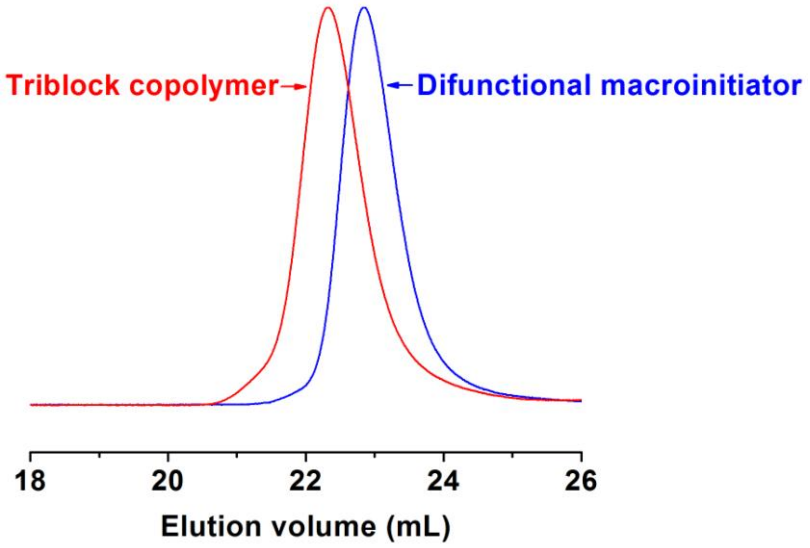

Figure 2.3 SEC traces of the CTA–PEO–CTA difunctional macroinitiator and P2VP–PEO–P2VP triblock copolymer.

2.1.2 Synthesis and Characterization of Poly(4-vinylphenol) Cross-linker

Poly(4-vinylphenol) (PVPh) cross-linker was also synthesized via RAFT polymerization, with the same CTA following a two-step process previously reported (Figure 2.4).[1,2] 4-*Tert*-butoxystyrene monomer was purchased from Aldrich and passed through a neutral alumina column to remove inhibitors prior to use. The purified monomer was degassed by multiple freeze-pump-thaw cycles and then polymerized in bulk at 130 ℃. The poly(4-*tert*-butoxystyrene) (P*t*BOS) precursor was purified by multiple precipitations into a methnol/water mixture (85/15, v/v). The protective *tert*-butyl groups were removed by hydrolysis with concentrated hydrochloric acid in dioxane at 40 ℃ for 48 hours to afford the targeted PVPh polymer, which was purified by

multiple precipitations into water. The hydrolysis efficiency of the *tert*-butyl groups was estimated by ^{1}H NMR spectroscopy (Figure 2.5). Complete removal of the protective *tert*-butyl groups and the generation of the phenolic hydroxyl groups after hydrolysis were verified, and thus the degree of hydrolysis was determined to be greater than 99%.

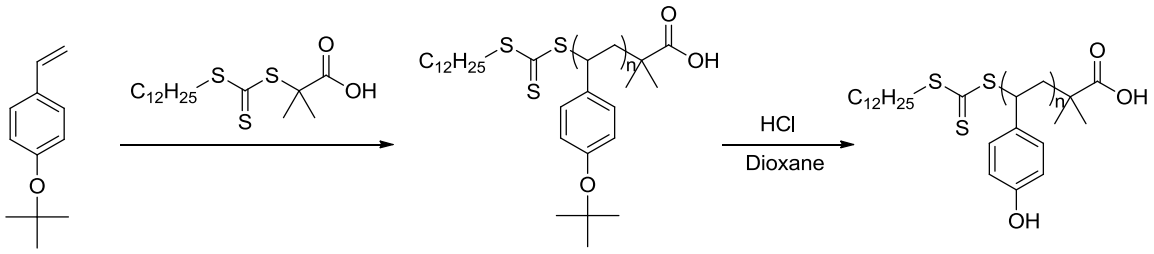

Figure 2.4 Synthetic scheme of PVPh homopolymer.

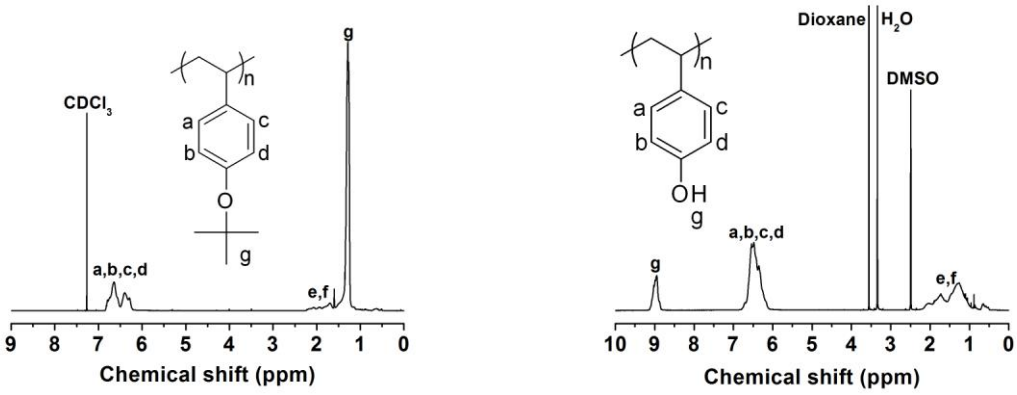

Figure 2.5 ^{1}H NMR spectra of P*t*BOS precursor and PVPh homopolymer.

2.2 Ionic Liquid Synthesis and Characterization

A common hydrophobic room-temperature ionic liquid, 1-ethyl-3-methylimidazolium bis(trifluoromethylsulfonyl)amide ([EMIM][TFSA]), was prepared via an ion exchange reaction following a reported procedure.[6] Equal moles of 1-ethyl-3-methylimidazolium bromide ([EMIM][Br]) (IoLiTec, 99%) and lithium bis(trifluoromethylsulfonyl)amide ([Li][TFSA]) (3M, HQ-115) were mixed in HPLC water and vigorously stirred at 70 ℃ for 24 h. The hydrophobic ionic liquid phase was separated and then washed with HPLC water four times, followed by passing through a neutral alumina column using dichloromethane as a diluent. Dichloromethane was subsequently removed using a rotary evaporator and the ionic liquid was dried in a vacuum oven at 60 ℃ for 2 days. The ionic liquid was clear and colorless, and stored in a glove box to avoid water absorption.

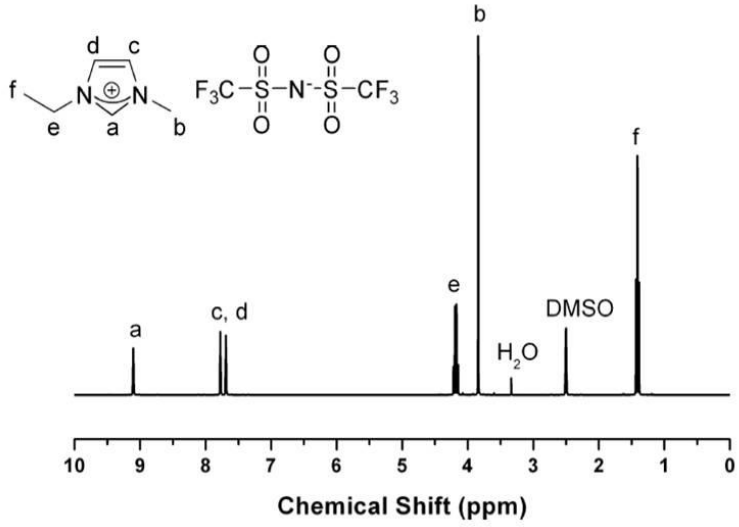

Figure 2.6 ^{1}H NMR spectrum of [EMIM][TFSA].

The ionic liquid was characterized by ^{1}H NMR spectroscopy (Figure 2.6). The temperature dependence of the viscosity of [EMIM][TFSA] over the range of 20–100 ℃ was also characterized (Figure 2.7). The zero shear viscosity (η_0) of [EMIM][TFSA] was measured by steady shear tests on a strain-controlled Rheometric Fluids Spectrometer (RFS II) using couette geometry (bob radius: 16.0 mm; cup radius: 17.0 mm; bob length: 33.2 mm). The temperature was controlled using a Rheometrics environmental circulator. All steady shear viscosity data were taken at several shear rates spanning at least two decades. The temperature dependence of η_0 was fitted with the Vogel–Fulcher–Tammann (VFT) equation

$$\log\left(\frac{\eta(T)}{\eta_\infty}\right) = \frac{B}{T - T_0} \qquad (2.1)$$

where η_∞ = 0.17 cP, B = 350.9 K, and T_0 = 143.5 K. These values are in excellent agreement with the literature results.[7]

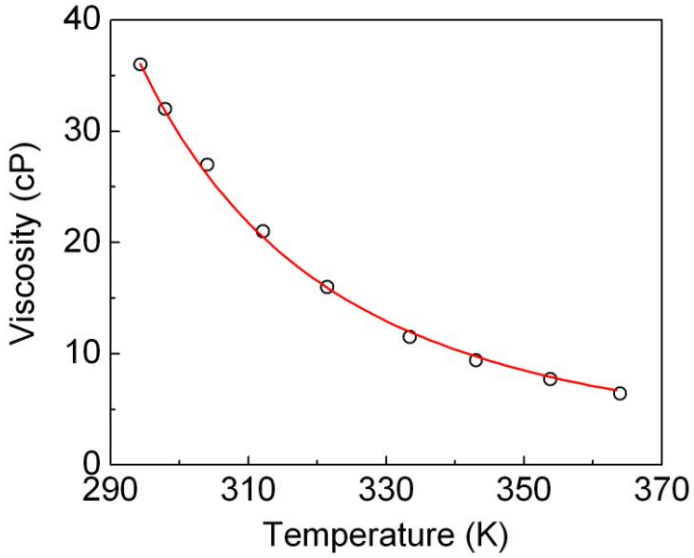

Figure 2.7 Temperature dependence of zero shear viscosity of [EMIM][TFSA]. The solid line represents a fit to the Vogel–Fulcher–Tammann (VFT) equation.

2.3 Size Exclusion Chromatography

Size exclusion chromatography (SEC) is the most commonly employed technique in the molecular characterization of polymers, as with suitable column calibration or multiple detection schemes, both the average molecular weights and molecular weight distributions can be determined. In practice, a solution (mobile phase) passes through columns packed with porous particles of various pore sizes (stationary phase). The separation occurs because molecules of different sizes are excluded from the pores to varying degrees. The largest molecules are excluded from the pores to the greatest extent, and therefore are the first to elute from the column. Progressively smaller molecules

permeate the porous stationary phase to increasing extents and are eluted sequentially. As such, the separation mechanism is based on molecular size (hydrodynamic volume, V_h), as opposed to molecular weight directly. This leads to a limitation when the SEC column is calibrated by standards because accuracy in molecular weight requires the use of standards of the same polymer as the analyte. The major limitation of SEC, however, is that the separation has rather low resolution.

All SEC measurements described in this thesis were performed on an Alltech 426 HPLC pump combined with three Phenogel columns (Phenomenex). THF was used as the routine eluent and the flow rate was 1 mL/min. Both a refractive index (RI) detector (OPTILAB DSP interferometric reflectometer, Wyatt Technology Corporation) and a light scattering (LS) detector (DAWN DSP laser photometer, Wyatt Technology Corporation) were used to monitor the eluting solution. The response of the RI detector (voltage signal) is proportional to the concentration in g/mL of the eluting polymer (c) and the proportionality factor, known as the refractive index increment ($\partial n/\partial c$), depends on the polymer/solvent system. The LS detector measures scattering intensity at a series of scattering angles simultaneously. A Zimm plot can be constructed to determine both the radius of gyration ($R_{g,i}$) and weight-average molecular weight ($M_{w,i}$) of the eluting polymer. The crucial advantage of the LS detector is the possibility of obtaining an absolute $M_{w,i}$ of each slice of the chromatogram without any column calibration. As a result, both the average molecular weights and dispersities can be extracted.

2.4 Rheology

If the time-dependent stress–strain relationships of polymeric materials are examined, we will find that they are generally viscoelastic in nature, *i.e.*, an intermediate behavior between the viscous flow of liquids and the elastic deformation of solids.[8–11] The molecular origin is the long-chain nature of polymer molecules. When a polymeric material is subjected to a deformation, the individual chains will be stretched in the direction of the force and adopt a non-equilibrium distribution of conformations. After a characteristic relaxation time, the chains will relax back to an equilibrium distribution of conformations, whereby energy is dissipated as heat due to the relative motion of the molecules through the surroundings. Viscoelastic properties of polymeric materials are described by a variety of material functions, such as steady flow viscosity, stress relaxation modulus, creep compliance, and dynamic modulus.

The most common experimental approach is to apply a small-amplitude oscillatory shear, in which the sample is subjected to a sinusoidal shear strain given by

$$\gamma(t) = \gamma_0 \sin(\omega t) \tag{2.2}$$

where ω is the frequency of the oscillation, t is the time, and γ_0 is the maximum strain amplitude. In the linear response regime, *i.e.*, sufficiently small strain amplitudes and strain rates such that material functions do not depend on the strain amplitude or rate, the stress is also sinusoidal with the same frequency, but shifted from the strain by a phase angle δ

$$\sigma(t) = \sigma_0 \sin(\omega t + \delta) \tag{2.3}$$

The elastic and viscous components of the response can be resolved concurrently, which is the primary advantage of this approach. The elastic component is in phase with the strain and the viscous component is in phase with the strain rate

$$\frac{\sigma(t)}{\gamma_0} = G' \sin(\omega t) + G'' \cos(\omega t) \qquad (2.4)$$

where G' is the elastic or storage modulus and G'' is the viscous or loss modulus, G''. The phase angle between strain and stress is determined by the ratio of G'' and G'

$$\tan \delta = \frac{G''}{G'} \qquad (2.5)$$

All rheological measurements described in this thesis were performed on an Advanced Rheometric Expansion System (ARES) equipped with a force transducer featuring a 0.02 g cm lower torque limit. Temperature was always controlled to within ±0.1 ℃ of the set values via a convection oven using dry nitrogen gas. Either 50 or 25 mm diameter parallel plates were used, depending on the modulus, and the gap was *ca.* 1 mm. At each temperature, the gap was adjusted to compensate for thermal expansion, and the sample loading was checked visually to ensure a flat edge. The actual gap was calculated based on the thermal expansion coefficient of the stainless steel plates (2.4 μm/K) assuming linear expansion with temperature. Samples were allowed to equilibrate for 15 min at each temperature and then a dynamic strain sweep was performed to identify the linear viscoelastic regime.

Dynamic frequency sweeps were carried out over the frequency range of 0.1–100 rad/s, limited by the capability of the rheometer at higher frequencies and by the

experimental convenience at lower frequencies. Original data collected over a range of temperatures can be reduced to a single master curve to extend the accessible frequency range, by applying the time–temperature superposition (tTS) principle. The frequency dependence of a viscoelastic function, for example, stress relaxation modulus, $G(\omega,T)$, at two different temperatures is given by a simple scaling

$$G(\omega,T) = b_T G(\omega a_T, T_r) \tag{2.6}$$

where T_r is the reference temperature, and a_T and b_T are the horizontal and vertical shift factors, respectively. Small vertical shift factors can be applied to correct for density variation with temperature, which is given by

$$b_T = \frac{\rho_r T_r}{\rho T} \tag{2.7}$$

In practice, the tan δ spectrum is shifted horizontally to obtain a_T and then the same shift factors are applied to the dynamic moduli to obtain master curves. Finally, small vertical shifts can be applied based on knowledge of $\rho(T)$. For tTS to apply, the single and crucial requirement is that all the relevant relaxation times have the same temperature dependence over the measured temperature range.

2.5 Small-Angle Scattering

Small-angle scattering is a non-invasive structural characterization technique based on deflection of a collimated beam of radiation (light, X-rays and neutrons) away from the straight trajectory after it interacts with structures that are much larger than the

wavelength of the radiation.[12] Information about the size, shape and orientation of structures can be obtained over length scales from 1 nm to 10 μm. In a scattering experiment, an unpolarized incident wave with intensity I_0 illuminates the sample, and the scattered wave with intensity I_s is detected at an angle θ. The amplitude of a wave travelling in the $\vec{k}_i$ direction at the position $\vec{r}$ and time t is given by

$$\Psi_0 \exp\left[i\left(\omega t - \vec{k}_i \cdot \vec{r}\right)\right] \tag{2.8}$$

Here ω is the frequency in rad/s and $\vec{k}_i$ has amplitude $2\pi/\lambda$, where λ is the wavelength in the sample. The change in the direction of propagation of the scattered wave relative to the incident wave is quantified by the scattering vector, $\vec{q}$, also known as the momentum transfer vector, which is defined by the difference between incident and scattered wave vectors

$$\vec{q} \equiv \vec{k}_i - \vec{k}_s \tag{2.9}$$

For elastic scattering, in which the scattered wave has the same frequency as the incident wave, both incident and scattered wave vectors have magnitude $2\pi/\lambda$, and thus the magnitude of $\vec{q}$ can be obtained

$$|\vec{q}| \equiv q = \frac{4\pi}{\lambda} \sin\left(\frac{\theta}{2}\right) \tag{2.10}$$

The magnitude of $\vec{q}$ has dimensions of inverse length. Scattering experiments explore fluctuations and thus are sensitive to structures on the length scale of q^{-1}.

Scattering arises from three factors: the amplitude of the mean square concentration fluctuations, the spatial correlations among the fluctuations, and the contrast factor. The concentration fluctuations, which are random in nature, give rise to incoherent scattering, from which one cannot extract any structural correlation present in the sample, because there is no preferred distance, or spatial correlation, among the fluctuations. The intensity of incoherent scattering is independent of scattering angle. Spatial correlations among different scattering centers lead to scattered waves travelling different distances to the detector, which give rise to phase differences among them. This phenomenon is known as coherent scattering. Analysis of the phase differences yields valuable information about the orientation of scattering centers in the sample. The path difference (δ) between the waves scattered by two scattering centers separated by a distance of $\vec{r}_{jk}$ is given by $d_j - d_k$, which can be related to $\vec{q}$ through the following equation

$$\delta = \frac{2\pi}{\lambda}\left(d_j - d_k\right) = \frac{2\pi}{\lambda}\left(\vec{k}_i \cdot \vec{r}_{jk} - \vec{k}_s \cdot \vec{r}_{jk}\right) \qquad (2.11)$$

The structure factor contains the information about the spatial correlations of the sample and is defined by the superposition of all waves at a particular $\vec{q}$, normalized by the square of the number of scattering centers

$$S(\vec{q}) = \frac{1}{N^2}\sum_{j}^{N}\sum_{k}^{N}\left\langle \exp\left[-\mathrm{i}\vec{q}\cdot\vec{r}_{jk}\right]\right\rangle \qquad (2.12)$$

The scattered intensity per unit volume can be obtained from the structure factor and is given by

$$I(\vec{q}) \sim \frac{K}{v} S(\vec{q}) \qquad (2.13)$$

where K is the contrast factor and v is the scattering volume. The contrast factor quantifies the degree to which a given concentration fluctuation modulates the relevant material parameter: dielectric constant (refractive index) for light, electron density for X-rays, and scattering cross section for neutrons. If there is no scattering contrast present in the sample, structural correlations will be invisible and only scattering originating from random concentration fluctuation will be present.

Small-angle X-ray scattering (SAXS) data presented in this thesis were collected at the synchrotron facility of Advanced Photon Source (APS), Argonne National Laboratory (ANL). Synchrotron sources provide an incident flux of X-rays that is several orders of magnitude larger than a laboratory source. Furthermore, it can be much better collimated, and wavelength may be tuned to a convenient value. These features together provide scattering patterns with much better resolution in much shorter exposure time.

Small-angle neutron scattering (SANS) measurements were performed on the CG-2 General Purpose SANS instrument at the High Flux Isotope Reactor (HFIR) facility at Oak Ridge National Laboratory (ORNL). The neutron wavelength was 4.75 Å and the sample-to-detector distance was 14 m. Temperature was calibrated using a thermocouple immersed in oil in a quartz cell. Samples were sandwiched between two quartz disks separated by an aluminum spacer and sealed by high-temperature adhesives. Data reduction was performed using the Igor package provided by ORNL. Scattering data were corrected for sample transmission, empty cell, background scattering, and detector

sensitivity. Absolute intensity curves $I(q)$ were obtained using the direct beam method, followed by azimuthal averaging.

2.6 References

(1) Noro, A.; Matsushita, Y.; Lodge, T. P. *Macromolecules* **2008,** *41*, 5839–5844.

(2) Noro, A.; Matsushita, Y.; Lodge, T. P. *Macromolecules* **2009,** *42*, 5802–5810.

(3) Chiefari, J.; Chong, Y. K.; Ercole, F.; Kristina, J.; Jeffery, J.; Le, T. P. T.; Mayadunne, R. T. A.; Meijs, G. F.; Moad, C. L.; Moad, G.; Rizzardo, E.; Thang, S. H. *Macromolecules* **1998,** *31*, 5559−5562.

(4) Moad, G.; Rizzardo, E.; Thang, S. H. *Aust. J. Chem.* **2005,** *58*, 379−410.

(5) Lai, J. T.; Filla, D.; Shea, R. *Macromolecules* **2002,** *35*, 6754−6756.

(6) Susan, M. A. B. H.; Kaneko, T.; Noda, A.; Watanabe, M. *J. Am. Chem. Soc* **2005,** *127*, 4976–4983.

(7) Tokuda, H.; Hayamizu, K.; Ishii, K.; Susan, M. A. B. H.; Watanabe, M. *J. Phys. Chem. B* **2005,** *109*, 6103–6110.

(8) Ferry, J. D. *Viscoelastic Properties of Polymers*, 3rd ed.; John Wiley & Sons: New York, 1980.

(9) Macosko, C. W. *Rheology: Principles, Measurements and Applications*; Wiley-VCH: New York, 1994.

(10) Larson, R. G. *The Structure and Rheology of Complex Fluids*; Oxford University Press: New York, 1999.

(11) Hiemenz, P. C.; Lodge, T. P. *Polymer Chemistry,* 2nd ed.; CRC Press: New York, 2007.

(12) Roe, R. J. *Methods of X-ray and Neutron Scattering in Polymer Science*; Oxford University Press: New York, 2000.

Chapter 3

Effects of Component Molecular Weight on the Viscoelastic Properties*

3.1 Introduction

In 2008, Noro *et al.* reported a special approach to thermoreversible ion gels by adding an additional poly(4-vinylphenol) (PVPh) cross-linker to a poly(2-vinylpyridine-*b*-ethyl acrylate-*b*-2-vinylpyridine) (P2VP–PEA–P2VP) triblock solution in a room-temperature ionic liquid, 1-ethyl-3-methylimidazolium bis(trifluoromethylsulfonyl)amide ([EMIM][TFSA]), a good solvent for the entire triblock chain, where hydrogen bonding between the P2VP blocks and PVPh cross-linkers generates a transient polymer network.[1,2] Initial results from a representative sample containing 10 wt% triblock and 4 wt% cross-linker revealed remarkably thermosensitive viscoelastic properties in the sense that its longest relaxation time (τ_1) varied by a factor of 10^{12} from gel temperature ($T_{gel} \approx$ 140 ℃) down to room temperature. This extreme temperature sensitivity was attributed to the formation of multiple hydrogen bonds in a single P2VP↔PVPh association. It was further hypothesized that τ_1 is determined by the average lifetime of a P2VP↔PVPh association, which is directly related to the number of hydrogen bonds involved. On the basis of this hypothesis, the many orders of magnitude variation in τ_1 was interpreted in

* *Reproduced by permission of The Royal Society of Chemistry* from Lei, Y.; Lodge, T. P. *Soft Matter* **2012,** *8*, 2110–2120. http://dx.doi.org/10.1039/c2sm06652a

terms of the variation in the number of hydrogen bonds on a P2VP↔PVPh association, and therefore, the activation energy barrier to junction dissociation, as temperature changes. However, further experimental work is needed to test this hypothesis.

In this chapter, we investigate the viscoelastic properties of supramolecular ion gels via hydrogen bonding, with particular attention paid to how τ_1 and T_{gel} vary with the P2VP block and PVPh cross-linker lengths at constant poly(ethylene oxide) (PEO) midblock length and polymer concentration. The results enhance understanding of the underlying gelation and relaxation mechanisms in this versatile supramolecular ion gel system. The PEA midblock used in the previous system was relatively disperse ($Đ \approx 1.6$),[1,2] and therefore we have switched to a PEO midblock, which can provide a narrower molecular weight distribution.

3.2 Experimental Section

3.2.1 Polymer Synthesis and Characterization

The molecular characterization information of all polymers used in this chapter is summarized in Table 3.1, including the molecular weight of each block and overall dispersities (*Đ*s). Their detailed synthesis was described in Chapter 2. For simplicity, each P2VP–PEO–P2VP triblock copolymer is denoted as VOV(*x*-*y*-*z*), where *x*, *y*, and *z* refer to the average block molecular weights in kg/mol, and each PVPh homopolymer is denoted as PVPh-*m*, where *m* represents the molecular weight in kg/mol.

Table 3.1 Molecular Characterization of Polymers

Polymers	$M_{n,P2VP}$[a] (kg/mol)	$M_{n,PEO}$[b] (kg/mol)	$M_{n,PVPh}$[c] (kg/mol)	$Đ$[d]
VOV(2-35-2)	2	35		1.06
VOV(3-35-3)	2.6	35		1.08
VOV(4-35-4)	4	35		1.08
VOV(6-35-6)	5.8	35		1.09
VOV(15-35-15)	15	35		1.12
PVPh-5[e]			5	1.04
PVPh-8[f]			8	1.12
PVPh-10[g]			10	1.10
PVPh-35[e]			35	1.22

[a] Block M_n determined by ^{1}H NMR spectroscopy. [b] Determined by SEC with light scattering detection (the $\partial n/\partial c$ value for PEO homopolymer in THF solvent at a laser wavelength of 633 nm is 0.068 mL/g). [c] Determined by ^{1}H NMR spectroscopy. [d] Determined by SEC. [e] These two PVPh homopolymers were previously synthesized by Ozair using anionic polymerization.[3] [f] This PVPh homopolymer was synthesized by RAFT polymerization as described in Chapter 2. [g] This PVPh homopolymer was purchased from Sigma–Aldrich.

3.2.2 Supramolecular Ion Gel Preparation

All supramolecular ion gels were prepared by mixing weighed amounts of the respective polymers (triblock and cross-linker) and ionic liquid in a THF cosolvent. After these ternary mixtures were stirred for a few hours, most of the cosolvent was removed under a flow of nitrogen gas for 1 day followed by drying in a vacuum oven at 110 °C for 1 day to completely remove the cosolvent. All samples were stored in a vacuum desiccator to minimize water absorption.

3.2.3 Rheology

Rheological experiments were performed on an ARES rheometer (TA instruments) using parallel plate geometry. Temperatures were controlled to within ±0.1 °C of the set values via a convection oven using dry nitrogen gas. Special care was taken during sample loading to exclude bubbles. Gels were annealed above their respective T_{gel}s while shearing at a shear rate of 10 s^{-1} for 10–15 minutes before further experiments were conducted, allowing any small bubbles to flow to the center of the geometry, where they minimally affect the torque.[4] At each temperature, the gap was adjusted to compensate for thermal expansion, and the sample loading was checked visually to ensure a flat edge. The actual gap was calculated based on the thermal expansion coefficient of the stainless steel plates (2.4 μm/K) assuming linear expansion with temperature. Gels were allowed to equilibrate for 15 minutes at each measurement temperature and then a dynamic strain sweep was performed to identify the linear viscoelastic regime. Dynamic temperature ramps were performed both on heating and cooling at a strain amplitude of 3%, an angular frequency of 0.3 rad/s, and a heating/cooling rate of 1 °C/min. Dynamic

frequency sweeps were performed at a strain amplitude of 3% over an angular frequency range of 0.1–100 rad/s at various temperatures.

3.2.4 Small-Angle X-ray Scattering

Small-angle X-ray scattering (SAXS) experiments were performed at the Dupont–Northwestern–Dow Collaborative Access Team (DND–CAT) beamline 5-ID-D at the Advance Photon Source, Argonne National Laboratory. Gels were sealed into hermetic differential scanning calorimetry (DSC) pans, which were then mounted to a washer sandwiched between two Kapton layers. Two-dimensional SAXS data were collected and then azimuthally integrated to generate one-dimensional data presented as intensity (I) vs scattering vector ($q = 4\pi\sin(\theta/2)/\lambda$), where θ is the scattering angle and λ is the X-ray wavelength.

3.3 Results and Discussion

Seven supramolecular ion gels were prepared and investigated, in which either the P2VP block or PVPh cross-linker length was varied, as summarized in Table 3.2. The triblock concentration was fixed at 10 wt% and the cross-linker concentration at 4 wt%.

Table 3.2 Characteristics of Supramolecular Ion Gels

P2VP–PEO–P2VP	PVPh	X_{ph}/X_{py} [a]	T_{gel} [b] (℃)	G_N [c] (Pa)
VOV(2-35-2)	PVPh-8	340/100	119	8700
VOV(3-35-3)	PVPh-8	240/100	137	11500
VOV(6-35-6)	PVPh-8	140/100	162	3000
VOV(15-35-15)	PVPh-8	75/100	163	500
VOV(4-35-4)	PVPh-5	190/100	140	14500
VOV(4-35-4)	PVPh-10	190/100	145	14000
VOV(4-35-4)	PVPh-35	190/100	155	13500

[a] Molar ratio of phenol/pyridine units. [b] T_{gel} determined from the crossover temperature at which $G' = G''$ in Figures 3.1 and 3.2. [c] Plateau modulus.

3.3.1 Dynamic Temperature Ramp

Dynamic temperature ramps from each of the seven supramolecular ion gels examined are shown in Figures 3.1 and 3.2, in which the dynamic storage modulus (G') and loss modulus (G'') are plotted against temperature in a semi-logarithmic format. These plots illustrate the significant changes in viscoelastic properties of these gels over the temperature ranges investigated. At low temperatures, the rheological response is highly elastic with $G' >> G''$, whereas at high temperatures, the rheological response is predominantly viscous with $G'' > G'$. Wide temperature-independent rubbery plateaus in G' are evident at low temperatures, indicating the formation of a well-defined network structure which does not evolve appreciably with temperature. Additionally, all gels undergo a sharp transition from viscous liquid-like behavior to elastic gel-like behavior with a well-defined transition temperature termed T_{gel}. Above T_{gel}, gels rapidly soften into viscoelastic liquids over a narrow temperature interval with steep drop in the moduli. The crossover temperature at which $G' = G''$ is used as a convenient indicator of T_{gel}, which represents the temperature at which the gel has a longest relaxation time comparable to the time scale of the experiment ($\tau_1 \approx \omega^{-1}$). Since dynamic temperature ramps were performed at ω = 0.3 rad/s, the rheological response of these gels was probed on a time scale of ~3.3 s. These gels are thermoreversible, and rheological data collected on heating and cooling are highly reproducible with negligible hysteresis in T_{gel} (1–2 ℃ difference).

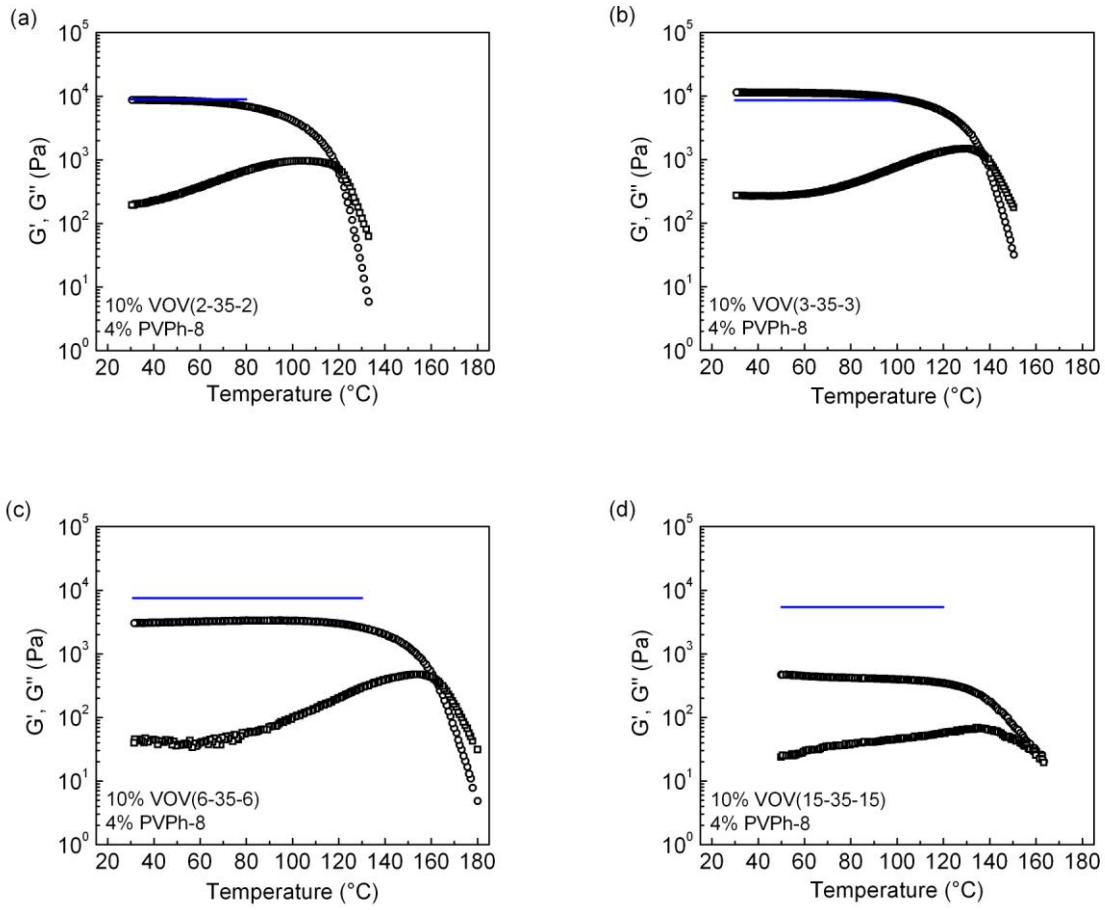

Figure 3.1 Temperature dependence of dynamic storage modulus G' (○) and loss modulus G'' (□) for four supramolecular ion gels showing the effect of varying the P2VP block length: (a) 2 kg/mol; (b) 2.6 kg/mol; (c) 5.8 kg/mol; (d) 15 kg/mol. All other variables are held constant (see the lower left-hand corner of each plot for details). All measurements were performed at a strain amplitude of 3%, an angular frequency of 0.3 rad/s, and a heating rate of 1 ℃/min. The blue lines represent the "ideal" plateau modulus assuming every midblock is elastically effective, as discussed in Section 3.3.5.

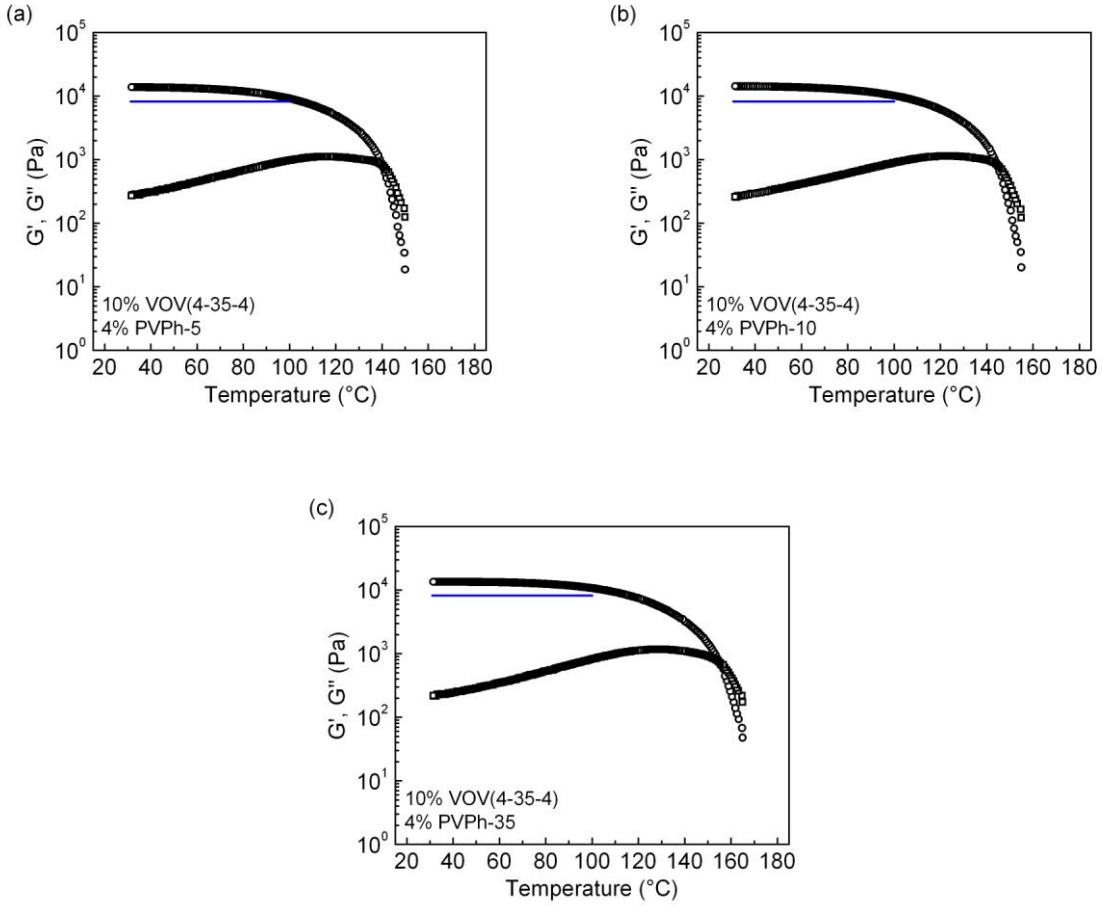

Figure 3.2 Temperature dependence of dynamic storage modulus G' (○) and loss modulus G'' (□) for three supramolecular ion gels showing the effect of varying the PVPh cross-linker length: (a) 5 kg/mol; (b) 10 kg/mol; (c) 35 kg/mol. All other variables are held constant (see the lower left-hand corner of each plot for details). All measurements were performed at a strain amplitude of 3%, an angular frequency of 0.3 rad/s, and a heating rate of 1 ℃/min. The blue lines represent the "ideal" plateau modulus assuming every midblock is elastically effective, as discussed in Section 3.3.5.

3.3.2 Dynamic Frequency Sweep

For each gel, the time-temperature superposition (tTS) principle was applied to construct a master curve by shifting the isothermal dynamic frequency sweep data collected at various temperatures along the frequency axis. Figures 3.3 and 3.4 show the tTS master curves in which G' and G'' are plotted against reduced frequency (ωa_T) in a double-logarithmic format (see Figure 3.5 for resulting shift factors). The applicability of tTS suggests that the underlying origin of viscoelasticity in these gels does not evolve over the temperature range investigated. At low reduced frequencies, all samples behave as viscoelastic liquids, as revealed by the terminal relaxation behavior where G' and G'' scale with second and first powers of frequency, respectively. The terminal region in the VOV(15-35-15)-based gel was not accessed because the relatively low-viscosity yielded low-torque values that approached the sensitivity limitation of the rheometer transducer. At high reduced frequencies, pronounced frequency-independent rubbery plateaus in G' are evident extending up to ten orders of magnitude in reduced frequency; concurrently, G'' is considerably smaller than G', exemplifying the rheological features that characterize a gel.[5] The appearance of systematic upturns in G'' at the high-frequency end of low-temperature data is attributed to the relaxation of the PEO network strands, which possesses a distinct temperature dependence compared with the gel relaxation. As noted previously,[1,2] shifting these G'' upturns along the frequency axis by an amount equal to the relative solvent viscosity causes the data to superpose (see Figures 3.6 and 3.7 for master curves and resulting shift factors, respectively).

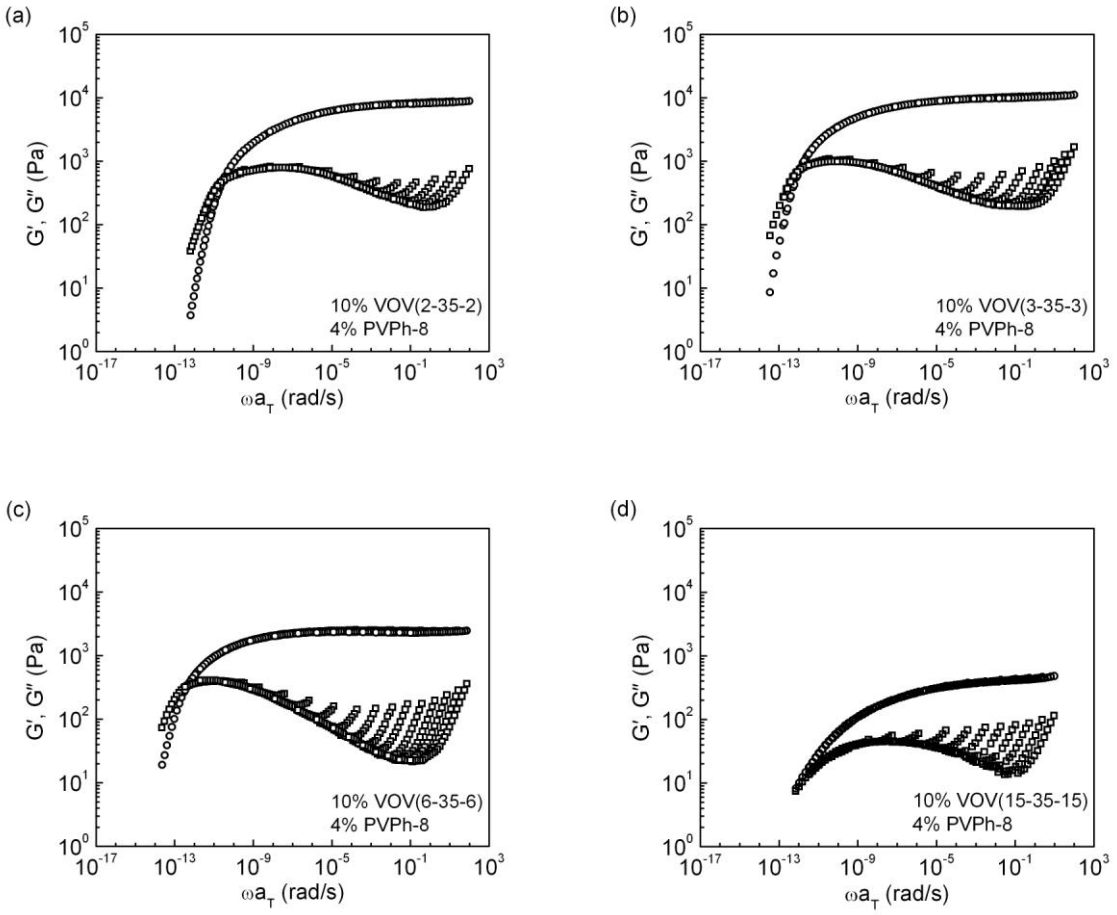

Figure 3.3 tTS master curves of dynamic storage modulus G' (○) and loss modulus G'' (□) referenced to 30 ℃ for four supramolecular ion gels showing the effect of varying the P2VP block length: (a) 2 kg/mol; (b) 2.6 kg/mol; (c) 5.8 kg/mol; (d) 15 kg/mol. All other variables are held constant (see the lower right-hand corner of each plot for details).

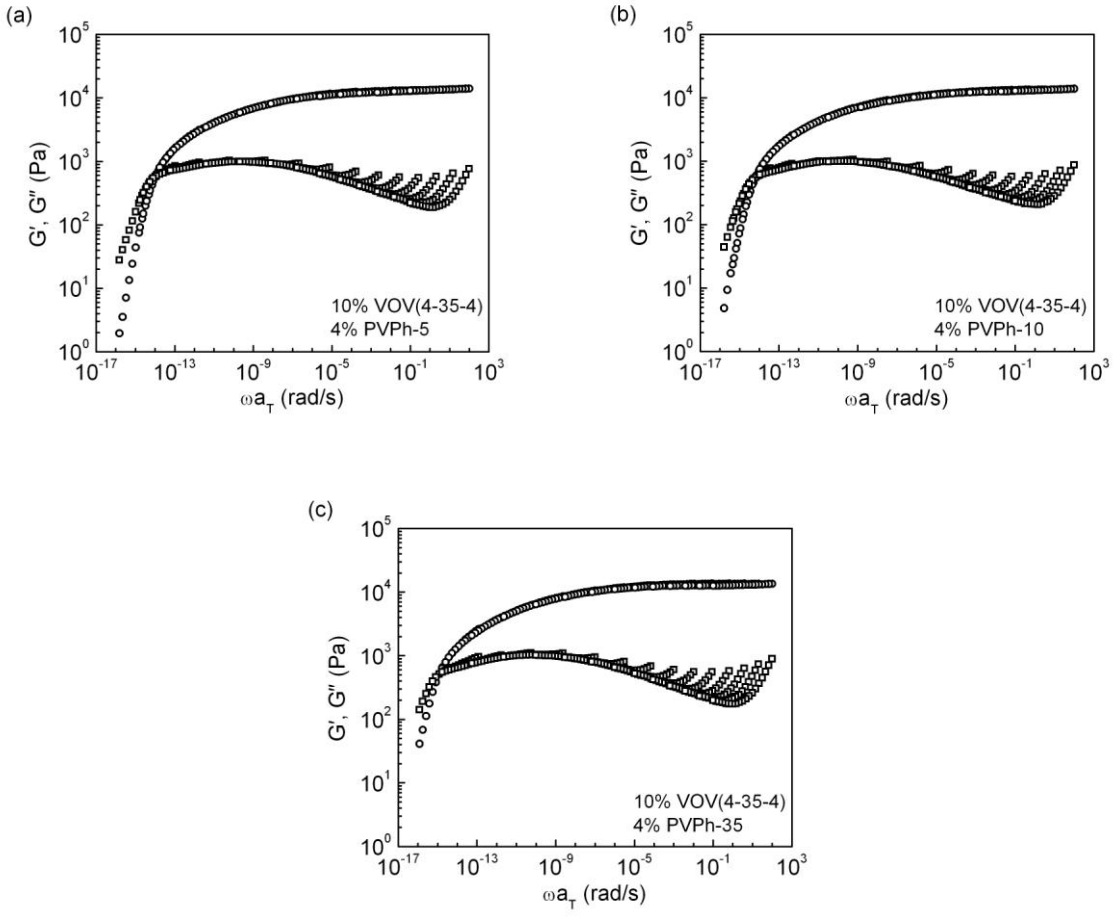

Figure 3.4 tTS master curves of dynamic storage modulus G' (○) and loss modulus G'' (□) referenced to 30 ℃ for three supramolecular ion gels showing the effect of varying the cross-linker length: (a) 5 kg/mol; (b) 10 kg/mol; (c) 35 kg/mol. All other variables are held constant (see the lower right-hand corner of each plot for details).

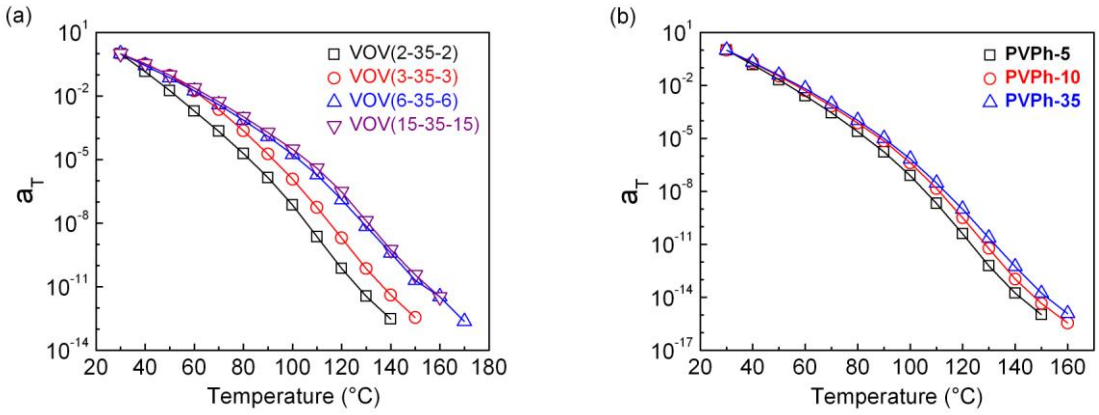

Figure 3.5 Temperature dependence of tTS shift factors used in generating the master curves of (a) Figure 3.3 and (b) Figure 3.4.

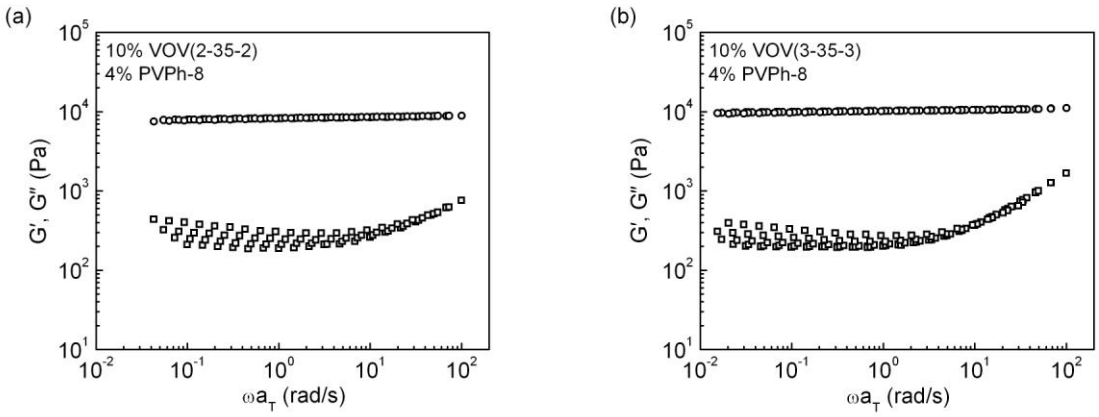

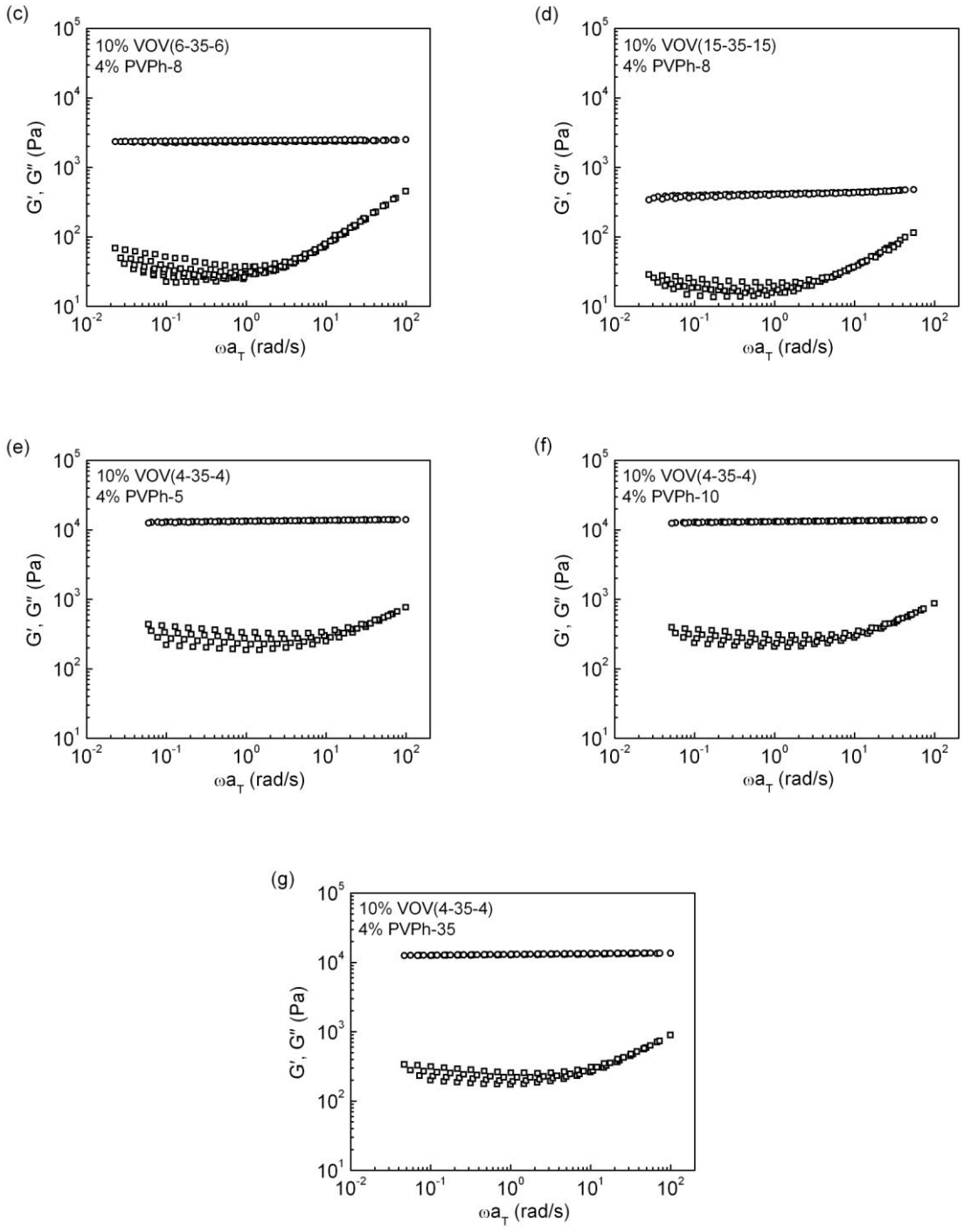

Figure 3.6 tTS master curves from superposing the *G″* upturns at the high-frequency end of low-temperature data, with a uniform reference temperature of 30 ℃.

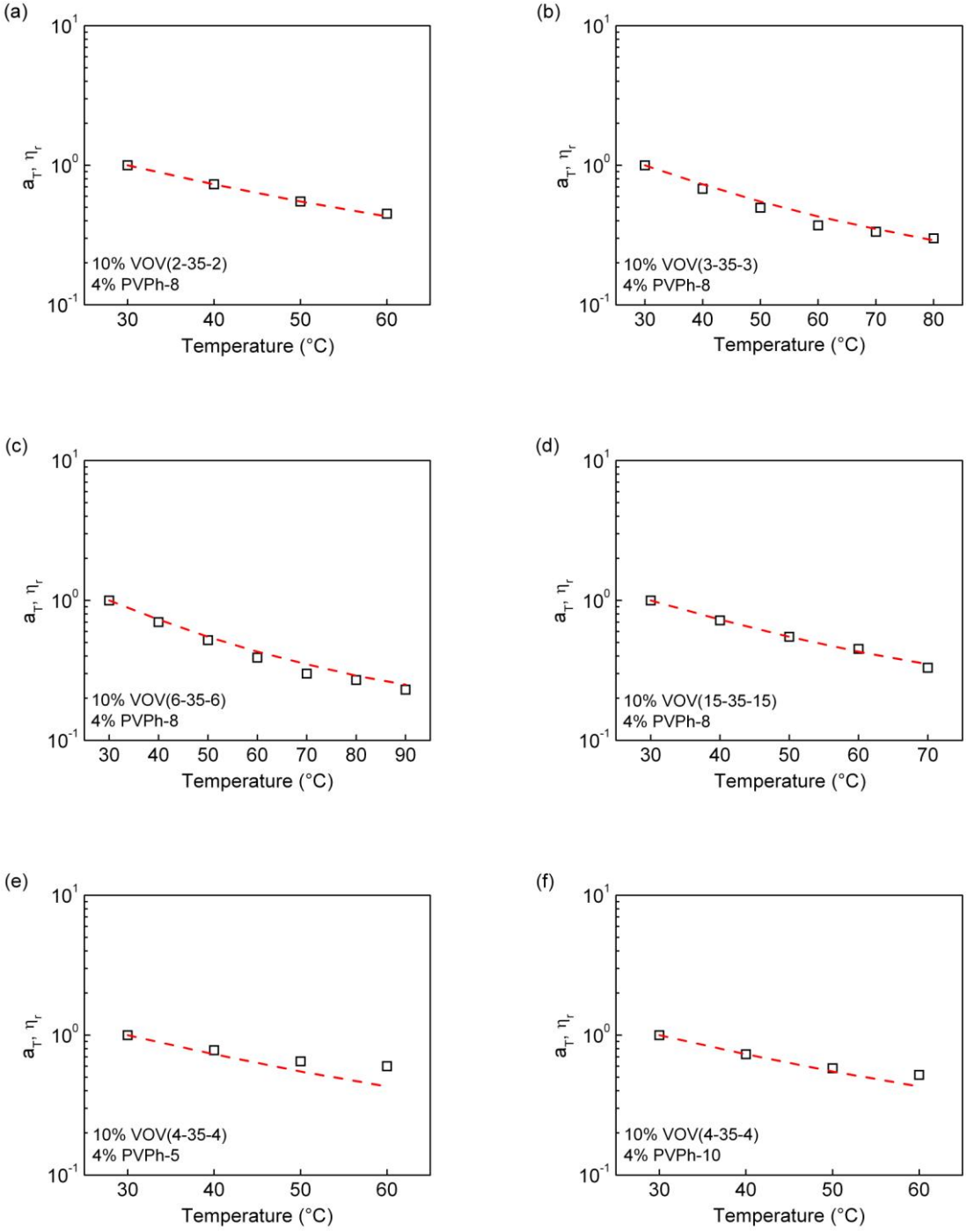
(a)
10% VOV(2-35-2)
4% PVPh-8
(b)
10% VOV(3-35-3)
4% PVPh-8
(c)
10% VOV(6-35-6)
4% PVPh-8
(d)
10% VOV(15-35-15)
4% PVPh-8
(e)
10% VOV(4-35-4)
4% PVPh-5
(f)
10% VOV(4-35-4)
4% PVPh-10
a_T, η_r
Temperature (°C)

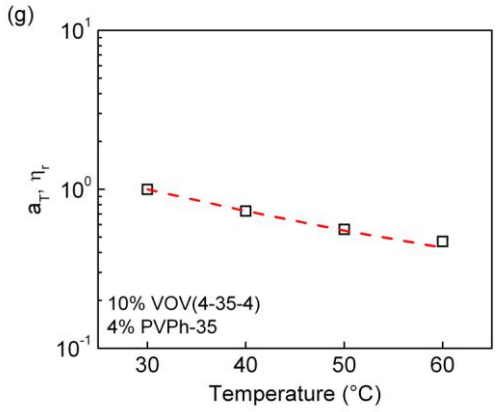

Figure 3.7 Temperature dependence of tTS shift factors (□) used in generating the master curves of Figure 3.6. The viscosities of [EMIM][TFSA] relative to its value at the tTS reference temperature (30 ℃) are also included (red dashed lines) for comparison.

3.3.3 Effects of P2VP Block Length

As mentioned earlier, the remarkable temperature sensitivity observed in this supramolecular ion gel system was hypothesized to originate from the temperature dependence of the average lifetime of a P2VP↔PVPh association. For the purpose of testing this hypothesis, we examine the rheological consequences of varying the P2VP block length while holding all other variables constant, with the expectation that increasing the P2VP block length would increase the number of hydrogen bonds in a P2VP↔PVPh association, which would change τ_1 and T_{gel}. It is worth emphasizing that a P2VP↔PVPh association refers to a block↔cross-link association, which generally involves multiple hydrogen bonds, instead of a monomer↔monomer association, which is a single hydrogen bond. Additionally, an important structural feature of this system is

that the cross-links are comprised of intermolecularly hydrogen-bonded PVPh chains instead of a single PVPh chain, due to the self-association of phenol units, and therefore an aggregation number is employed to denote the number of PVPh chains associated in one cross-link.

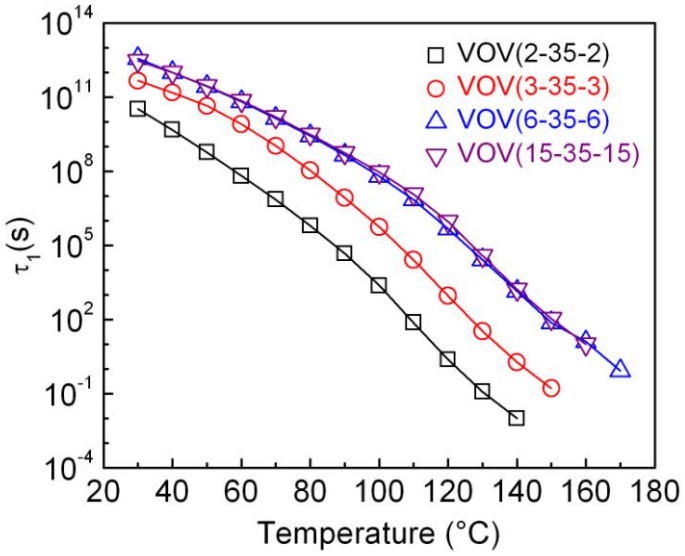

Figure 3.8 Effect on temperature-dependent τ_1 of varying the P2VP block length over the range of 2–15 kg/mol while holding all other variables constant.

Dynamic temperature ramps and tTS master curves for four supramolecular ion gels showing the effect of varying the P2VP block length over the range of 2–15 kg/mol are shown in Figures 3.1 and 3.3, respectively. From the tTS master curves, τ_1 at any given temperature is calculated from

$$\tau_1(T) = \tau_1(T_{ref})a_T \quad (3.1)$$

where $\tau_1(T_{ref})$ is the longest relaxation time at the tTS reference temperature, which is determined by the crossover frequency (ω_c) at which $G' = G''$ in the tTS master curve, $\tau_1(T_{ref}) = \omega_c^{-1}$, and a_T is the tTS shift factor for the temperature of interest, which denotes the ratio of any relaxation time at one temperature to its value at the chosen reference temperature. This allows us to generate a plot showing the effect on temperature-dependent τ_1 of varying the P2VP block length over the range of 2–15 kg/mol (Figure 3.8). It is immediately clear that τ_1 is considerably influenced by the P2VP block length over the range of 2–5.8 kg/mol. Specifically, the VOV(3-35-3)-based gel relaxes about 1000 times slower than the VOV(2-35-2)-based gel, but about 500 times faster than the VOV(6-35-6)-based gel. Since the number of hydrogen bonds per P2VP↔PVPh association should increase with increasing P2VP block length in this series, the dramatically slower terminal relaxation dynamics observed with longer P2VP blocks is in excellent agreement with the hypothesis that τ_1 is determined by the average lifetime of a P2VP↔PVPh association, which is directly related to the number of hydrogen bonds involved. Furthermore, there is some indication that τ_1 approaches fixed values at long enough P2VP block lengths, as manifested by the near equivalence of VOV(6-35-6)- and VOV(15-35-15)-based gels. This apparent saturation is attributed to the finite number of effective phenol units in a cross-link capable of associating with pyridine units on the P2VP blocks, which does not fluctuate significantly at fixed cross-linker concentration, and therefore would prevent unlimited enhancement in τ_1 with increasing P2VP block length. It is noteworthy that PVPh does not dissolve in the ionic liquid when hydrogen-

bonded with P2VP, whereas PVPh by itself initially dissolves in the ionic liquid. The PVPh aggregates shrink into a compact phase to minimize contact with the solvent, whereby a certain fraction of phenol units is hidden inside the aggregates. Therefore, only a small fraction of free phenol units that are exposed to the surface of the cross-links are available to form hydrogen bonds with pyridine units on the P2VP blocks. This interpretation is supported by the modest number of hydrogen bonds actually formed on a P2VP↔PVPh association, as will be shown later. As the P2VP block length increases progressively, the eventual exhaustion of the effective phenol units would result in the saturation of τ_1, because further increase in the P2VP block length would not contribute to an increase in the number of hydrogen bonds for a given P2VP↔PVPh association. Thus, this apparent saturation of τ_1 is also consistent with the idea that τ_1 is determined by the average lifetime of a P2VP↔PVPh association. Based on these results, we propose that the most straightforward relaxation mechanism implicates P2VP block detachment from associated cross-links, which requires simultaneous breaking of all hydrogen bonds involved.

A similar trend with respect to the dependence of T_{gel} on the P2VP block length was also observed, as summarized in Table 3.2. From a physical perspective, a reasonable assumption for T_{gel} is that the gel point should occur at about one hydrogen bond per P2VP↔PVPh association. At equivalent cross-linker concentration, the fraction of hydrogen-bonded pyridine units on a P2VP block needed to reach T_{gel} decreases with increasing P2VP block length. The fraction of hydrogen-bonded units is further correlated with the equilibrium constant. The natural consequence of a reduction in the

equilibrium constant is the shift of T_{gel} to higher temperatures. Additionally, at sufficiently long P2VP block lengths, T_{gel} saturates at ~160 ℃, which is essentially of the same origin as the saturation of τ_1, *i.e.*, due to the finite number of effective phenol units in a cross-link. Note that T_{gel} depends on the fraction of hydrogen-bonded units to reach approximately eight hydrogen bonds per P2VP↔PVPh association, whereas τ_1 depends on the absolute number of hydrogen bonds per P2VP↔PVPh association.

We may extend these qualitative analyses to estimate the actual number of hydrogen bonds per P2VP↔PVPh association. Since the dissociation of hydrogen bonds is a thermally activated process, τ_1 is expected to follow an Arrhenius relation

$$\tau_1 \propto \exp\left(\frac{nE}{RT}\right) \tag{3.2}$$

where n is the number of hydrogen bonds per P2VP↔PVPh association and E is the activation energy required to break a single hydrogen bond, which was estimated to be 13 ± 2.5 kJ/mol from Arrhenius plot of the corrected FT-IR absorbance. In addition, as will be shown in Chapter 6, $n(T_{gel}) \approx 8$ for T_{gel} in the range of 120–160 ℃. Based on these two relationships, $n(T)$ is expressed as

$$n(T) = 8\frac{T}{T_{gel}} + \frac{RT}{E}\ln\frac{a_T}{a_{T_{gel}}} \tag{3.3}$$

From equation 3.3, the temperature dependence of $n(T)$ for gels with various P2VP block lengths is generated and shown in Figure 3.9. It can be seen that $n(T)$ for each gel saturates at low temperatures, which simply reflects the formation of the maximum number of hydrogen bonds on a P2VP↔PVPh association. Furthermore, the absolute

number of hydrogen bonds per P2VP block is really quite modest, consistent with both the plausibility of the interpretation and the extreme sensitivity of the gel properties to this parameter.

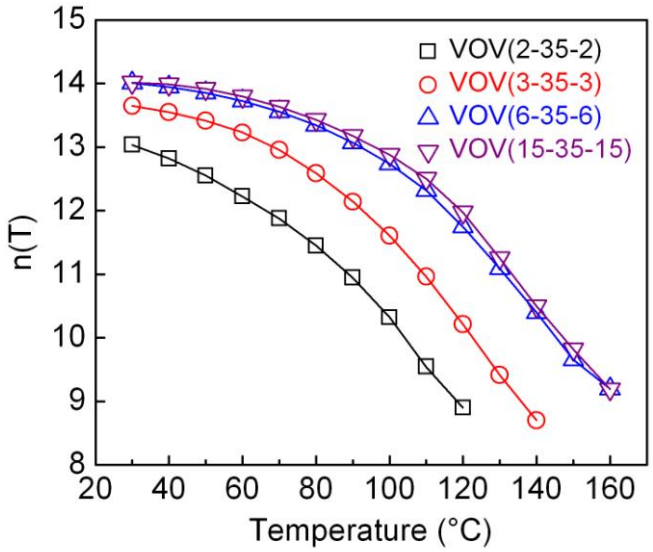

Figure 3.9 Effect on temperature-dependent $n(T)$ of varying the P2VP block length over the range of 2–15 kg/mol while holding all other variables constant.

3.3.4 Effects of PVPh Cross-linker Length

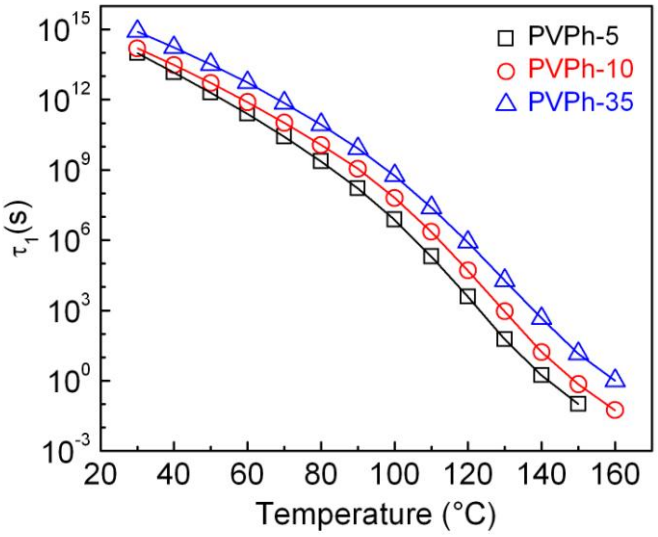

Figure 3.10 Effect on temperature-dependent τ_1 of varying the cross-linker length over the range of 5–35 kg/mol while holding all other variables constant.

The effect on rheological properties of varying the cross-linker length was also evaluated while holding all other variables constant, for a comparison with the effect of P2VP block length. Dynamic temperature ramps and tTS master curves for three supramolecular ion gels showing the effect of varying the cross-linker length over the range of 5–35 kg/mol are shown in Figures 3.2 and 3.4, respectively. The temperature dependence of τ_1 for gels with various cross-linker lengths is shown in Figure 3.10. It is evident from a comparison of Figures 3.8 and 3.10 that the cross-linker length influences

the terminal relaxation dynamics of hydrogen-bonded supramolecular networks to a much lesser extent than the P2VP block length, the reason for which is revealed by room temperature SAXS. As shown in Figure 3.11, varying the cross-linker length has little discernible influence on the SAXS patterns in general, and on the locations of the scattering peaks in particular. The primary low-q scattering peaks represent the structure factor, which arises from interactions between cross-links and reflects the average distance between scattering centers. The fact that the location of the structure factor peak is almost independent of the cross-linker length suggests that the number density of cross-links is not strongly correlated with the cross-linker length at fixed concentration, revealing an approximately inversely proportional relationship between the cross-link aggregation number and cross-linker length. Furthermore, the broad high-q maxima at the tail of the small-angle region, which represent the form factor of the scattering cross-links and depend on the geometry of the individual cross-links, show little discernible shift in position either, offering further evidence that the average size of the cross-links is not appreciably affected by the cross-linker length. In other words, at constant cross-linker concentration, an increase in the cross-linker length is largely compensated by a corresponding reduction in the aggregation number of the cross-links, while leaving the average number and size of the cross-links essentially unperturbed. Consequently, varying the cross-linker length at fixed concentration would not appreciably alter the number of hydrogen bonds on a P2VP↔PVPh association. Again, this result is also consistent with the idea that τ_1 is determined by the average lifetime of a P2VP↔PVPh association, which is directly related to the number of hydrogen bonds involved. Finally,

it should be noted that the cross-link size indeed increases very slightly with increasing cross-linker length, as exemplified by the small enhancements in τ_1 and T_{gel}.

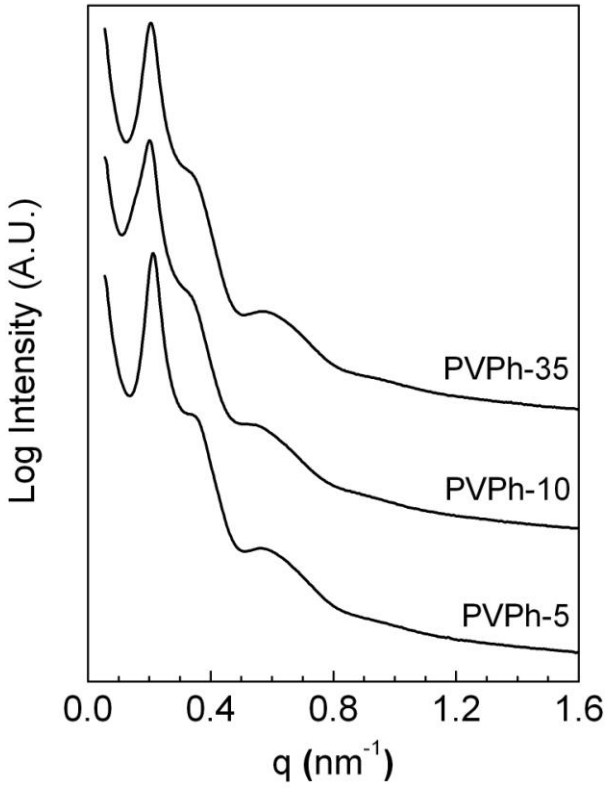

Figure 3.11 Room temperature SAXS profiles for three supramolecular ion gels showing the effect of varying the cross-linker length over the range of 5–35 kg/mol while holding all other variables constant.

For a quantitative treatment, values of average domain spacing (D) and aggregation number (N_{agg}) can be extracted from the scattering profiles and are listed in Table 3.3. Average domain spacing is estimated by presuming the location of the primary scattering peak (q_1) is related to the Bragg spacing for cross-links with a body-centered cubic packing, $D \approx 2\pi/q_1$. The aggregation number, defined here as the number of PVPh chains associated inside a cross-link, can be estimated by

$$N_{agg} = \frac{cN_A}{2M_{PVPh}}\left(\frac{2\sqrt{2}\pi}{q_1}\right)^3 \qquad (3.4)$$

Table 3.3 Estimated Parameters from SAXS Profiles

$M_{n,\,PVPh}$[a] (kg/mol)	q_1[b] (nm^{-1})	D[c] (nm)	N_{agg}[d]
5	0.212	29.6	249
10	0.202	31.1	144
35	0.205	30.6	39

[a] PVPh molecular weight. [b] Scattering vector of the primary peak in Figure 3.11. [c] Average domain spacing estimated by $D \approx 2\pi/q_1$. [d] Aggregation number estimated by equation 3.4.

3.3.5 Plateau Modulus

According to simple rubber elasticity theory, the plateau modulus (G_N) for a supramolecular ion gel is given by

$$G_N = \nu_e k_B T = \frac{fcN_A k_B T}{M} \qquad (3.5)$$

where ν_e is the number density of elastically effective strands, k_B is the Boltzmann constant, T is the absolute temperature, c is the triblock concentration (w/v), N_A is Avogadro constant, M is the triblock molecular weight, and f is the fraction of bridging or elastically effective molecules. Consider a perfect gel in which every midblock adopts bridging conformation and is thus elastically effective (f = 1), the anticipated G_N for each gel was estimated using equation 3.5 and represented by the horizontal lines in Figures 3.1 and 3.2. It is interesting that simple rubber elasticity theory can overestimate (Figures 3.1(c) and 3.1(d)), underestimate (Figures 3.1(b) and 3.2), and satisfactorily estimate (Figure 3.1(a)) G_N of these supramolecular ion gels investigated in this chapter. While the overestimation is not surprising since a certain fraction of midblocks is expected to form loops instead of bridges, the underestimation can be accounted for by the presence of trapped PEO midblock entanglements. A prerequisite for equation 3.5 to apply is that systems under consideration are in the concentration range where midblock entanglements are not present. Trapped midblock entanglements must be taken into account in defining elastically effective strands because they behave as temporary cross-links and provide additional constraints which magnify the change of entropy with deformation.[6] The number of entanglements per midblock ($n_{e,mid}$) is estimated by

$$n_{e,mid} = \frac{M_{mid}}{M_{e,mid}} \varphi_{mid} - 1 \qquad (3.6)$$

where M_{mid} is the midblock molecular weight, $M_{e,mid}$ is the entanglement molecular weight of the midblock in the melt, and φ_{mid} is the midblock volume fraction. For the current system, M_{mid} = 35000 g/mol, $M_{e,mid}$ = 1600 g/mol, φ_{mid} = 9%, and an estimation using equation 3.6 yields $n_{e,mid} \sim 1$. In this sense, every bridging midblock chain is separated into two elastically effective strands, which will increase the anticipated G_N by at most a factor of 2. Therefore, the overestimation, underestimation, and satisfactory estimation of G_N by simple rubber elasticity theory can be rationalized by a fraction of elastically effective molecules below, above, and approximately equal to 50%, respectively.

The significant variation in the experimental G_N itself, as summarized in Table 3.2, may reflect combined effects from triblock molecular weight, stoichiometry of phenol and pyridine units, and steric constraints. The anticipated G_N for each gel differs by a small amount due to the difference in triblock molecular weight. The more important contributor is the stoichiometry of phenol and pyridine units, which will be demonstrated to control the highly tunable G_N of this system in Chapter 4. Specifically, G_N does not increase monotonically with the molar ratio of phenol/pyridine units but goes through a maximum at an optimal ratio ~2/1 (Figure 3.2), which represents a certain stoichiometric balance between phenol and pyridine units. At low molar ratios of phenol/pyridine units (Figures 3.1(c) and 3.1(d)), the existence of a significant amount of dangling ends, due to the exhaustion of the cross-links, results in rather low G_N, whereas at high molar ratios of

phenol/pyridine units (Figures 3.1(a) and 3.1(b)), the mechanism responsible for the decrease in G_N will be discussed in Chapter 4. Also, it is evident that inadequate amount of cross-linker affects G_N to a much greater extent than excess amount of cross-linker. Furthermore, the fact that the functionality of the cross-links is at least partly controlled by steric factors suggests a possible reduction in the functionality of the cross-links with increasing P2VP block length as the P2VP block gets bulkier, which would further increase the amount of dangling ends. For the VOV(15-35-15)-based gel, the relatively bulky P2VP blocks would even give rise to monofunctional and difunctional cross-links because there might be not enough space to accommodate three or more P2VP blocks around a given cross-link, as illustrated by the cartoon in Figure 3.12. Since a functionality of at least three is required for the formation of a network structure, both monofunctional and difunctional cross-links are network defects and will not contribute to the equilibrium elasticity of the network. As a matter of fact, albeit a rubbery plateau is still present in the VOV(15-35-15)-based gel, G' decays continuously with increasing temperature or decreasing frequency, as shown in Figures 3.1(d) and 3.3(d). This indicates a very weak gel without a high level of connectivity because of the presence of a significant amount of network defects, which probably include dangling ends due to the low molar ratio of phenol/pyridine units and monofunctional/difunctional cross-links due to the relatively bulky P2VP blocks.

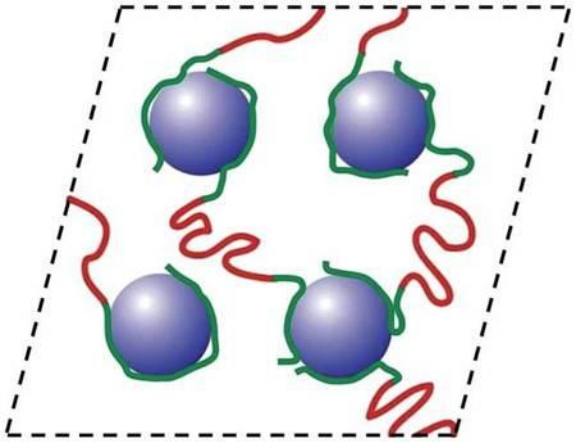

Figure 3.12 Schematic illustration of the formation of monofunctional and difunctional cross-links from bulky P2VP blocks.

3.3.6 Comparison with Self-Assembled Systems

The structures and viscoelastic properties of physical gels from the self-assembly of ABA triblock copolymers in midblock-selective solvents have been extensively studied because of their importance in both theoretical studies and industrial applications.[7–15] Microphase separation of the insoluble endblocks results in assemblies of endblock domains bridged by the well-solvated midblocks into three-dimensional networks. Under conditions where the solvent is not too poor for the endblock and the temperature is above the glass transition of the micelle core, the weakly associated endblocks are able to reversibly exchange between micelle cores,[16] thus generating a transient network with a finite longest relaxation time, which is determined by the time scale of endblock detachment from associated micelle cores either by thermal motion or tension. This endblock pull-out process in self-assembled systems is analogous to the breaking of

hydrogen bonds in the supramolecular system. However, the free energy functions that describe the breaking of transient junctions in these two systems are quite different, namely approximately $\chi_{AS}N_A k_B T$[17–20] for the endblock pull-out and nE for the breaking of hydrogen bonds, where χ_{AS} is the Flory-Huggins interaction parameter between the endblock and the solvent, and N_A is the degree of polymerization of the endblock. The fundamental distinction is that $\chi_{AS}N_A k_B T$ is essentially temperature-independent while nE is strongly temperature-dependent. These self-assembled and supramolecular polymer networks might be described using transient network theory developed by Tanaka and Edwards[21] for a hypothetical system comprised of telechelic polymers with sticky functional groups at both chain ends in which junctions are continuously generated and destroyed.

3.3.7 Comparison with Existing Supramolecular Systems via Hydrogen Bonding

Supramolecules employing hydrogen bonding of terminal units or sequences of telechelic polymers constitute a scientifically fascinating and technologically important class of materials, and numerous illustrations of such systems have been described in the literature.[22–34] For example, Sijbesma *et al.* synthesized polymeric materials using well-defined dimerization of 2-ureido-4-pyrimidone units with quadruple cooperative hydrogen bonds. While these materials are highly analogous in terms of strongly temperature-dependent viscoelastic properties, these supramolecular ion gels have a unique feature that distinguishes them from previous systems. At the get point, the material is a rather weak gel with about eight hydrogen bonds per P2VP↔PVPh association. Upon subsequent cooling, the number of hydrogen bonds per P2VP↔PVPh

association increases from about 8 at gel point to about 13 at room temperature, while no substantial rearrangement of network connectivity takes place due to very high activation energy required to break multiple hydrogen bonds simultaneously. Therefore, the unique feature of this system is that the strength of a given P2VP↔PVPh association is greatly enhanced as temperature decreases, while the network structure is essentially locked in place at the gel point.

3.4 Conclusions

In this chapter, we have demonstrated that the utilization of complementary hydrogen bonding interactions between the endblocks of a P2VP–PEO–P2VP triblock copolymer and an additional cross-linker PVPh homopolymer in an ionic liquid [EMIM][TFSA] allows for the facile preparation of a thermoreversible supramolecular ion gel with well-defined longest relaxation time, gelation temperature, and plateau modulus. The terminal relaxation dynamics of hydrogen-bonded supramolecular networks is dramatically influenced by the P2VP block length, as reflected by the large enhancements in τ_1 and T_{gel} before the eventual saturation appears. This is because progressively increasing the P2VP block length results in a continuous increase in the number of hydrogen bonds on a P2VP↔PVPh association until the exhaustion of the effective phenol units in a cross-link. In contrast, varying the cross-linker length while holding all other variables constant has only minor effects on τ_1 and T_{gel}, because the average size of the cross-links is not significantly affected by the cross-linker length. These results at least establish the plausibility of the hypothesis that τ_1 is determined by the average lifetime of a

P2VP↔PVPh association, which is directly related to the number of hydrogen bonds involved. Estimating the anticipated G_N by assuming every midblock is elastically effective reveals the inadequacy of simple rubber elasticity theory in describing entangled gel systems. Combined effects from triblock molecular weight, steric constraints, and especially stoichiometry of phenol and pyridine units contribute to a significant variation in experimental G_N. In conclusion, we envision the most straightforward molecular description of this system that is consistent with our results is an entangled supramolecular polymer network formed by hydrogen bonding between the endblocks of a P2VP–PEO–P2VP triblock copolymer and aggregates of intermolecularly hydrogen-bonded PVPh cross-linkers, in which stress relaxation is due to P2VP block detachment from associated cross-links through simultaneous breaking of all hydrogen bonds involved.

3.5 References

(1) Noro, A.; Matsushita, Y.; Lodge, T. P. *Macromolecules* **2008,** *41*, 5839–5844.

(2) Noro, A.; Matsushita, Y.; Lodge, T. P. *Macromolecules* **2009,** *42*, 5802–5810.

(3) Ozair, S. N. Ph.D. Dissertation, University of Minnesota, 2009.

(4) Zeroni, I.; Ozair, S.; Lodge, T. P. *Macromolecules* **2008,** *41*, 5033–5041.

(5) Almdal, K.; Dyre, J.; Hvidt, S.; Kramer, O. *Polym. Gels Networks* **1993,** *1*, 5–17.

(6) Ferry, J. D. *Viscoelastic Properties of Polymers,* 3rd ed.; John Wiley & Sons: New York, 1980.

(7) Raspaud, E.; Lairez, D.; Adam, M.; Carton, J.-P. *Macromolecules* **1994,** *27*, 2956–2964.

(8) Raspaud, E.; Lairez, D.; Adam, M.; Carton, J.-P. *Macromolecules* **1996,** *29*, 1269–1277.

(9) Inomata, K.; Nakanishi, D.; Banno, A.; Nakanishi, E.; Abe, Y.; Kurihara, R.; Fujimoto, K.; Nose, T. *Polymer* **2003,** *44*, 5303–5310.

(10) Drzal, P. L.; Shull, K. R. *Macromolecules* **2003,** *36*, 2000–2008.

(11) Seitz, M. E.; Burghardt, W. R.; Faber, K. T.; Shull, K. R. *Macromolecules* **2007,** *40*, 1218–1226.

(12) Bras, R. E.; Shull, K. R. *Macromolecules* **2009,** *42*, 8513–8520.

(13) He, Y.; Boswell, P. G.; Buhlmann, P.; Lodge, T. P. *J. Phys. Chem. B* **2007,** *111*, 4645–4652.

(14) He, Y.; Lodge, T. P. *Macromolecules* **2008,** *41*, 167–174.

(15) Zhang, S.; Lee, K. H.; Frisbie, C. D.; Lodge, T. P. *Macromolecules* **2011,** *44*, 940–949.

(16) Halperin, A.; Alexander, S. *Macromolecules* **1989,** *22*, 2403–2412.

(17) Yokoyama, H.; Kramer, E. J. *Macromolecules* **1998,** *31*, 7871–7876.

(18) Cavicchi, K. A.; Lodge, T. P. *Macromolecules* **2003,** *36*, 7158–7164.

(19) Choi, S.-H.; Lodge, T. P.; Bates, F. S. *Phys. Rev. Lett.* **2010,** *104*, 047802.

(20) Choi, S.-H.; Lodge, T. P.; Bates, F. S. *Macromolecules* **2011,** *44*, 3594–3604.

(21) Tanaka, F.; Edwards, S. F. *Macromolecules* **1992,** *25*, 1516–1523.

(22) Nair, K. P.; Breedveld, V.; Weck, M. *Macromolecules* **2008,** *41*, 3429–3438.

(23) Noro, A.; Hayashi, M.; Ohshika, A.; Matsushita, Y. *Soft Matter* **2011,** *7*, 1667–1670.

(24) Suzuki, T.; Shinkai, S.; Sada, K. *Adv. Mater.* **2006,** *18*, 1043–1046.

(25) Sijbesma, R. P.; Beijer, F. H.; Brunsveld, L.; Folmer, B. J. B.; Hirschberg, J. H. K. K.; Lange, R. F. M; Lowe, J. K. L.; Meijer, E. W. *Science* **1997,** *278*, 1601–1604.

(26) Hirschberg, J. H. K. K.; Beijer, F. H.; van Aert, H. A.; Magusin, P. C. M. M.; Sijbesma, R. P.; Meijer, E. W. *Macromolecules* **1999,** *32*, 2696–2705.

(27) Lange, R. F. M.; van Gurp, M.; Meijer, E. W. *J. Polym. Sci., Part A: Polym. Chem.* **1999,** *37*, 3657–3670.

(28) Folmer, B. J. B.; Sijbesma, R. P.; Versteegen, R. M.; van der Rijt, J. A. J.; Meijer, E. W. *Adv. Matter.* **2000,** *12*, 874–878.

(29) Müller, M.; Dardin, A.; Seidel, U.; Balsamo, V.; Iván, B.; Spiess, H. W.; Stadler, R. *Macromolecules* **1996,** *29*, 2577–2583.

(30) Yamauchi, K.; Lizotte, J. R.; Long, T. E. *Macromolecules* **2003,** *36*, 1083–1088.

(31) Montarnal, D.; Tournilhac, F.; Hidalgo, M.; Couturier, J.-L.; Leibler, L. *J. Am. Chem. Soc.* **2009,** *131*, 7966–7967.

(32) Nair, K. P.; Breedveld, V.; Weck, M. *Soft Matter* **2011,** *7*, 553–559.

(33) Nair, K. P.; Breedveld, V.; Weck, M. *Macromolecules* **2011,** *44*, 3346–3357.

(34) Feldman, K. E.; Kade, M. J.; Meijer, E. W.; Hawker, C. J.; Kramer, E. J. *Macromolecules* **2009,** *42*, 9072–9081.

Chapter 4

Mechanical Properties Modulated by Stoichiometry of Complementary Hydrogen Bonding Units

4.1 Introduction

Hydrogen-bonded polymeric networks can be classified broadly into two categories depending on whether the hydrogen bonding recognition motifs are self-complementary or hetero-complementary. In self-complementary polymeric networks, intermolecular cross-linking results from the intrinsic tendency for self-association (*i.e.*, dimerization) of the hydrogen bonding recognition units covalently attached to the polymer backbone. As a result, these systems are inherently cross-linked and do not require the addition of external cross-linking agents. For example, Stadler and coworkers studied the structure and junction dynamics of reversible polymer network through intermolecular hydrogen bonding in telechelic polyisobutylene end-functionalized by 4-urazoylbenzoic acid groups.[1] Sijbesma *et al.* developed synthetically easily accessible 2-ureido-4[1*H*]-pyrimidinone (UPy) derivatives, which strongly dimerize through a quadruple hydrogen bond array.[2] It has further been demonstrated that the enhanced specificity and strength of UPy derivatives through cooperative multiple hydrogen bonds enable more precise design of hydrogen-bonded polymer networks.[3,4] However, while the self-complementary strategy simplifies the synthesis to just one molecule and is highly successful in controlling the network structure, a crucial limitation of these systems is that they are

always cross-linked at ambient temperature and lack the flexibility to modulate the strength and degree of cross-linking.

The second category of hydrogen-bonded polymeric networks requires the addition of external cross-linking agents to achieve cross-linking. Because the hydrogen bonding functional groups attached to the polymer backbone do not undergo self-association and therefore cannot achieve effective cross-linking, an external cross-linking agent has to be added. One of the advantages of these two-component systems is the flexibility to tailor the macroscopic network properties through subtle modifications in the chemistry of the cross-linking agent. For example, Nair *et al.* have designed systems in which the network microstructure can be modulated by varying the molecular architecture of the cross-linking agents, leading to materials with highly tunable rheological properties from the same polymer backbone functionalized by cyanuric acid functional groups.[5,6] They found that the intrinsically weak triple cyanuric acid–2,4-diaminotriazine hydrogen bonding recognition motif produced viscoelastic gels, while the intrinsically strong sextuple cyanuric acid–Hamilton wedge motif led to high-viscosity fluids. This illustrates the importance of the molecular architecture of the cross-linking agent in determining the network structure. They have further demonstrated that the extent of cross-linking can be modulated by varying the concentration of the cross-linking agent added, leading to materials with highly tunable mechanical properties. They found that the modulus initially increased with the concentration of the cross-linking agent, and eventually reached a plateau at high concentrations.

In this chapter, we further test the hypothesis that the amount of cross-linker added controls the network microstructure, which ultimately determines the macroscopic mechanical properties of these hydrogen-bonded supramolecular ion gels. We demonstrate that low-viscosity solutions of the parent triblock copolymer could be changed into thermoreversible viscoelastic gels with tunable modulus by simply varying the concentration of the PVPh cross-linker. Interestingly, the modulus goes through a maximum instead of increasing monotonically with the cross-linker concentration. As a result, these materials offer a high degree of control over the final mechanical properties, and the underlying strategy shall be useful in designing tailor-made materials.

4.2 Experimental Section

4.2.1 Polymer Synthesis and Characterization

A P2VP–PEO–P2VP triblock copolymer was synthesized via reversible addition–fragmentation chain transfer (RAFT) polymerization, as described in Chapter 2. The number-average molecular weights (M_n) for the P2VP and PEO blocks are 2 and 35 kg/mol, respectively. The triblock has an overall dispersity ($Đ$) of 1.06 and is denoted as VOV(2-35-2). A PVPh homopolymer was also synthesized by RAFT polymerization, as described in Chapter 2. It has a molecular weight of 7 kg/mol and a dispersity of 1.09, and is denoted as PVPh-7.

4.2.2 Supramolecular Ion Gel Preparation

All supramolecular ion gels were prepared by mixing weighed amounts of the respective polymers (triblock and cross-linker) and ionic liquid in a THF cosolvent. After these ternary mixtures were stirred for a few hours, most of the cosolvent was removed under a flow of nitrogen gas for 1 day followed by drying in a vacuum oven at 110 ℃ for 1 day to completely remove the cosolvent. All samples were stored in a vacuum desiccator to minimize water absorption.

4.2.3 Rheology

Rheological experiments were performed on an Advanced Rheometric Expansion System (ARES) rheometer (TA instruments) with parallel plate geometry. Temperature was always controlled within ±0.1 ℃ of the set value via a convection oven using dry nitrogen gas. In order to minimize the effect of air bubbles, each sample was annealed above its gel temperature while shearing at a moderate shear rate for 10–15 minutes before any further experiments were carried out, allowing whatever small air bubbles to flow to the center of the geometry. At each temperature, the gap was adjusted to compensate for the thermal expansion of the stainless steel plates and the sample loading was checked visually to ensure a flat edge. The actual gap was calculated based on the thermal expansion coefficient of the stainless steel plates (2.4 μm/K) assuming linear expansion with temperature. Samples were allowed to equilibrate for 15 minutes at each temperature and then a dynamic strain sweep was performed to identify the linear viscoelastic regime. Dynamic temperature ramps and dynamic frequency sweeps were performed in small-amplitude oscillatory shear mode.

4.2.4 Small-Angle X-ray Scattering

Small-angle X-ray scattering (SAXS) experiments were performed at the Dupont–Northwestern–Dow Collaborative Access Team (DND–CAT) beamline 5-ID-D at the Advance Photon Source (APS), Argonne National Laboratory (ANL). Samples were sealed into hermetic differential scanning calorimetry (DSC) pans, which were then mounted to a washer with Kapton tapes. Two-dimensional SAXS data were collected and then azimuthally integrated to generate one-dimensional data presented as intensity (I) vs scattering vector ($q = 4\pi\sin(\theta/2)/\lambda$) where θ is the scattering angle and λ is the X-ray wavelength.

4.3 Results and Discussion

In order to study the effect of stoichiometry of complementary hydrogen bonding donors and acceptors, we investigated the cross-linking profile of our system by varying the concentration of the cross-linker over the range of 0–6% while holding that of the triblock constant at 10%. The resulting materials were characterized quantitatively using rheology, but a telling qualitative picture can be obtained from initial visual observations. While solutions with 0 and 0.5% cross-linker yielded freely flowing low-viscosity fluids, all the rest resulted in viscoelastic gels. The fact that the pure triblock does not gel in the ionic liquid excludes any appreciable effect due to the self-assembly of the triblock in the ionic liquid. The addition of 0.5% cross-linker was not sufficient to induce gelation, which simply reflects the existence of a minimum degree of cross-linking required for the

formation of a continuous percolating network. The rightmost column of Table 4.1 quantifies the mechanical properties of these polymer networks in terms of the magnitude of the elastic modulus. Although this representation does not provide the complete rheological features of the samples, it effectively highlights the marked differences between samples, which are the primary focus of this chapter.

Table 4.1 Characteristics of Supramolecular Ion Gels

Triblock	Cross-linker	X_{ph}/X_{py} [a]	T_{gel} [b] (℃)	G_N [c] (Pa)
10% VOV(2-35-2)	0% PVPh-7	100/0	–	–
10% VOV(2-35-2)	0.5% PVPh-7	100/42	–	–
10% VOV(2-35-2)	1% PVPh-7	100/85	118.5	2500
10% VOV(2-35-2)	1.5% PVPh-7	100/128	123	9500
10% VOV(2-35-2)	2% PVPh-7	100/170	127.5	14000
10% VOV(2-35-2)	3% PVPh-7	100/225	124	14200
10% VOV(2-35-2)	4% PVPh-7	100/340	121	10500
10% VOV(2-35-2)	6% PVPh-7	100/510	110	4500

[a] Molar ratio of phenol/pyridine units. [b] T_{gel} determined from the crossover temperature at which $G' = G''$ in Figure 4.1. [c] Plateau modulus.

4.3.1 Rheological Characterization

In order to investigate the effect of the amount of cross-linker on network formation, the resulting materials were characterized quantitatively using rheology. Figure 4.1 illustrates that the rheological response is a strong function of temperature. At low temperatures such as 30 ℃, the network structure apparently becomes frozen, forming an elastic, macromolecular network with extraordinarily large relaxation times. As the temperature is increased, the response of the network changes from predominantly elastic to viscoelastic, with G'' increasing relative to G'. At these intermediate temperatures, stress relaxation is accelerated and relaxation times become shorter. As the temperature is further increased above the gelation temperature, hydrogen-bonded cross-links are created and annihilated rapidly, giving rise to a freely flowing, viscous liquid.

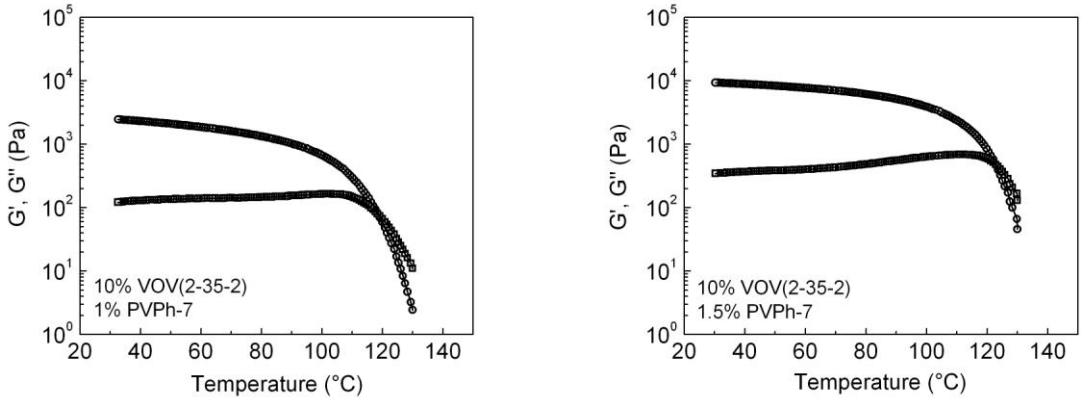

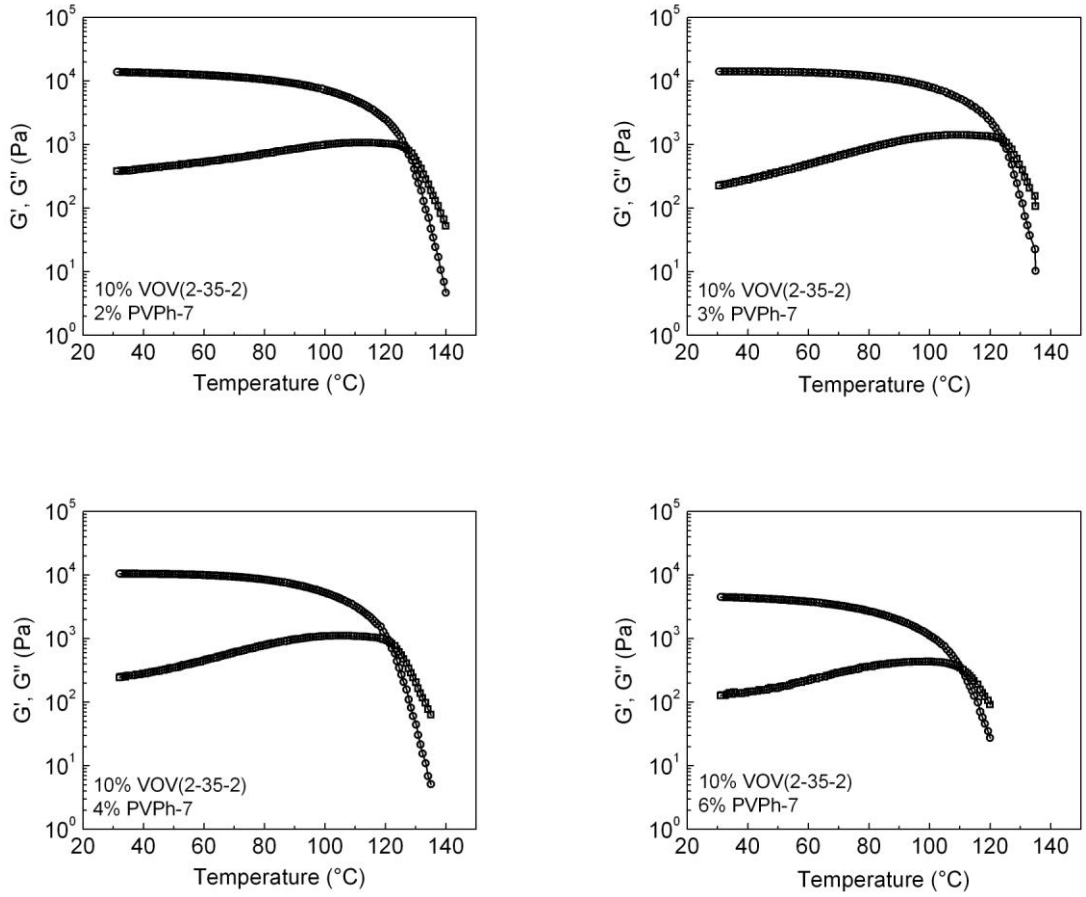

Figure 4.1 Temperature dependence of dynamic storage modulus G' (○) and loss modulus G'' (□) showing the effect of varying the cross-linker concentration. All other variables are held constant (see the lower left-hand corner of each plot for details). All measurements were performed at a strain amplitude of 3%, an angular frequency of 0.3 rad/s, and a temperature ramp rate of 1 ℃/min.

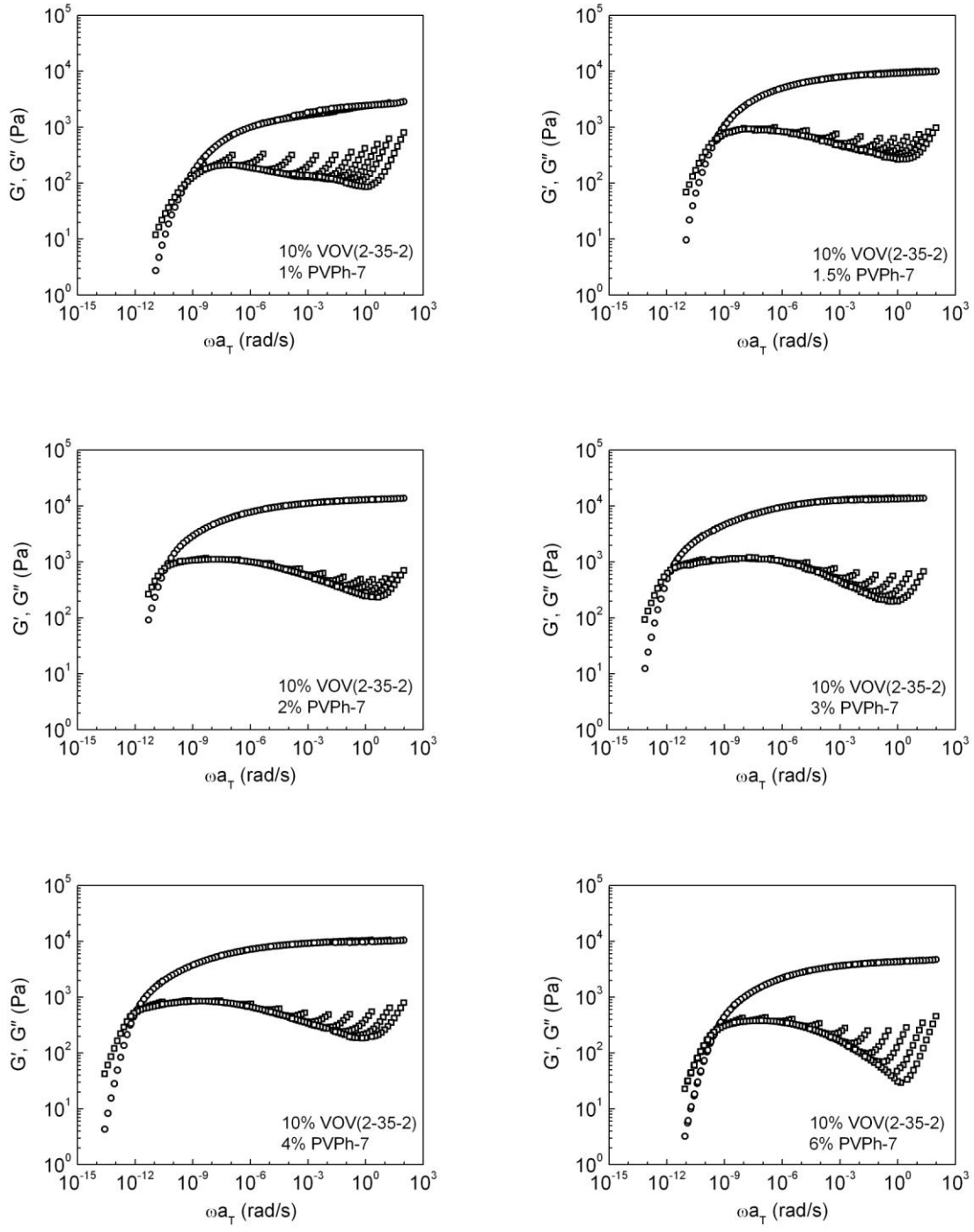

Figure 4.2 tTS master curves of *G′* (○) and *G″* (□) referenced to 30 ℃. All other variables are held constant (see the lower right-hand corner of each plot for details).

The time-temperature superposition (tTS) principle was applied to construct master curves by shifting the isothermal dynamic frequency sweep data collected at various temperatures along the frequency axis. The loss tangent (tan δ) spectra were shifted horizontally, and then the same shift factors were applied to G' and G'' to obtain master curves, as shown in Figure 4.2. The fact that tTS is applicable suggests that the underlying origin of viscoelasticity in these gels is not evolving over the temperature range investigated. At low reduced frequencies, all samples behave as viscoelastic liquids, as revealed by the terminal relaxation behavior where G' and G'' scale with second and first powers of frequency, respectively. At high reduced frequencies, G' exhibits a pronounced plateau extending over 10 decades in reduced frequency and G'' is considerably smaller than G' in the plateau region, which are the rheological signatures that characterize a gel. The appearance of systematic upturns in G'' at the high-frequency end of the data for each temperature is attributed to the relaxation of the PEO network strands, which obviously possesses distinct temperature dependence compared to gel relaxation. Figure 4.3 shows the temperature dependences of the resulting shift factors (a_T), which denote the ratio of any relaxation time at one temperature to its value at the chosen reference temperature. They show similar general trends for the various samples, such as a strong temperature dependence and saturation at low temperatures. The strong temperature dependence is ascribed to the formation of multiple hydrogen bonds on a single P2VP↔PVPh association, while the saturation at low temperatures simply reflects the formation of the maximum number of the hydrogen bonds.

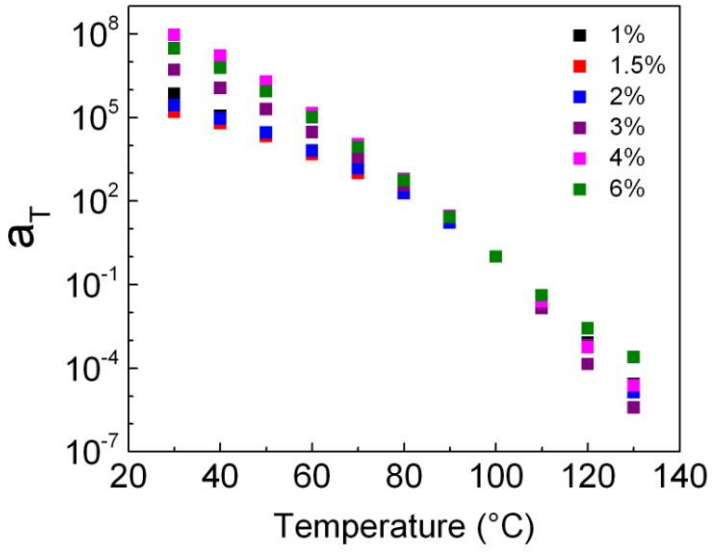

Figure 4.3 Temperature dependence of the tTS shift factors used in generating the master curves of Figure 4.2. The reference temperature is 100 ℃.

4.3.2 Small-Angle X-ray Scattering

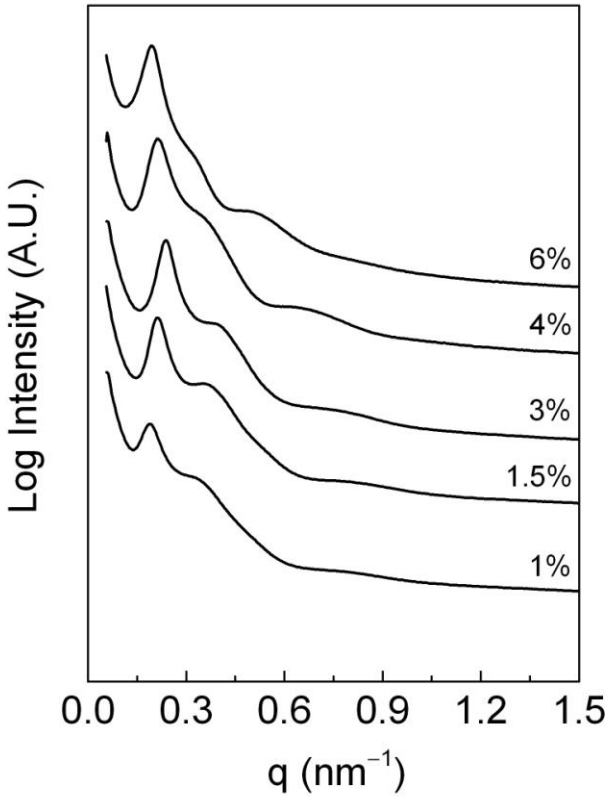

Figure 4.4 Room temperature synchrotron SAXS data showing the effect of varying the cross-linker concentration.

Small-angle X-ray scattering (SAXS) experiments were performed to assess the gel structures, as shown in Figure 4.4. The characteristic features of the scattering patterns include two maxima at low-*q* values, a strong one and a weak one, followed by a steep decrease in intensity, and a broad maximum in the tail of the small-angle region.

Scattering contrast in these gels arises from the electron density difference between the dense hydrogen-bonded network microdomains and the well-solvated network strands.

For a quantitative analysis, the interdomain distance (D), aggregation number (N_{agg}), and functionality of cross-links (X) can be extracted from the scattering profiles and are listed in Table 4.2. The principal lattice spacing (d_{110}) is estimated by presuming the location of the primary scattering peak (q_1) is related to the Bragg spacing for cross-links with a body-centered cubic packing, $d_{110} = 2\pi/q_1$. This gives a lattice constant of $a = \sqrt{2}d_{110}$. The interdomain distance (D) between the centers of two nearest cross-links can be estimated by

$$D = \frac{\sqrt{3}}{2} a = \frac{\sqrt{6}}{2} \frac{2\pi}{q_1} \tag{4.1}$$

The aggregation number (N_{agg}), defined here as the number of PVPh chains associated in a cross-link, can be estimated by

$$N_{agg} = \frac{c_{PVPh} N_A}{2M_{PVPh}} \left(\frac{2\sqrt{2}\pi}{q_1} \right)^3 \tag{4.2}$$

The functionality of the cross-link (X), defined as the number of network strands that are connected, can be estimated by

$$X = \frac{c_{VOV} N_A}{2M_{VOV}} \left(\frac{2\sqrt{2}\pi}{q_1} \right)^3 \tag{4.3}$$

Table 4.2 Extracted Parameters from SAXS Profiles

PVPh content (wt%)	d_{110} (nm)	D (nm)	N_{agg}	X
1	33.0	40.4	62	110
1.5	29.4	36.0	66	80
3	26.5	32.5	96	60
4	29.4	36.0	173	80
6	32.4	39.7	345	100

4.3.3 Mechanical Properties Modulated by Stoichiometry

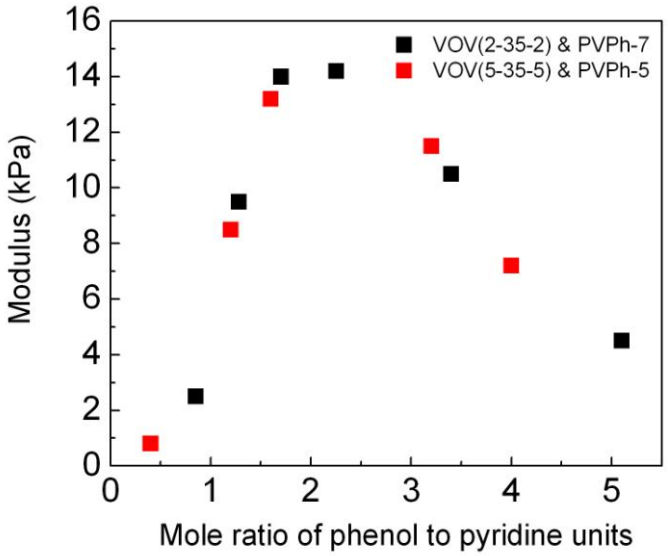

Figure 4.5 Dependence of plateau modulus on cross-linker concentration. The triblock concentration is held constant at 10%.

Figure 4.5 reveals an interesting dependence of the elastic modulus on the cross-linker concentration at constant triblock concentration; G_N goes through a maximum instead of increasing monotonically with the cross-linker concentration. For example, in VOV(2-35-2)/PVPh-7 systems, upon increasing the cross-linker concentration from 1% to 3%, G_N increases from 2500 Pa to 14000 Pa. However, further addition of cross-linker results in a dramatic decrease in G_N. We speculate that this distinct difference in modulus of networks formed from the same parent triblock copolymer backbone can be explained on the basis of differences in hypothesized network microstructures, which are schematically illustrated in Figure 4.6. At low cross-linker concentrations where the number of pyridine units is much greater than phenol units, the cross-links are not able to accommodate all the P2VP blocks around them due to the limited number of phenol units, leaving a significant amount of dynamic chains. This will be further explored in Chapter 6. At moderate cross-linker concentrations where the amounts of pyridine and phenol units are present under certain stoichiometric balance, the highest modulus is achieved. The decrease at high cross-linker concentration is more surprising; G_N would be expected to exhibit a plateau at high cross-linker concentrations, as reported in some systems.[5,6] The mechanism that is responsible for the dramatic drop in G_N at high cross-linker concentrations was previously ascribed to the formation of monofunctional and difunctional cross-links. However, values of the functionality of cross-links listed in Table 4.2 actually exclude the possibility of forming monofunctional and difunctional cross-links. We now propose that the formation of looping midblocks is responsible for the dramatic drop in modulus at high cross-linker concentrations. An increase in the

aggregation number gives rise to larger cross-links which favors loop formation. Moreover, an increase in average domain spacing between cross-links requires stronger stretching of midblocks to adopt bridging conformations, and therefore loop formation is favored. It is also noteworthy that the aggregation number's dependence on cross-linker concentration starts to increase sharply around 3% cross-linker, below which the aggregation number is relatively insensitive to changes in cross-linker concentration. Note that 3% is the cross-linker concentration where pyridine and phenol units are present under appropriate stoichiometric balance and the highest modulus is achieved. This suggests that as cross-linker concentration increases progressively, the new cross-linker chains are primarily accommodated by creating more cross-links at low cross-linker concentrations and by increasing the aggregation number at high cross-linker concentrations, with the boundary being a cross-linker concentration where pyridine and phenol units are present under appropriate stoichiometric balance and the highest modulus is achieved.

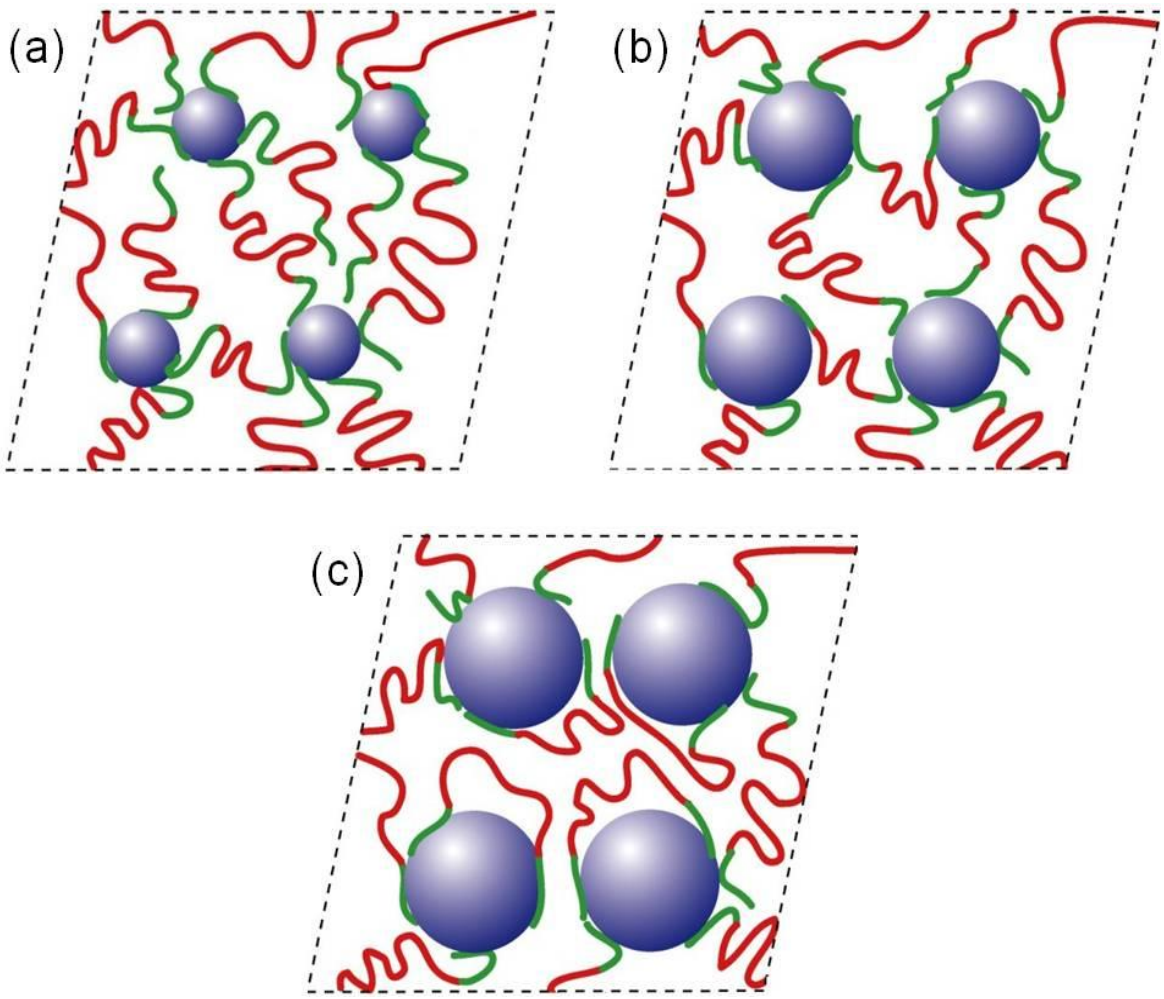

Figure 4.6 Cartoon illustration of the stoichiometric effect on the microstructure of the hydrogen-bonded supramolecular polymer network: (a) inadequate amount of cross-linker leads to dynamic chains; (b) stoichiometric balance; (c) excess amount of cross-linker leads to the formation of loops.

4.3.4 Competitive Hydrogen Bonding from Component Polymers

In addition to the hydrogen bonding between P2VP and PVPh, PEO is also a weak hydrogen bonding acceptor and therefore has the potential to form hydrogen bonds with PVPh. Miscible blends of P2VP/PVPh and PEO/PVPh have been studied by different groups and it is known that hydrogen bonding is the driving force for their miscibility.[8–12] Then the question arises, what is the contribution of the hydrogen bonding between the PEO midblock and PVPh cross-linker? In all the described systems, tTS works over the whole temperature range, suggesting the negligibility of hydrogen bonding between P2VP and PEO; otherwise, there should be multiple relaxation processes contributing, resulting in the failure of the tTS due to distinct temperature dependence. However, if the amount of phenol is in huge excess compared with that of pyridine units, the hydrogen bonding between PEO and PVPh starts to play a role. While adding 6% cross-linker into 10% triblock solution results in a clear, homogeneous gel, further increasing the amount of cross-linker to 10% results in clear phase separation. This turbidity presumably arises from the hydrogen bonding between PEO and PVPh. This is consistent with the fact that although both PEO and PVPh initially dissolve in the ionic liquid and clear solutions are obtained, their mixture is co-precipitated from the ionic liquid, resulting in a cloudy solution. Upon heating the cloudy solution, it becomes clear at 80 ℃, suggesting the breakup of hydrogen bonding. This relatively low temperature where hydrogen bonding between PEO and PVPh dissociates confirms that it is relatively weak.

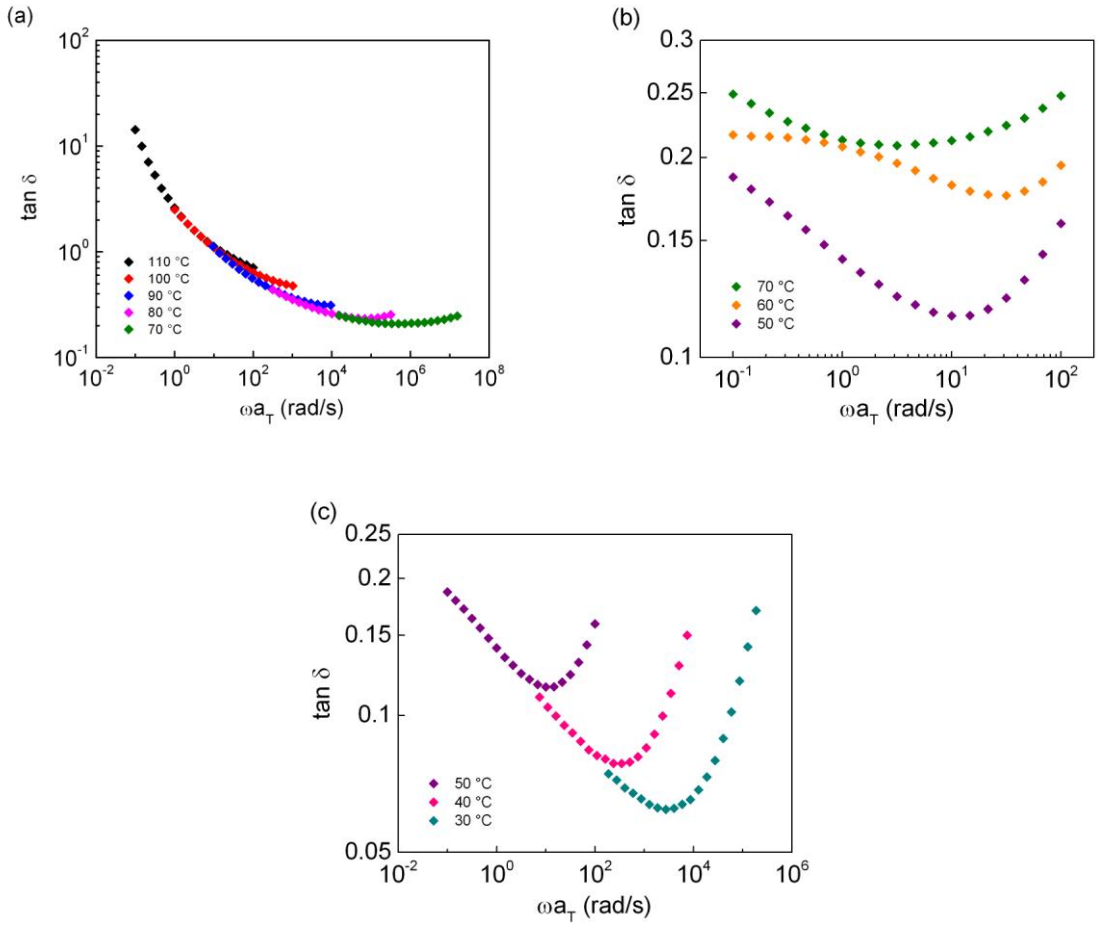

Figure 4.7 The applicability of tTS for a sample with 10% VOV(3-35-3) and 10% PVPh-5. Tan δ curves are shifted horizontally along the frequency axis: (a) tTS applicable over the temperature range of 110–70 ℃; (b) tTS not applicable over the temperature range of 70–50 ℃; (c) tTS applicable over the temperature range of 50–30 ℃.

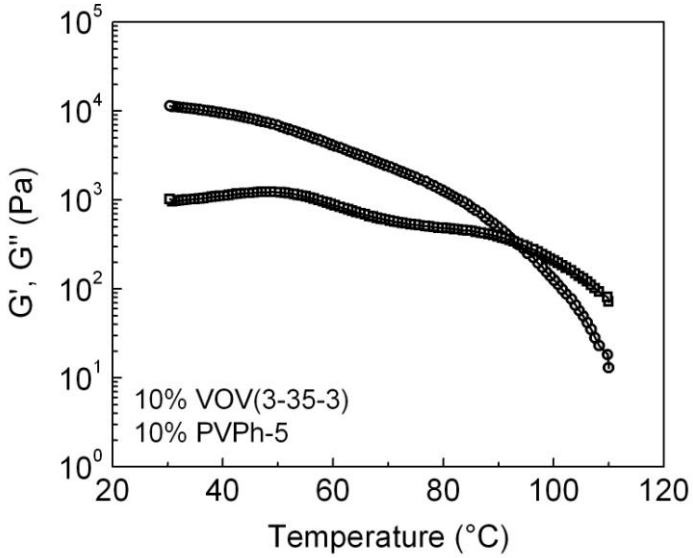

Figure 4.8 Temperature dependence of G' (○) and G'' (□) for a supramolecular ion gel containing 10% VOV(3-35-3) and 10% PVPh-5.

Figure 4.7 shows the applicability of tTS for a sample with 10 wt% VOV(3-35-3) and 10 wt% PVPh-5. Tan δ curves at 50, 60, and 70 ℃ unambiguously shows that tTS is not applicable over this temperature range. At high temperatures, the relaxation process is dominated by the dissociation of phenol–pyridine hydrogen bonds. At low temperatures, the relaxation process is dominated by the dissociation of phenol–ether hydrogen bonds. In the intermediate temperature range (70–50 ℃), tTS fails because both relaxations are evident. The solubility test described earlier in this section confirms that phenol–ether hydrogen bonds completely break above 80 ℃, which is in excellent consistency with the tTS applicability temperature range. Furthermore, values of a_T are unusually large at low temperatures, for example, a_T = 75 at 40 ℃ with a reference temperature of 50 ℃. In all

previous systems, a_T is less than 10 at low temperature, suggesting a different relaxation process.

Overall, our important conclusion is that phenol–ether hydrogen bonds are negligible at low molar ratios of phenol/pyridine units (smaller than 500/100) but become significant at high molar ratios of phenol/pyridine units (greater than 600/100).

4.3.5 Participation in Hydrogen Bonding from Ionic Liquids

The role of ionic liquids in this supramolecular system is at least twofold. First, their substantially wide liquidus temperature range without evaporation and chemical degradation enables an elaborate exploration of the fundamental behavior of this system. Second, ionic liquids clearly form hydrogen bonding with the component polymers. Concurrently, it is possible to modulate the ion structure such that the solvent can compete to a greater or lesser extent with the interpolymer hydrogen bonding that is responsible for the formation of the polymer network. This flexibility is not readily accessible in water without adding further ingredients. Here, we replace the most acidic proton of the imidazole ring (in the C2 position) with a methyl group to produce 1-ethyl-2,3-methylimidazolium bis(trifluoromethylsulfonyl)amide ([EMMIM][TFSA]), with the expectation that hydrogen bonding between the solvent and component polymers will be depressed while enhancing the interpolymer hydrogen bonding.

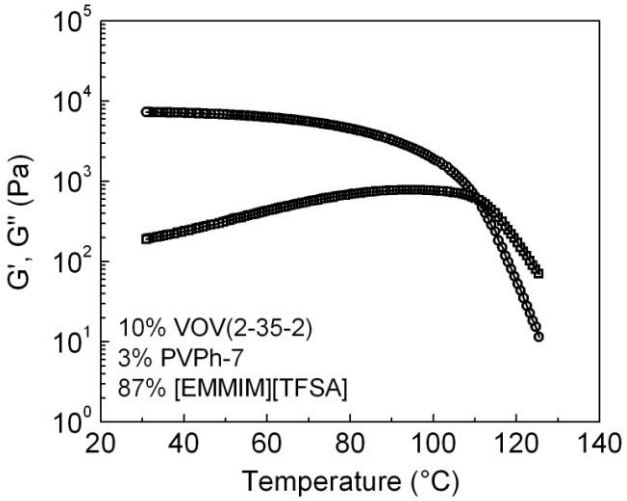

Figure 4.9 Temperature dependence of G' (○) and G'' (□) for an ion gel in which ionic liquid is [EMMIM][TFSA].

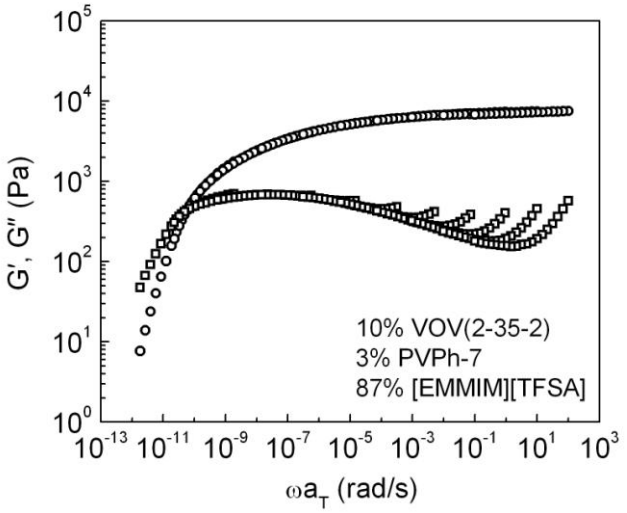

Figure 4.10 tTS master curve of G' (○) and G'' (□) referenced to 30 ℃ for an ion gel in which ionic liquid is [EMMIM][TFSA].

As can be seen from Figures 4.9 and 4.10, the general rheological behavior is very similar to [EMIM][TFSA]-based gels. Compared to the [EMIM][TFSA]-based gel with the same polymer, the [EMMIM][TFSA]-based gel has a lower T_{gel} (110.5 ℃) than the [EMIM][TFSA]-based gel (124 ℃), which might be explained by smaller activation energy to break a phenol–pyridine hydrogen bond in [EMMIM][TFSA] than in [EMIM][TFSA]. Furthermore, the [EMMIM][TFSA]-based gel has a lower modulus (9000 Pa) than the [EMIM][TFSA]-based gel (14000 Pa). As will be described in Chapter 6, multiple hydrogen bonds are required on a given P2VP↔PVPh association to generate elastically effective chains, and the specific values depend on the lifetime of a single hydrogen bond. Since the hydrogen bond in [EMMIM][TFSA] has a lower dissociation energy than in [EMIM][TFSA], it should have a smaller lifetime and therefore more hydrogen bonds are required on a P2VP block to generate elastically effective chains. Given that the P2VP block is not very long (2 kg/mol), the lower modulus of the [EMIM][TFSA]-based gel might come from the inadequate number of hydrogen bonds on a certain fraction of P2VP blocks, resulting in a significant amount of dynamic chains. Overall, the applicability of different ionic liquids confirms the versatility of this supramolecular ion gel system.

4.4 Conclusions

In this chapter, we have demonstrated that low-viscosity solutions of the parent triblock copolymer could be changed into thermally reversible highly viscous liquids or

elastic gels with tunable modulus by simply varying the amount of cross-linker added. It is hypothesized that the microstructure is essential in determining the macroscopic mechanical properties of these hydrogen-bonded polymer networks. For small cross-linker concentrations, the hydrogen bonding between the PEO midblock and PVPh cross-linker is negligible, implied by the applicability of tTS over the whole temperature range investigated. For high cross-linker concentrations, the hydrogen bonding between PEO midblock and PVPh cross-linker becomes significant, as suggested by the visual phase separation and failure of tTS over the intermediate temperature range. The use of another ionic liquid which competes with the interpolymer hydrogen bonding to a lesser extent than [EMIM][TFSA] suggests the versatility of this supramolecular ion gel system.

4.5 References

(1) Müller, M.; Dardin, A.; Seidel, U.; Balsamo, V.; Iván, B.; Spiess, H. W.; Stadler, R. *Macromolecules* **1996,** *29,* 2577–2583.

(2) Beijer, F. H.; Sijbesma, R. P.; Kooijman, H.; Spek, A. L.; Meijer, E. W. *J. Am. Chem. Soc.* **1998,** *120,* 6761–6769.

(3) Sijbesma, R. P.; Beijer, F. H.; Brunsveld, L.; Folmer, B. J. B.; Hirschberg, J. H. K. K.; Lange, R. F. M.; Lowe, J. K. L.; Meijer, E. W. *Science* **1997,** *278,* 1601–1604.

(4) Lange, R. F. M.; van Gurp, M.; Meijer, E. W. *J. Polym. Sci., Part A: Polym. Chem.* **1999,** *37,* 3657−3670.

(5) Nair, K. P.; Breedveld, V.; Weck, M. *Macromolecules* **2008,** *41,* 3429–3438.

(6) Nair, K. P.; Breedveld, V.; Weck, M. *Soft Matter* **2011,** *7*, 553–559.

(7) Noro, A.; Matsushita, Y.; Lodge, T. P. *Macromolecules* **2009,** *42*, 5802–5810.

(8) Dai, J.; Goh, S. H.; Lee, S. Y.; Siow, K. S. *Polym. J.* **1994,** *26*, 905–911.

(9) Zeng, X.-M.; Chan, C.-M.; Weng, L.-T.; Li, L. *Polymer* **2000,** *41*, 8321–8329.

(10) Cai, H.; Ait-Kadi, A.; Brisson, J. *Polymer* **2003,** *44*, 1481–1489.

(11) Lee, L.-T.; Woo, E. M.; Hou, S. S.; Förster, S. *Polymer* **2006,** *47*, 8350–8359.

(12) Salim, N. V.; Hameed, N.; Guo, Q. *J. Polym. Sci., Part B: Polym. Phys.* **2009,** *47*, 1894–1905.

Chapter 5

A High-Temperature Hexagonally Ordered Morphology of the Hydrogen-Bonded Microdomains

5.1 Introduction

Thermoplastic elastomer gels, consisting of symmetric ABA triblock copolymers immersed in a midblock-selective solvent, are ubiquitous in a wide range of technologies, including pressure-sensitive adhesives, substrates for microfluidic systems, thickening agents in surface coatings and cosmetics, oil recovery, wastewater treatment, and tissue engineering.[1] Complementary experimental and theoretical efforts have been devoted to enriching the current understanding of their phase behavior, morphology, and rheological properties.[2–12] The insoluble A-blocks self-assemble into hard microdomains that are bridged by the flexible and well-solvated B-blocks, giving rise to a micellar network structure. Typically the microdomains are randomly distributed within the solvated midblock matrix in as-prepared systems.[13] However, by appropriate selection of the processing conditions, they can rearrange into crystalline-type structures on a mesoscopic length scale,[14–21] which is favored at high volume fractions of the microdomains where correlations among microdomains are pronounced, and at high temperatures where chain exchange can take place. These structures may be cubic spheres, hexagonal cylinders, or lamellar disks, where the equilibrium morphology is determined by the free energy balance between interfacial tension and chain stretching entropy.[1] The disordering and

eventual dissolution of the microdomains upon heating is macroscopically observed by a solid–liquid transition.

The utilization of intermolecular non-covalent interactions,[22] for example, hydrogen bonding,[23–34] metal–ligand coordination,[35,36] and electrostatic interactions,[37,38] to construct reversible alternatives for covalent polymer networks has attracted considerable interest since the pioneering work by Sijbesma *et al.* in 1997,[23] in which trifunctional polymers functionalized by 2-ureido-4[1*H*]-pyrimidinone (UPy) units were shown to assemble through quadruple cooperative hydrogen bonds in an array, yielding reversible polymer networks with strongly temperature-dependent rheological properties and thermodynamically controlled architectures. One of the key challenges is to incorporate highly directional, sufficiently strong, but still reversible interactions to create a robust structure yet with dynamic reversibility. It was recognized from the pioneering work of Sijbesma *et al.* that multiple hydrogen bonds satisfy these requirements combined with synthetic accessibility. Their strength and specificity vary significantly, from weakly complementary pyridine–phenol pairs to extraordinarily strong sextuple hydrogen bonding motifs,[39,40] with association constants ranging from 1 M^{-1} to as high as 10^9 M^{-1}. In addition to self-complementary functionalities such as UPy,[41,42] hetero-complementary units have also been synthesized and incorporated into polymeric networks.[31,32,39,40] While the self-complementary strategy simplifies the synthesis to just one molecule and avoids complications of exact stoichiometry of components, they are always cross-linked and lack the flexibility to tune the macroscopic network properties. On the other hand, the hetero-complementary approach provides opportunities to tailor materials properties

through the design of the cross-linking agent, whereby providing excellent control over the association strength of the cross-links, the degree of cross-linking, and the network microstructure. Hydrogen-bonded supramolecular polymer networks exhibit interesting properties such as enhanced processability, stimuli-responsiveness,[23–38] self-healing,[26] and shape-memory.[43] Furthermore, they are also important for fundamental research of polymer physics, because their "living" nature provides a special condition to test classical theories of polymer physics.[44,45]

Recently, we have developed a thermoreversible supramolecular polymer gel system consisting of a poly(4-vinylpyridine-*b*-ethylene oxide-*b*-4-vinylpyridine) (P4VP–PEO–P4VP) triblock copolymer, a poly(4-vinylphenol) (PVPh) homopolymer, and a room-temperature ionic liquid, 1-ethyl-3-methylimidazolium bis(trifluoromethylsulfonyl)amide ([EMIM][TFSA]). This system exhibits interesting physical properties, such as strongly temperature-dependent rheology and homopolymer clustering in the cross-links. From a practical perspective, the incorporation of ionic liquids into cross-linked polymeric networks imparts fascinating properties that enable their applications in a variety of technologies,[46] including solid polymer electrolytes with high ionic conductivity,[47] high-performance membranes for gas separation technology,[48] high-capacitance dielectric materials for organic thin-film transistors,[49–52] and electroresponsive materials for electromechanical actuators.[53,54] In this chapter, we describe rheological and small-angle X-ray scattering (SAXS) studies which give unique insight into the thermally induced morphological changes in this system. The influence of thermal history on the rheological properties and morphology of such materials is discussed.

5.2 Experimental Section

5.2.1 Polymer Synthesis and Characterization

A P4VP–PEO–P4VP triblock copolymer was synthesized via reversible addition–fragmentation chain transfer (RAFT) polymerization, as described in Chapter 2. The number-average molecular weights (M_n) for the P4VP and PEO blocks are 3 and 35 kg/mol, respectively. The triblock has an overall dispersity ($Đ$) of 1.08. A PVPh homopolymer was previously synthesized by Dr. Ozair via anionic polymerization.[55] It has a molecular weight of 5 kg/mol and a dispersity of 1.04. Their molecular characterization information is summarized in Table 5.1.

Table 5.1 Molecular Characterization of Polymers

Polymers	$M_{n,P4VP}$ (kg/mol)[a]	$M_{n,PEO}$ (kg/mol)[b]	$M_{n,PVPh}$ (kg/mol)[c]	$Đ$[d]
P4VP–PEO–P4VP	3	35		1.08
PVPh			5	1.04

[a] Block M_n determined by ^{1}H NMR spectroscopy. [b] Determined by size exclusion chromatography (SEC) with light scattering detection (the $\partial n/\partial c$ value for PEO/THF is 0.068 mL/g at a laser wavelength of 633 nm. [c] Determined by matrix-assisted laser desorption/ionization (MALDI) mass spectrometry. [d] Determined by SEC.

5.2.2 Rheology

Rheological experiments were conducted on an Advanced Rheometric Expansion System (ARES) with parallel plate geometry (25 mm diameter and *ca.* 1 mm gap). Temperature was precisely controlled to within ±0.1 ℃ of the set value via a convection oven using dry nitrogen gas. Gels were annealed above their respective melting temperatures while shearing at a moderate shear rate for 10–15 min before further experiments were performed. Dynamic temperature ramps were performed both on cooling and heating at a strain amplitude of 3%, an angular frequency of 0.3 rad/s, and a cooling/heating rate of 1 ℃/min. The instrument automatically adjusted the gap during measurement based on the thermal expansion coefficient of the stainless steel plates (2.4 μm/K) assuming linear expansion with temperature.

5.2.3 Small-Angle X-ray Scattering

Small-angle X-ray scattering (SAXS) experiments were performed at the synchrotron facility at the Advanced Photon Source (APS), Argonne National Laboratory. Gels were sealed into hermetic differential scanning calorimetry (DSC) pans, which were either heated and cooled in a Linkam DSC sample holder for high-temperature experiments or mounted in a washer sandwiched between two Kapton layers for room-temperature experiments. An annealing time of 5 min was allowed on the beamline at each temperature. Two-dimensional SAXS patterns were recorded by a Mar-CCD detector, and then azimuthally integrated to generate one-dimensional data presented as intensity (I) versus scattering vector (q). The X-ray wavelength was 0.728 Å and the sample-to-detector distance was 4.626 m.

5.3 Results and Discussion

In this chapter, three supramolecular ion gels were examined by rheology and SAXS. The concentration of the P4VP–PEO–P4VP triblock was varied between 10–30 wt%, and that of the PVPh cross-linker was chosen such that the amounts of the hydrogen bonding donors and acceptors were under a certain stoichiometric balance, as described in Chapter 4. For simplicity, each supramolecular ion gel is denoted as **T-*x*/C-*y***, where ***x*** and ***y*** refer to the weight fraction of the triblock and cross-linker, respectively.

5.3.1 Rheological Characterization

In order to quantitatively investigate the thermal reversibility of the hydrogen-bonded supramolecular ion gels, we carried out dynamic temperature ramps in which the storage modulus (G') and loss modulus (G'') were monitored at a constant frequency and strain amplitude during a cooling–heating cycle, which consisted of first decreasing the temperature from their respective loading temperatures to ambient temperature and then increasing the temperature back to their original loading temperatures, with cooling and heating rates of 1 ℃/min (Figure 5.1). All gels were loaded onto the rheometer *ca.* 10 ℃ higher than their respective melting temperatures, where they flowed and behaved as viscoelastic liquids with $G'' > G'$. Upon subsequent cooling, all materials experienced a sharp transition from viscous liquid-like behavior to elastic gel-like behavior with a well-defined transition temperature termed gel temperature (T_{gel}), which can be determined by the crossover temperature at which $G' = G''$. Wide temperature-independent rubbery plateaus in G' are evident below T_{gel}, indicating the formation of a well-defined network structure which does not evolve appreciably with temperature. This arises from the

extraordinarily large relaxation times due to the high activation energy barrier to break multiple hydrogen bonds simultaneously, which resembles thermoplastic elastomer gels below the glass transition temperature of the micelle core, whereby the network structure is locked in place and no network rearrangement takes place. The recovery of these gels during heating was remarkably different. While **T-10%/C-3%** recovered quantitatively over the entire temperature range, the recovery behavior in **T-20%/C-6%** and **T-30%/C-9%** can be divided into two distinct regions: low-temperature quantitative recovery and high-temperature significant hysteresis. After completion of the cooling–heating cycle, **T-20%/C-6%** and **T-30%/C-9%** exhibited solid-like behavior with $G' > G''$, whereas they were liquid-like with $G'' > G'$ before the start of the cooling–heating cycle. G' entered into a second plateau instead of dropping rapidly. We attempt to elucidate the origin of this high-temperature rheological hysteresis observed in **T-20%/C-6%** and **T-30%/C-9%**.

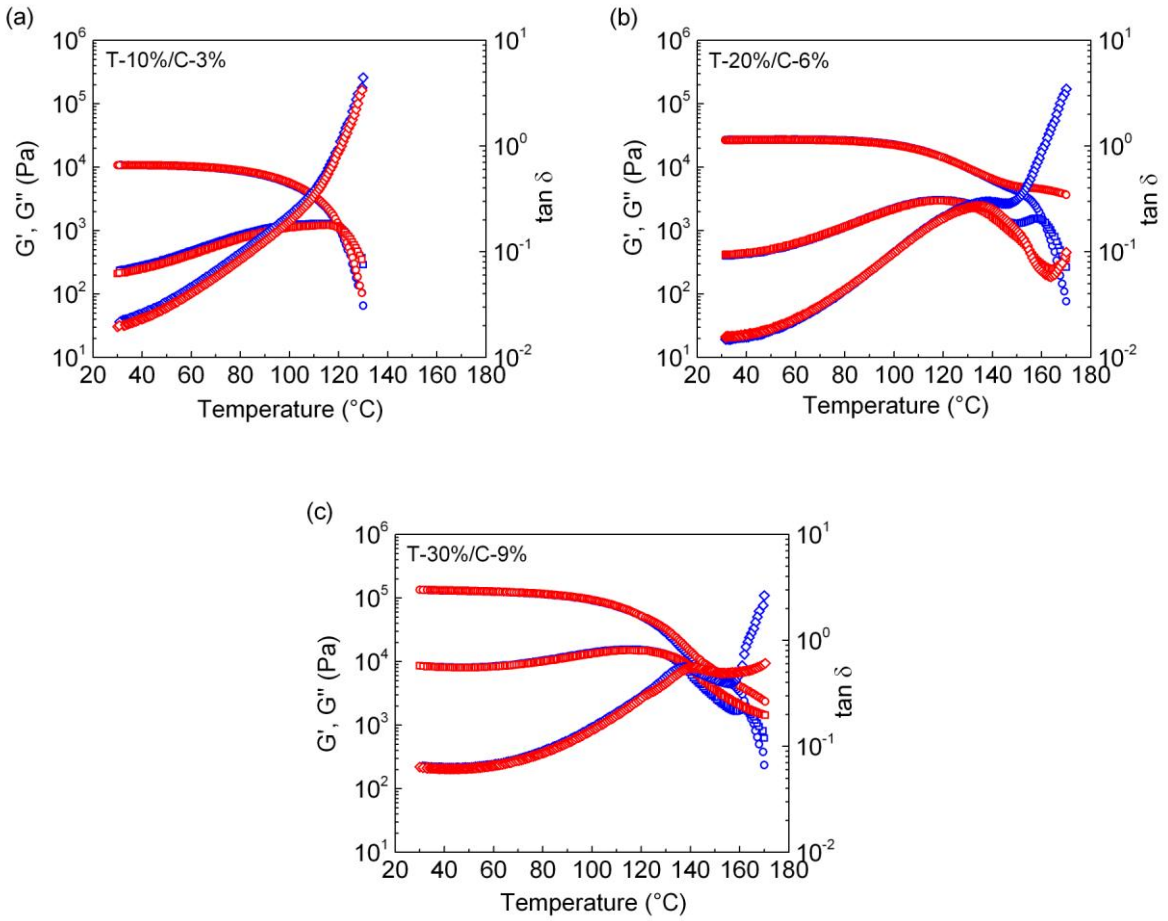

Figure 5.1 Temperature dependence of the dynamic storage modulus G' (○), loss modulus G'' (□), and tan δ (◇) during a cooling–heating cycle: (a) **T-10%/C-3%**; (b) **T-20%/C-6%**; (c) **T-30%/C-9%**. The blue curves denote cooling and the red curves denote heating. All measurements were performed at a strain amplitude of 3%, an angular frequency of 0.3 rad/s, and a cooling/heating rate of 1 ℃/min.

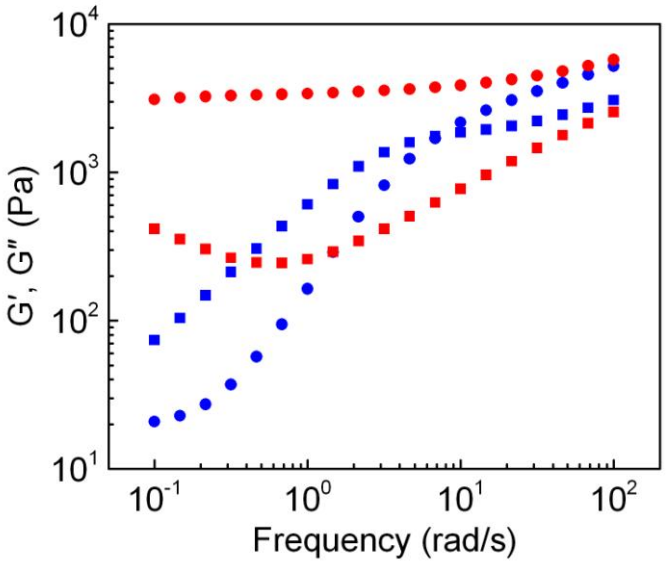

Figure 5.2 Dynamic frequency sweeps from **T-20%/C-6%** before (blue) and after (red) the cooling–heating cycle. Both measurements were performed at a strain amplitude of 3% over an angular frequency range of 0.1–100 rad/s at 170 ℃.

To probe the rheological recovery during the cooling–heating cycle in more detail, we also conducted two dynamic frequency sweeps: the first at 170 ℃ before the sample was cooled and the second also at 170 ℃ after the sample was heated back (Figure 5.2). Before the start of the cooling–heating cycle, terminal relaxation behavior was observed at low frequencies, where G' and G'' scale with second and first powers of frequency, respectively. After completion of the cooling–heating cycle, G' showed a frequency-independent rubbery plateau; concurrently, G'' is considerably smaller than G' and passes through a minimum, exemplifying the rheological signatures of a typical viscoelastic solid. Figure 5.3 also reiterates the effect of thermal history, in which tan δ is plotted as a

function of frequency after the completion of the cooling–heating cycle with different annealing periods. It is clear that it slowly evolves toward an equilibrium state in an hour, suggesting that a slow structural development is taking place.

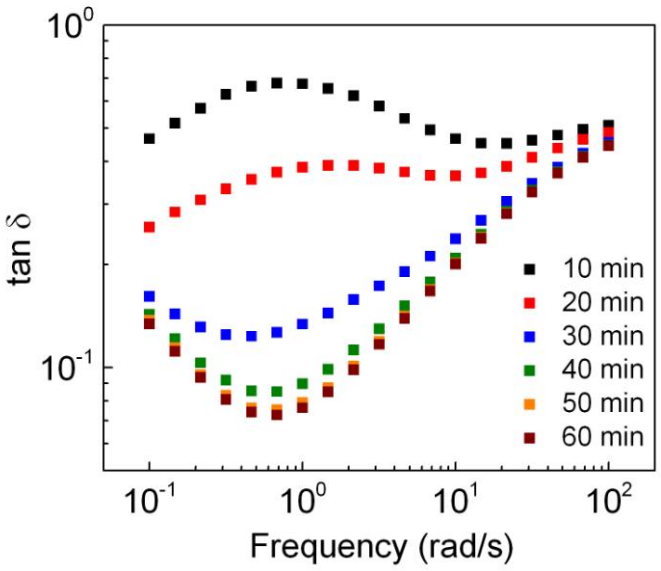

Figure 5.3 Frequency dependence of tan δ for **T-20%/C-6%**, showing the effect of different annealing periods as indicated.

Two distinct maxima in G'' during cooling were observed in **T-20%/C-6%** and **T-30%/C-9%**: a broad one around 120 ℃ and a sharp one around 160 ℃ (see Figure 5.1, parts (b) and (c)). We tentatively attribute the broad maximum around 120 ℃ to chain dynamics, where the P4VP blocks start to dissociate from their associated cross-links and diffuse into the PEO/[EMIM][TFSA] matrix, as the number of hydrogen bonds on a

given P4VP↔PVPh association may vary greatly from one to another; associations with fewer hydrogen bonds starts to dissociate at lower temperatures. This interpretation is supported by the concurrent decrease in G' by almost an order of magnitude. The sharp maximum around 160 ℃ represents a solid–liquid transition, driven by the dissociation of all hydrogen bonds between the P4VP blocks and PVPh cross-linkers.

5.3.2 Morphology of Nonannealed Gels at Ambient Temperature

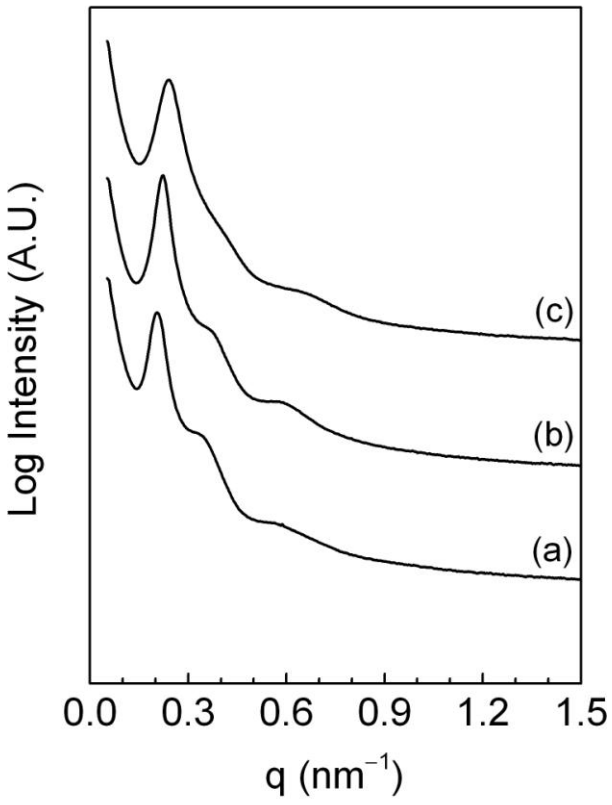

Figure 5.4 Room temperature synchrotron SAXS patterns of nonannealed gels: (a) **T-10%/C-3%**; (b) **T-20%/C-6%**; (c) **T-30%/C-9%**.

SAXS experiments were conducted to investigate the morphology of nonannealed gels at ambient temperature and scattering patterns are shown in Figure 5.4. Scattering contrast in these gels arises from the electron density difference between the less solvated hydrogen-bonded network microdomains and the well-solvated network strands. It is noteworthy that both P4VP and PVPh initially dissolve in the ionic liquid. However, their hydrogen-bonded interpolymer complexes are co-precipitated from their common solvent, probably because the hydrogen bonding between P4VP and PVPh is more favorable than either polymer–solvent affinity. The primary low-q peak represents the structure factor, which arises from interactions between microdomains and depends on the domain spacing, while the undulations at higher q are related to the form factor, which accounts for the geometry of the individual microdomain. With increasing polymer concentration, the structure factor maxima shift to higher q values as a consequence of shorter domain spacing. Nevertheless, the most important feature is that the scattering patterns revealed no higher order reflections for any of the nonannealed gels, indicating a random distribution of microdomains rather than crystalline packing. Indeed, the extraordinarily large relaxation times are expected suppress any structural rearrangement of the network at ambient temperature.

5.3.3 Morphology of Preannealed Gels at Ambient Temperature

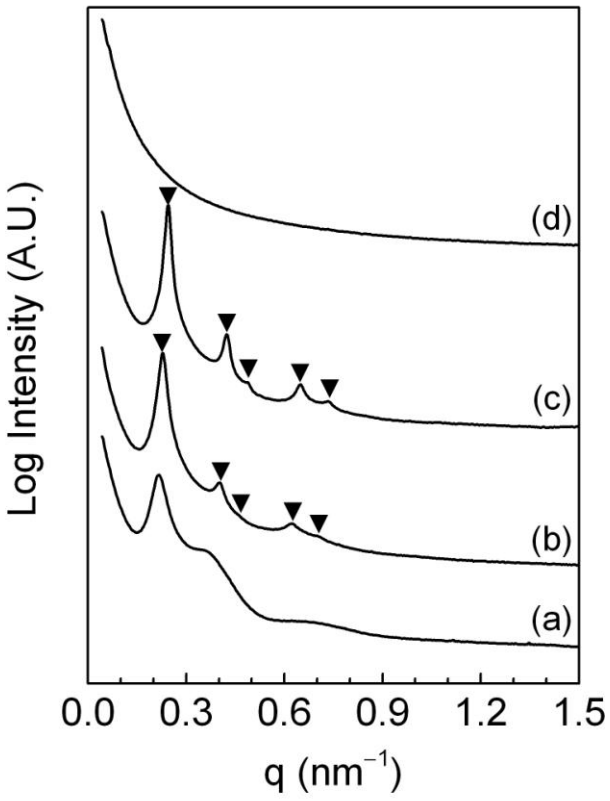

Figure 5.5 Synchrotron SAXS patterns of preannealed gels taken at ambient temperature: (a) **T-10%/C-3%**; (b) **T-20%/C-6%**; (c) **T-30%/C-9%**; (d) **T-30%/C-0%** Solid triangles correspond to expected intensity maxima for hexagonally packed cylinders at q/q_1 values of 1:√3:√4:√7:√9.

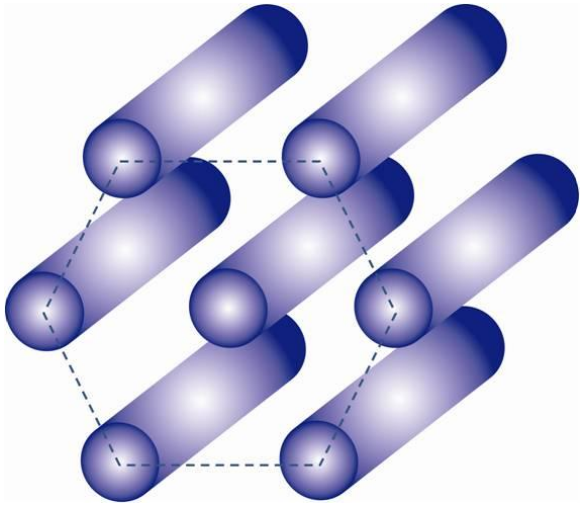

Figure 5.6 Cartoon representation of hexagonally packed cylindrical morphology after high-temperature annealing for a sufficiently long period of time.

In order to achieve equilibrium-like morphologies, gels were annealed at high temperatures for extended periods of time. Due to limited beam time, instead of annealing the samples on the beamline, they were preannealed at 140 ℃ for 2 h and subsequently quenched to room temperature. The key hypothesis behind this approach is that rapid quenching results in a kinetic freezing of the equilibrium-like morphology that has been developed during the annealing process and can be preserved for a long time at ambient temperature, due to extraordinarily large relaxation times. It is evident from a comparison of Figure 5.4 and Figure 5.5 that **T-20%/C-6%** and **T-30%/C-9%** undergo a well-defined transition from short-range order in nonannealed systems to long-range order in preannealed systems, as confirmed by a strong increase in the scattering intensity, a significant decrease in the width of the primary interference maxima, and appearance of higher-order interference maxima. Furthermore, the presence of well-

pronounced structure factor maxima with positions corresponding to ratios of 1:√3:√4:√7:√9 correspond to a hexagonally packed lattice. In contrast, **T-10%/C-3%** still displays only short-range microdomain order in preannealed systems. We speculate that ordering might take place in **T-10%/C-3%**, but on a much longer time scale, which appears to be a result of a lower number density of microdomains in the material. Therefore, a possible origin of the rheological hysteresis is that an ordered hexagonal morphology has been developed in **T-20%/C-6%** and **T-30%/C-9%** during the cooling–heating cycle, whereas this transition takes place in **T-10%/C-3%** on a time scale that is much longer than the cooling–heating cycle. This concentration-dependent ordering kinetics also accounts for the stronger hysteresis in **T-20%/C-6%** than **T-30%/C-9%**, since faster kinetics allows the ordering to take place in **T-30%/C-9%** during heating, and thus the structural difference during cooling and heating is smaller. Indeed, a high-temperature plateau can already be seen during cooling in **T-30%/C-9%**.

To determine whether there is any appreciable effect due to the self-assembly of the pure triblock in the ionic liquid, we measured the pure triblock without the addition of the cross-linker in the ionic liquid (**T-30%/C-0%)**, which showed no scattering peaks at all. This confirms that the hexagonally packed cylindrical morphology is not due to the self-assembly of the triblock in the ionic liquid, but from a supramolecular polymer network by hydrogen bonding. Indeed, although no flow was initially observed in **T-30%/C-0%** for several minutes after vial inversion, it gradually flowed after a period of several hours at room temperature, indicative of a high-viscosity liquid. The marked differences in flow

and scattering behavior between **T-30%/C-0%** and **T-30%/C-9%** confirm the role of cross-linker in generating the polymer network.

The reason that cylinders are formed can be understood by the volume fraction of the hydrogen-bonded phase (P2VP/PVPh) in the material. Assuming a density of 1 g/cm^3 and 1.5 g/cm^3 for polymers and the ionic liquid, respectively, the volume fraction of the hydrogen-bonded phase is estimated to be 12% and 19% in **T-20%/C-6%** and **T-30%/C-9%**, respectively, consistent with the formation of cylinders, based on block copolymer precedents.[1]

For a quantitative analysis, values of the domain spacing (D) and cylinder radius (r) can be extracted from the scattering profiles. From the positions of the primary Bragg peak (q_1) we can estimate the principal lattice spacing, $d_{100} = 2\pi/q_1$. The domain spacing between two nearest cross-links can be estimated by $D = (2/\sqrt{3})d_{100}$. The position of the first minimum (q_{min}) of the form factor can be related to the cylinder radius by $r = 3.83/q_{min}$. Table 5.2 summarizes the estimated values.

Table 5.2 Extracted Parameters from SAXS Profiles

Triblock content (wt%)	d_{110} (nm)	D (nm)	r (nm)
10	29.0	33.5	6.9
20	27.4	31.6	7.1
30	25.5	29.5	7.2

5.3.4 Temperature-Dependent Morphology of Nonannealed and Preannealed Gels

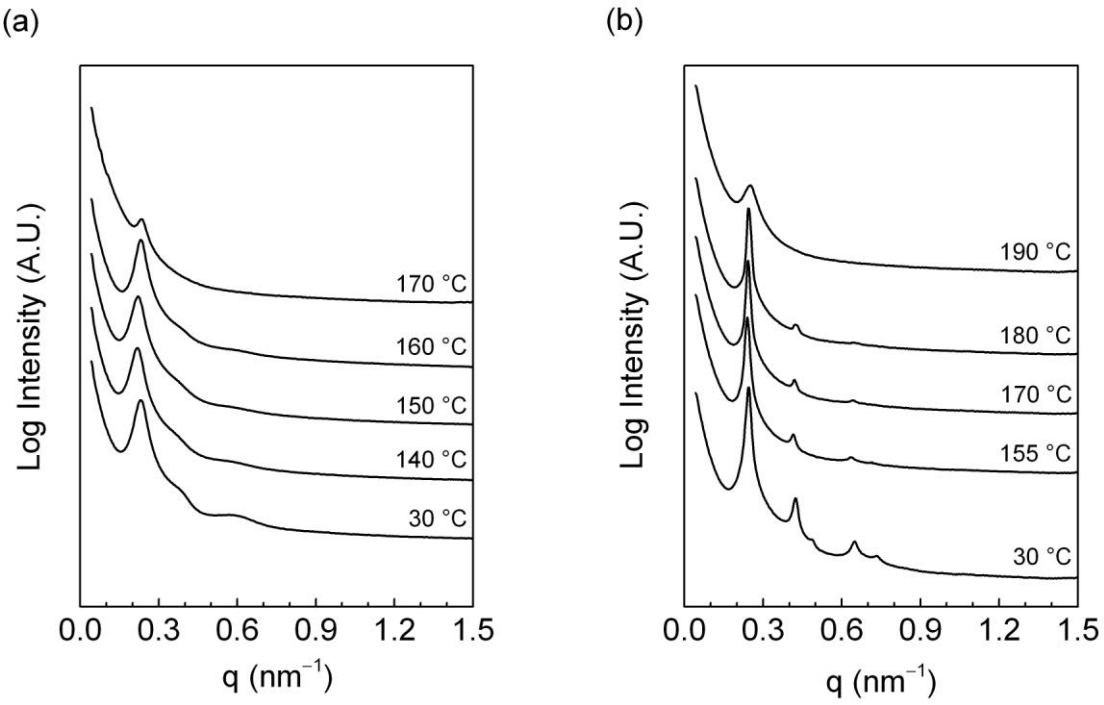

Figure 5.7 Evolution of synchrotron SAXS patterns with temperature, recorded on heating from **T-30%/C-9%**: (a) nonannealed; (b) preannealed at 140 ℃ for 2 h.

The effect of temperature on the morphological evolution of nonannealed **T-30%/C-9%** is shown in Figure 5.7(a). SAXS patterns were recorded upon heating the gel from room temperature to 170 ℃, with 5 min equilibration time at each measurement temperature. In the absence of any additional thermal treatment, only short-range ordered morphologies were observed during the heating process, with little discernible changes below 160 ℃. At 170 ℃, the primary structure factor reveals a significant decrease in intensity and increase in width, indicating dissolution of the microdomains and the

network. However, even at temperatures above the solid–liquid transition, the main peak does not completely go away, suggestive the presence of random clusters of hydrogen-bonded microdomains. Similar observations have been seen in bulk block copolymer systems. The main peak is still evident after a block copolymer is heated through its order–disorder transition temperature (T_{ODT}).[56] This temperature is consistent with the rheological data, in which a solid–liquid transition temperature of 162 ℃ was observed during the cooling cycle prior to the development of well-ordered microdomains.

The effect of temperature on the morphological evolution of preannealed **T-30%/C-9%** is shown in Figure 5.7(b). During heating, the hexagonal morphology remains evident up to 180 ℃, as higher-order peaks are clearly resolved in the scattering patterns. At 190 ℃, the disappearance of higher-order interference maxima and the broadening of the primary interference maximum reflect a well-defined order–disorder transition. Annealing increases the stability of the structure, as no changes are observed if the sample is brought to 170 ℃. This is consistent again with the rheological observations; the flow temperature of the sample increased from 162 ℃ to 185 ℃ after completion of the cooling–heating cycle during which an ordered structure has been developed. One possible explanation for the enhanced solid–liquid transition temperature is that in ordered systems, the dissolution of the ordered microdomains takes place in a two-step process that involves lattice disordering followed by the dissolution of the microdomains.

5.3.5 Thermodynamically Favorable Window of Hexagonal Morphology

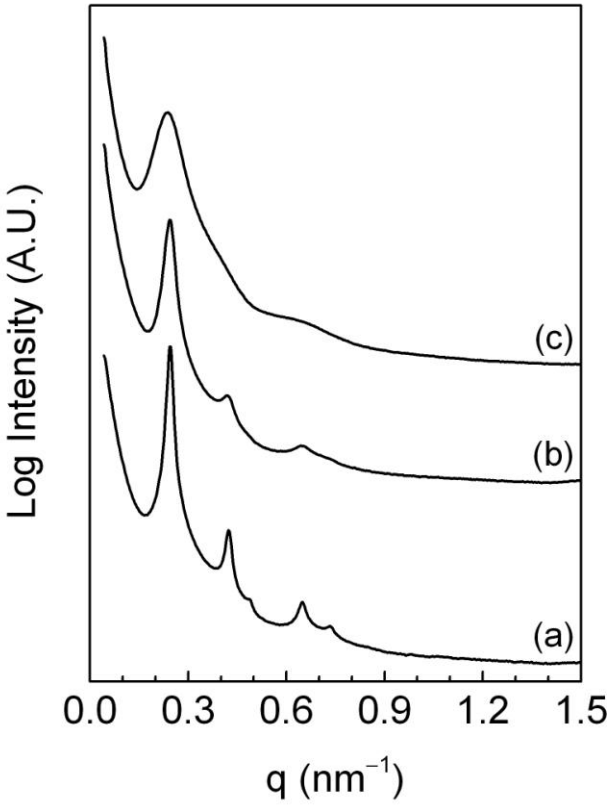

Figure 5.8 Room temperature synchrotron SAXS patterns of **T-30%/C-9%** with different thermal history: (a) preannealed at 140 ℃ for 2 h followed by rapid quenching to ambient temperature; (b) preannealed at 140 ℃ for 2 h followed by cooling to ambient temperature at a rate of 0.5 ℃/min; (c) nonannealed.

The long-range ordered hexagonal morphology represented an equilibrium-like thermodynamically favorable structure at 140 ℃ where the gel was annealed, and

corresponded to a kinetically frozen structure at ambient temperature due to rapid cooling. The question then arises as to whether the hexagonal morphology will still be present if the gel were cooled at a sufficiently slow rate, allowing sufficient time for potential rearrangements to take place. Therefore, we investigated the effect of cooling rate on the eventual morphology observed. Figure 5.8(b) was recorded after **T-30%/C-9%** was preannealed at 140 ℃ for 2 h and then cooled at a rate of 0.5 ℃/min, which was compared with rapid quenching (Figure 5.8(a)). The SAXS pattern of nonannealed **T-30%/C-9%** was also included for comparison (Figure 5.8(c)). Careful comparison of these SAXS patterns reveals that although a hexagonal morphology is still present, it becomes slightly distorted as indicated by a slight broadening of the interference maxima after slow cooling. It is reasonable to speculate that the long-range ordered hexagonal morphology could be highly distorted, or even vanish, if the sample were cooled at extremely slow rates. It is also possible that the hexagonal morphology is at equilibrium at ambient temperature, but domain spacing cannot adjust on cooling slowly, leading to distorted structures. Nevertheless, the extraordinarily large relaxation times make an evaluation of the equilibrium structures at ambient temperature rather difficult. Since the substantial displacement of one microdomain would require extraction of the copolymer involved, a prerequisite to achieve a thermodynamically stable structure is that chain exchange must be able to take place between neighboring microdomains. Based on the rheological results (see Figure 5.1), 120 ℃ could represent the onset of chain exchange between different microdomains, where a broad maximum in G'' was observed. There is no chain exchange below 120 ℃ because they are hydrogen-bonded. The activation

energy is too high to break multiple hydrogen bonds simultaneously and release the chains. Furthermore, the sharp peak in G'' around 160 °C represents the eventual dissolution of the polymer network, beyond which no stable structure is present and a homogeneous phase is obtained. Therefore, based on these analyses, a hypothesis is that the hexagonally ordered phase is only thermodynamically stable over the temperature range between the two peaks in G'', *i.e.*, between 120 and 160 ℃. This hypothesis is supported by the fact that only above this temperature were we able to detect the gradual development of this hexagonally ordered morphology. Figure 5.9 shows a SAXS pattern from a **T-30%/C-9%** sample preannealed at 100 ℃ for two days, which showed equivalent SAXS pattern with the nonannealed sample. The hypothesis is also consistent with the fact that there is a coexistence of short-range order and long-range order as indicated by SAXS, since only a certain fraction of P4VP blocks is able to exchange.

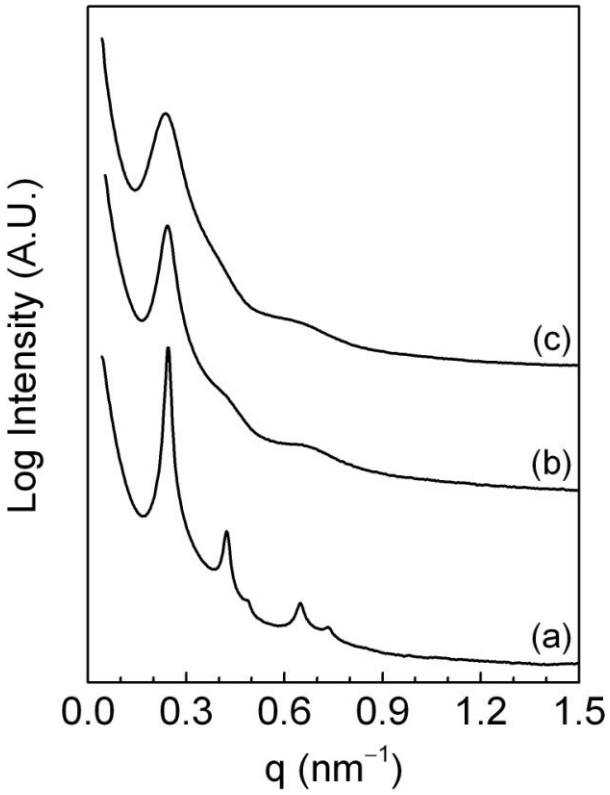

Figure 5.9 Synchrotron SAXS patterns recorded at ambient temperature from **T-30%/C-9%** with different thermal history: (a) preannealed at 140 ℃ for 2 h followed by rapid quenching to ambient temperature; (b) preannealed at 100 ℃ for 48 h followed by rapid quenching to ambient temperature; (c) nonannealed.

5.3.6 Concentration Dependence of Shear Modulus

At low temperatures, these gels behave as viscoelastic solids at accessible frequencies, with a well-defined plateau modulus (G_N). For triblock copolymer gels with

a midblock concentration in the unentangled regime, the plateau modulus (G_N) is described by classical theory of rubber elasticity[57]

$$G_N = \nu_e k_B T = \frac{fcRT}{M} \tag{5.1}$$

where ν_e is the number density of elastically effective strands, k_B is the Boltzmann constant, T is the absolute temperature, c is the triblock concentration in w/v, R is the ideal gas constant, M is the average molecular weight between cross-links, and f is the fraction of bridging or elastically effective molecules. For equation 5.1 to apply, gels must lack midblock entanglements. For the system under consideration, the polymer volume fraction (φ_{PEO}) at which PEO midblock forms one entanglement per chain is estimated by

$$\varphi_{PEO} \approx \frac{1}{N_e} = \frac{M_{e,PEO}}{M_{PEO}} \tag{5.2}$$

where N_e is the number of entanglements per PEO chain in the melt, $M_{e,PEO}$ is the entanglement molecular weight of PEO in the melt, and M_{PEO} is the molecular weight of PEO midblock under consideration. Since M_{PEO} = 35000 g/mol and $M_{e,PEO}$ = 1600 g/mol,[58] an estimation of φ_{PEO} using equation 5.2 yields $\varphi_{PEO} \approx 0.05$. Since the PEO volume fractions investigated here are all higher than the critical entanglement concentration, the existence of a plateau modulus reflects combined contributions from a hydrogen-bonded polymer network structure and trapped midblock entanglements.[11] Since trapped midblock entanglements behave as temporary cross-links and provide additional constraints that magnify the change of entropy with deformation,[59] M in

equation 5.1 must be replaced by the molecular weight between entanglements along the PEO chains (M_x) to describe the concentration dependence of G_N in our system

$$G_N = \nu_e k_B T = \frac{fcRT}{M_x} \tag{5.3}$$

where M_x can be estimated by $M_x = M_{e,PEO}/\varphi_{PEO}$. Assuming that all PEO chains adopt bridging conformations instead of looping conformations, the ideal values of G_N were calculated and plotted in Figure 5.10. As polymer concentration increases, the discrepancy between measured and anticipated values gets smaller. The reason that accounts for this phenomenon is twofold. At lower concentrations, the stronger midblock chain stretching due to greater domain spacing favors loop formation. Therefore, the fraction of bridging chains should increase with polymer concentration. Furthermore, with a fair amount of entanglements at high polymer concentration, for example, *ca.* 8 entanglements per PEO chain in **T-30%/C-9%**, looped midblocks are expected to contribute to the modulus almost the same as bridging midblocks, and the measured modulus would be expected to be closer to that of the ideal gel.

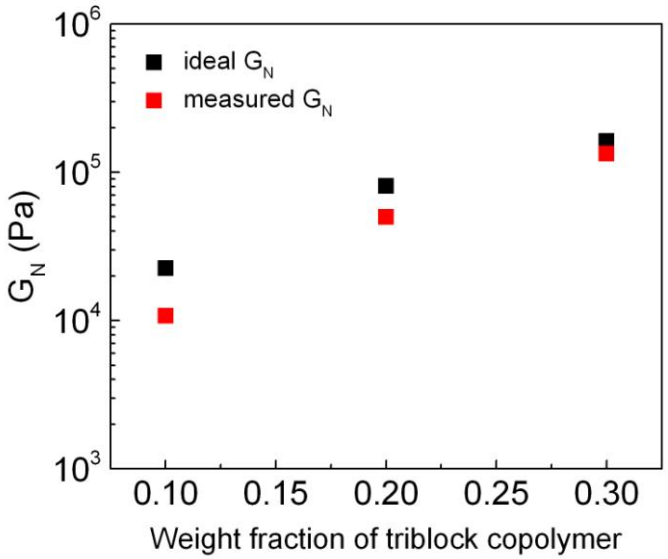

Figure 5.10 Concentration dependence of ideal (■) and measured G_N (■) for three supramolecular ion gels. Ideal G_N is calculated from equation 5.3 assuming every chain is elastically effective.

5.4 Conclusions

In this chapter, we have investigated thermally induced morphological evolution in a hydrogen-bonded supramolecular ion gel system using rheology and SAXS. In addition to the formation of a highly interconnected supramolecular polymer network as a result of hydrogen bonding between a P4VP–PEO–P4VP triblock copolymer and a PVPh cross-linker, the hydrogen-bonded phase can rearrange into a long-range ordered hexagonally packed cylindrical morphology under certain thermal conditions. Whether the network microdomains exhibit short-range order or long-range order strongly depends on factors

such as polymer concentration and thermal history. Only short-range order is found in as-prepared systems without additional thermal treatment. Long-range order is favored at high polymer concentration and may develop if the gel is annealed for a sufficiently long period of time at temperatures where P4VP endblocks are able to exchange. The present study also demonstrated that evolution of the network microdomains from short-range order toward long-range order takes place only in a limited temperature window and usually reveals slow kinetics on the time scale of several hours. The thermodynamically stable hexagonal phase is limited at high-temperature by eventual dissolution of network microdomains and at low-temperature by the absence of chain exchange. The slow development of this long-range ordered morphology results in a significant hysteresis at high temperatures in rheological experiments. This work enhances our understanding of the interplay between processing history, morphology, and properties, which is crucial to improve existing and develop new applications of these materials.

5.5 References

(1) Hamley, I. W. *Block Copolymers in Solution: Fundamentals and Applications*; John Wiley & Sons, Ltd.: Chichester, 2005.

(2) Laurer, J. H.; Bukovnik, R.; Spontak, R. J. *Macromolecules* **1996,** *29,* 5760–5762.

(3) Laurer, J. H.; Mulling, J. F.; Khan, S. A.; Spontak, R. J.; Bukovnik, R. *J. Polym. Sci., Part B: Polym. Phys.* **1998,** *36,* 2379–2391.

(4) Laurer, J. H.; Mulling, J. F.; Khan, S. A.; Spontak, R. J.; Lin, J. S.; Bukovnik, R. *J. Polym. Sci., Part B: Polym. Phys.* **1998,** *36*, 2513–2523.

(5) Laurer, J. H.; Khan, S. A.; Spontak, R. J.; Satkowski, M. M.; Grothaus, J. T.; Smith, S. D.; Lin, J. S. *Langmuir* **1999,** *15*, 7947–7955.

(6) Flanigan, C. M.; Crosby, A. J.; Shull, K. R. *Macromolecules* **1999,** *32*, 7251–7262.

(7) Drzal, P. L.; Shull, K. R. *Macromolecules* **2003,** *36*, 2000–2008.

(8) Seitz, M. E.; Burghardt, W. R.; Faber, K. T.; Shull, K. R. *Macromolecules* **2007,** *40*, 1218–1226.

(9) Seitz, M. E.; Burghardt, W. R.; Shull, K. R. *Macromolecules* **2009,** *42*, 9133–9140.

(10) Bras, R. E.; Shull, K. R. *Macromolecules* **2009,** *42*, 8513–8520.

(11) Vega, D. A.; Sebastian, J. M.; Loo, Y.-L.; Register, R. A. *J. Polym. Sci., Part B: Polym. Phys.* **2001,** *39*, 2183–2197.

(12) Chantawansri, T. L.; Duncan, A. J.; Ilavsky, J.; Stokes, K. K.; Berg, M. C.; Mrozek, R. A.; Lenhart, J. L.; Beyer, F. L.; Andzelm, J. W. *J. Polym. Sci., Part B: Polym. Phys.* **2011,** *49*, 1479–1491.

(13) Mischenko, N.; Reynders, K.; Koch, M. H. J.; Mortensen, K.; Pedersen, J. S.; Fontaine, F.; Graulus, R.; Reynaers, H. *Macromolecules* **1995,** *28*, 2054–2062.

(14) Soenen, H.; Berghmans, H.; Winter, H. H.; Overbergh, N. *Polymer* **1997,** *38*, 5653–5660.

(15) Soenen, H.; Liskova, A.; Reynders, K.; Berghmans, H.; Winter, H. H.; Overbergh, N. *Polymer* **1997,** *38*, 5661–5665.

(16) Kleppinger, R.; Reynders, K.; Mischenko, N.; Overbergh, N.; Koch, M. H. J.; Mortensen, K.; Reynaers, H. *Macromolecules* **1997,** *30*, 7008–7011.

(17) Kleppinger, R.; Mischenko, N.; Theunissen, E.; Reynaers, H. L. *Macromolecules* **1997,** *30*, 7012–7014.

(18) Reynders, K.; Mischenko, N.; Kleppinger, R.; Reynaers, H.; Koch, M. H. J.; Mortensen, K. *J. Appl. Cryst.* **1997,** *30*, 684–689.

(19) Kleppinger, R.; Mischenko, N.; Reynaers, H. L.; Koch, M. H. J. *J. Polym. Sci., Part A: Polym. Phys.* **1999,** *37*, 1833–1840.

(20) Mortensen, K.; Theunissen, E.; Kleppinger, R.; Almdal, K.; Reynaers, H. *Macromolecules* **2002,** *35*, 7773–7781.

(21) Zhang, S.; Lee, K. H.; Sun, J.; Frisbie, C. D.; Lodge, T. P. *Macromolecules* **2011,** *44*, 8981–8989.

(22) Noro, A.; Hayashi, M.; Matsushita, Y. *Soft Matter* **2012,** *8*, 2416–2429.

(23) Sijbesma, R. P.; Beijer, F. H.; Brunsveld, L.; Folmer, B. J. B.; Hirschberg, J. H. K. K.; Lange, R. F. M.; Lowe, J. K. L.; Meijer, E. W. *Science* **1997,** *278*, 1601–1604.

(24) Lange, R. F. M.; van Gurp, M.; Meijer, E. W. *J. Polym. Sci., Part A: Polym. Chem.* **1999,** *37*, 3657−3670.

(25) Suzuki, T.; Shinkai, S.; Sada, K. *Adv. Mater.* **2006,** *18*, 1043–1046.

(26) Cordier, P.; Tournilhac, F.; Souli é-Ziakovic, C.; Leibler, L. *Nature* **2008,** *451*, 977–980.

(27) Noro, A.; Matsushita, Y.; Lodge, T. P. *Macromolecules* **2008,** *41*, 5839–5844.

(28) Noro, A.; Matsushita, Y.; Lodge, T. P. *Macromolecules* **2009,** *42*, 5802–5810.

(29) Lei, Y.; Lodge, T. P. *Soft Matter* **2012,** *8*, 2110–2120.

(30) Noro, A.; Hayashi, M.; Ohshika, A.; Matsushita, Y. *Soft Matter* **2011,** *7*, 1667–1670.

(31) Nair, K. P.; Breedveld, V.; Weck, M. *Macromolecules* **2008,** *41*, 3429–3438.

(32) Nair, K. P.; Breedveld, V.; Weck, M. *Soft Matter* **2011,** *7*, 553–559.

(33) Nair, K. P.; Breedveld, V.; Weck, M. *Macromolecules* **2011,** *44*, 3346–3357.

(34) Feldman, K. E.; Kade, M. J.; Meijer, E. W.; Hawker, C. J.; Kramer, E. J. *Macromolecules* **2009,** *42*, 9072–9081.

(35) Yount, W. C.; Loveless, D. M.; Craig, S. L. *J. Am. Chem. Soc.* **2005,** *127*, 14488–14496.

(36) Piepenbrock, M.-O. M.; Lloyd, G. O.; Clarke, N.; Steed, J. W. *Chem. Rev.* **2010,** *110*, 1960–2004.

(37) Wathier, M.; Grinstaff, M. W. *Macromolecules* **2010,** *43*, 9529–9533.

(38) Aboudzadeh, M. A.; Mu ñoz, M. E.; Santamar á, A.; Fern ández-Berridi, M. J.; Irusta, L.; Mecerreyes, D. *Macromolecules* **2012,** *45*, 7599–7606.

(39) Berl, V.; Schmutz, M.; Krische, M. J.; Khoury, R. G.; Lehn, J.-M. *Chem. Eur. J.* **2002,** *8*, 1227–1244.

(40) Kolomiets, E.; Buhler, E.; Candau, S. J.; Lehn, J.-M. *Macromolecules* **2006,** *39*, 1173–1181.

(41) Beijer, F. H.; Kooijman, H.; Spek, A. L.; Sijbesma, R. P.; Meijer, E. W. *Angew. Chem. Int. Ed.* **1998,** *37*, 75–78.

(42) Beijer, F. H.; Sijbesma, R. P.; Kooijman, H.; Spek, A. L.; Meijer, E. W. *J. Am. Chem. Soc.* **1998,** *120*, 6761–6769.

(43) Li, J.; Viveros, J. A.; Wrue, M. H.; Anthamatten, M. *Adv. Mater.* **2007,** *19*, 2851–2855.

(44) Cates, M. E. *Macromolecules* **1987,** *20*, 2289–2296.

(45) Seiffert, S.; Sprakel, J. *Chem. Soc. Rev.* **2012,** *41*, 909–930.

(46) Lodge, T. P. *Science* **2008,** *321*, 50–51.

(47) Shin, J.-H.; Henderson, W. A.; Passerini, S. *J. Electrochem. Soc.* **2005,** *152*, A978–A983.

(48) Gu, Y.; Lodge, T. P. *Macromolecules* **2011,** *44*, 1732–1736.

(49) Lee, J.; Panzer, M. J.; He, Y.; Lodge, T. P.; Frisbie, C. D. *J. Am. Chem. Soc* **2007,** *129*, 4532–4533.

(50) Cho, J. H.; Lee, J.; He, Y.; Kim, B. S.; Lodge, T. P.; Frisbie, C. D. *Adv. Mater.* **2008,** *20*, 686–690.

(51) Cho, J. H.; Lee, J.; Xia, Y.; Kim, B.; He, Y.; Renn, M. J.; Lodge, T. P.; Frisbie, C. D. *Nat. Mater.* **2008,** *7*, 900–906.

(52) Lee, J.; Kaake, L. G.; Cho, J. H.; Zhu, X.-Y.; Lodge, T. P.; Frisbie, C. D. *J. Phys. Chem. C* **2009,** *113*, 8972–8981.

(53) Lu, W.; Fadeev, A. G.; Qi, B.; Smela, E.; Mattes, B. R.; Ding, J.; Spinks, G. M.; Mazurkiewicz, J.; Zhou, D.; Wallace, G. G.; MacFarlane, D. R.; Forsyth, S. A.; Forsyth, M. *Science* **2002,** *297*, 983−987.

(54) Ding, J.; Zhou, D.; Spinks, G.; Wallace, G.; Forsyth, S.; Forsyth, M.; MacFarlane, D. *Chem. Mater.* **2003,** *15*, 2392−2398.

(55) Ozair, S. N. Ph.D. Dissertation, University of Minnesota, 2009.

(56) Wang, X.; Dormidontova, E. E.; Lodge, T. P. *Macromolecules* **2002,** *35*, 9687–9697.

(57) Hiemenz, P. C.; Lodge, T. P. *Polymer Chemistry*, 2nd ed.; CRC Press: New York, 2007.

(58) Fetters, L. J.; Lohse, D. J.; Richter, D.; Witten, T. A.; Zirkel, A. *Macromolecules* **1994,** *27*, 4639–4647.

(59) Ferry, J. D. *Viscoelastic Properties of Polymers*, 3rd ed.; John Wiley & Sons: New York, 1980.

Chapter 6

How Many Hydrogen Bonds per Association are Required at the Gel Point?

6.1 Introduction

Hydrogen bonding is ubiquitous in a wide range of fundamental chemical and biological systems.[1,2] For instance, the extensive hydrogen-bonded network in water results in a liquid at ambient temperature rather than a gas; hydrogen bonding in proteins and DNA gives rise to their secondary and double-helix structures, respectively, which are crucial in the fulfillment of their physiological functions. The strength of hydrogen bonds is intermediate between van der Waals forces and covalent bonds, with dissociation enthalpies in the range of 5–30 kJ/mol. In contrast, a carbon–carbon single bond has a dissociation enthalpy of *ca.* 350 kJ/mol. Since relevant energies are on the order of a few k_BT (where k_B is the Boltzmann constant and T is the absolute temperature; k_BT is *ca.* 2.5 kJ/mol at room temperature), hydrogen bonds can reversibly dissociate and reform under thermal equilibrium conditions on very short time scales. This reversibility brings up an interesting and fundamental question: what is the lifetime of a hydrogen bond? Qualitatively, it would be expected that stronger hydrogen bonds persist longer. However, it was not until the recent advent of ultrafast infrared spectroscopy techniques that quantitative measurement of hydrogen bond lifetimes became possible,[3–10] especially for relatively weak hydrogen bonds with dissociation enthalpies smaller than 20 kJ/mol.

Hydrogen bonds are highly directional and sufficiently strong to direct small molecules to assemble into macromolecular architectures, yet with dynamic reversibility. In the pioneering work by Sijbesma *et al.*, 2-ureido-4[1*H*]-pyrimidinone (UPy) units were shown to assemble into long chains through quadruple cooperative hydrogen bonds in an array.[11] Thermodynamic and kinetic parameters of the dimerization process were presented in a subsequent work.[12] The dimerization constant (K_{dim}) was determined to be 10^7 M^{-1} at 298 K in chloroform by excimer fluorescence spectroscopy. Furthermore, the preexchange lifetime of the dimer was estimated to be 170 ms in chloroform by dynamic NMR spectroscopy, which was in excellent agreement with the longest relaxation time of the UPy-functionalized polymer, as determined from rheology assuming its relaxation is described by a pure Maxwell element.

In this chapter, we address an interesting and fundamental question in this supramolecular ion gel system, *i.e.*, how many hydrogen bonds per P2VP↔PVPh association are required at the gel point? It was previously assumed that there is about one hydrogen bond per P2VP↔PVPh association at the gel point of 140 ℃.[13,14] Upon subsequent cooling, the number of hydrogen bonds per P2VP↔PVPh association increases, while no substantial rearrangement of network connectivity takes place due to very high activation energy required to break multiple hydrogen bonds simultaneously. Therefore, the strength of a given P2VP↔PVPh association is greatly enhanced as temperature decreases, while the network structure is essentially locked in place at the gel point. In this chapter, theoretical analysis and experimental work will be presented for the

argument that one hydrogen bond per P2VP↔PVPh association is not enough to generate a sufficiently stable polymer network.

6.2 Results and Discussion

6.2.1 Estimation of the Lifetime of a Single Hydrogen Bond in [EMIM][TFSA]

Fayer and coworkers have applied ultrafast two-dimensional infrared vibrational echo chemical exchange spectroscopy to directly measure the lifetimes of a series of hydrogen bonds with different dissociation enthalpies under thermal equilibrium conditions at room temperature.[9,10] They found a linear relationship between the hydrogen bond lifetime and the Arrhenius factor of the hydrogen bond dissociation enthalpy (Figure 6.1). The relationship between hydrogen bond lifetime and dissociation enthalpy can be approximated by

$$1/k_{\mathrm{d}} = A\exp\left(\frac{\Delta H^{0}}{RT}\right) \qquad (6.1)$$

where the proportionality constant A was determined to be 0.5 ps from the slope of the linear fit, ΔH^{0} is the hydrogen bond dissociation enthalpy, R is the gas constant, and T is the absolute temperature. Therefore, it is straightforward to estimate the hydrogen bond lifetimes if the dissociation enthalpy is known.

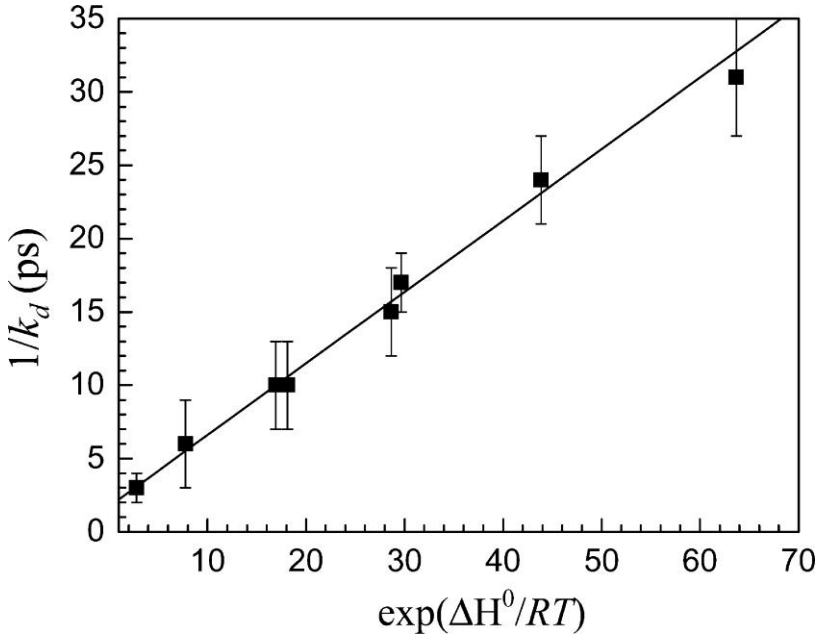

Figure 6.1 Hydrogen bond lifetimes ($1/k_d$, ps) versus $\exp(\Delta H^0/RT)$, where ΔH^0 is the hydrogen bond dissociation enthalpy, R is the gas constant, and T is the absolute temperature (300 K). Reprinted with permission from Zheng, J.; Fayer, M. D. *J. Am. Chem. Soc.* **2007,** *129*, 4328–4335. Copyright 2007 American Chemical Society.

The dissociation enthalpy of a single phenol–pyridine hydrogen bond in [EMIM][TFSA] was determined by measuring the temperature dependence of the infrared absorption spectrum of the hydroxyl stretching mode. An Arrhenius plot of the corrected FT-IR absorbance was constructed and a dissociation enthalpy of 13 ± 2.5 kJ/mol was extracted.[13]

The lifetime of a single phenol–pyridine hydrogen bond in [EMIM][TFSA] as a function of temperature is calculated based on equation 6.1 and presented in Figure 6.2; it varies by less than an order of magnitude over the temperature range of 30–200 ℃.

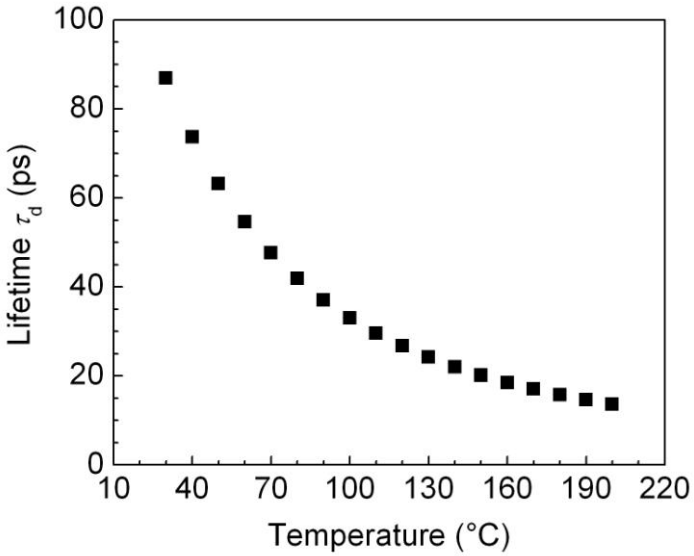

Figure 6.2 Temperature dependence of the lifetime of a single phenol–pyridine hydrogen bond in [EMIM][TFSA].

6.2.2 How Many Hydrogen Bonds per Association are Required at the Gel Point?

It was previously assumed that the gel point should occur at about one hydrogen bond per P2VP↔PVPh association.[13,14] From a physical perspective, with one hydrogen bond per association, effective cross-linking is achieved to generate a continuous percolating polymer network. However, the ultrafast dynamics of hydrogen bond formation and dissociation provides solid theoretical background to question this assumption, since the lifetime of a single phenol–pyridine hydrogen bond in [EMIM][TFSA] is on the order of sub-nanosecond, which is too transient to generate a sufficiently stable polymer network. In Chapter 3, the rheological relaxation times were qualitatively related to the lifetime of a P2VP↔PVPh association, which depends on the number of hydrogen bonds involved.

In rheology, the gel point is determined by the crossover temperature where $G' = G''$. By this definition, the average lifetime of a P2VP↔PVPh association at the gel point should be comparable to the timescale of a rheological experiment, which was performed on a timescale of seconds. Therefore, the average lifetime of a P2VP↔PVPh association should be on the order of seconds at the gel point. When multiple hydrogen bonds are involved, it is assumed that the total dissociation enthalpy is given by the product of the number of hydrogen bonds and the dissociation enthalpy of a single hydrogen bond. Therefore, equation 6.1 can be modified to give the lifetime of a P2VP↔PVPh association with *n* hydrogen bonds.

$$\tau_1 = A\exp\left(\frac{n\Delta H^0}{RT}\right) \tag{6.2}$$

Based on equation 6.2, the number of hydrogen bonds required at the gel point can be estimated and presented in Figure 6.3. The number of hydrogen bonds per association required at the gel point is weakly dependent on the gel point itself, which is attributed to the weak temperature dependence of the lifetime of a single hydrogen bond, as discussed in Section 6.2.1. One important conclusion is that $n(T_{gel}) \approx 6$ at 30 ℃, which means that at least 6 hydrogen bonds are required for a given P2VP↔PVPh association to persist over the timescale of seconds at room temperature and therefore an effective part of the polymer network. Based on equation 6.2, the lifetime of a P2VP↔PVPh association with 5 hydrogen bonds is on the order of milliseconds. Consequently, associations with less than 6 hydrogen bonds are dynamic and not considered effective part of the network.

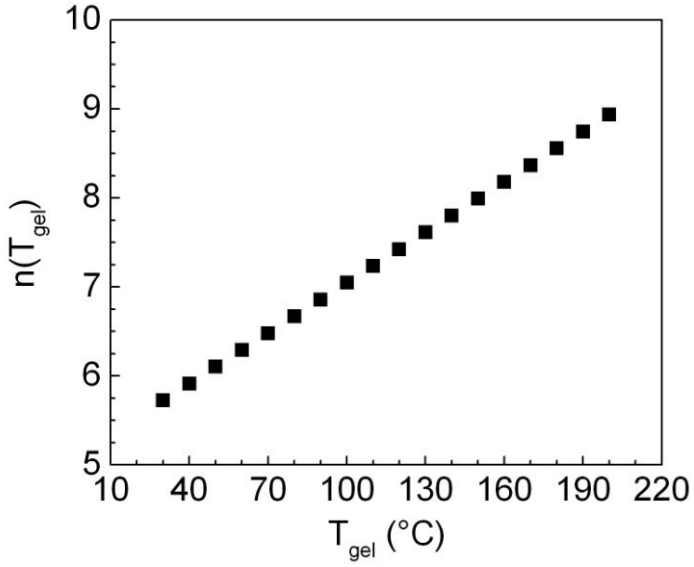

Figure 6.3 The number of hydrogen bonds per association required at gel point versus gel point.

6.2.3 Rheological Characterization

In order to qualitatively test the hypothesis that multiple hydrogen bonds per association are required at the gel point, we synthesized a P2VP–PEO–P2VP triblock copolymer in which the molecular weight of the P2VP block is 1 kg/mol. The key hypothesis is that fairly short P2VP blocks will result in a significant amount of dynamic chains, leading to the formation of rather weak gels or even viscous liquids. The results are quantitatively compared with similar gels with a longer P2VP block (2 kg/mol), in terms of the modulus and gel point.

Table 6.1 Characteristics of Supramolecular Ion Gels

Code	P2VP–PEO–P2VP	PVPh	X_{ph}/X_{py} [a]	T_{gel} [b] (℃)	G_N [c] (Pa)
1	10 wt% VOV(1-35-1)	1 wt% PVPh-5	160/100	72.5	1600
2	10 wt% VOV(1-35-1)	2 wt% PVPh-5	320/100	66.5	2800
3	10 wt% VOV(1-35-1)	1 wt% PVPh-5	85/100	118.5	2500
4	10 wt% VOV(1-35-1)	2 wt% PVPh-5	170/100	127	14000

[a] Molar ratio of phenol/pyridine units. [b] T_{gel} determined from the crossover temperature at which $G' = G''$ in Figure 6.4. [c] Plateau modulus at 30 ℃.

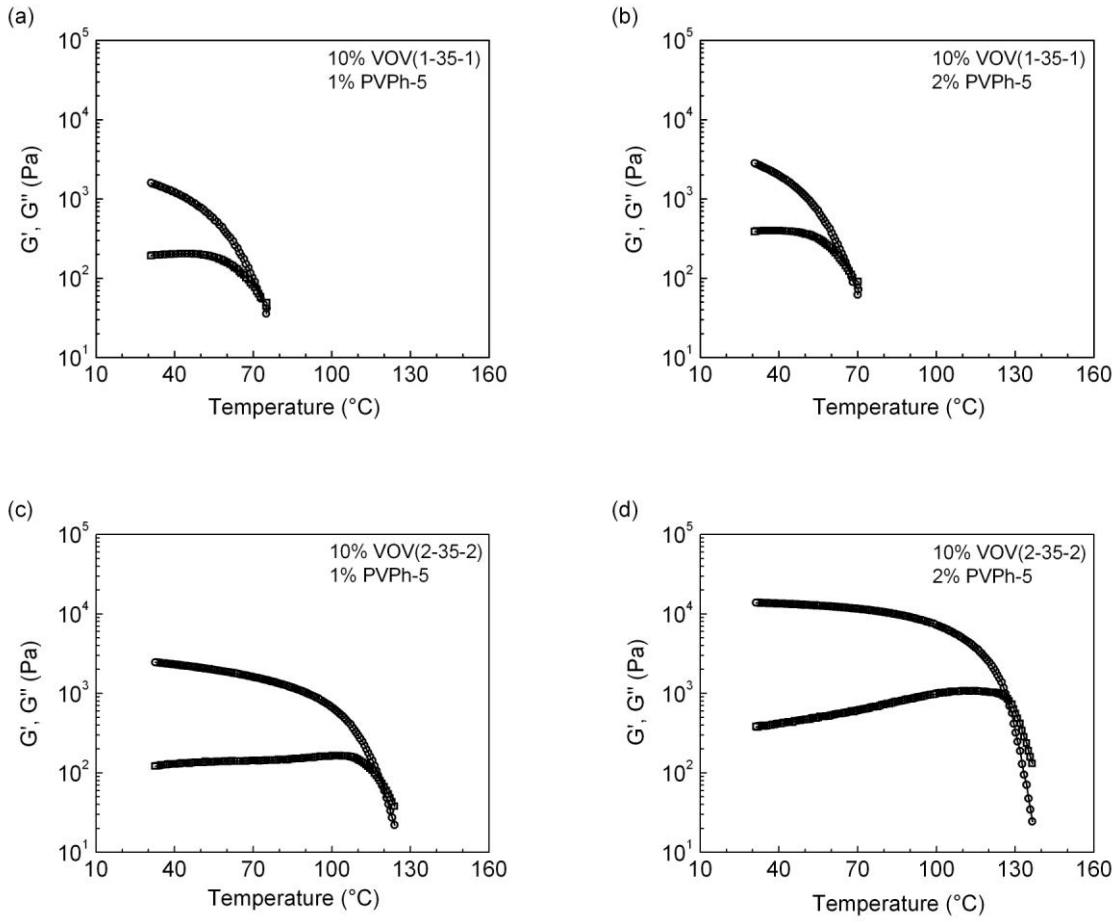

Figure 6.4 Temperature dependence of the dynamic shear storage modulus G' (○) and loss modulus G'' (□). See the upper right-hand corner of each plot for identity details. All measurements were performed at a strain amplitude of 3%, an angular frequency of 0.3 rad/s, and a temperature ramp rate of 1 ℃/min.

Dynamic temperature ramps were performed to evaluate the rheological changes with temperature (Figure 6.4). All gels exhibit predominantly viscous behavior at high temperatures and highly elastic behavior at low temperatures, with a well-defined transition temperature termed T_{gel}. The crossover temperature at which $G' = G''$ is used as a convenient indicator of T_{gel}, which represents the temperature at which the gel has a longest relaxation time comparable to the timescale of the experiment. The higher T_{gel}s of the VOV(2-35-2)-based gels (**3** and **4**) compared with the VOV(1-35-1)-based gels (**1** and **2**) are consistent with previous results described in Chapter 3, since the fraction of hydrogen-bonded pyridine units on a P2VP block needed to reach T_{gel} decreases with increasing P2VP block length. Furthermore, in **3** and **4**, wide temperature-independent rubbery plateaus in G' are evident at low temperatures, indicating the formation of a well-defined network structure, which does not evolve appreciably with temperature. In contrast, G' of **1** and **2** is still increasing upon cooling, suggesting the network structure is evolving with temperature.

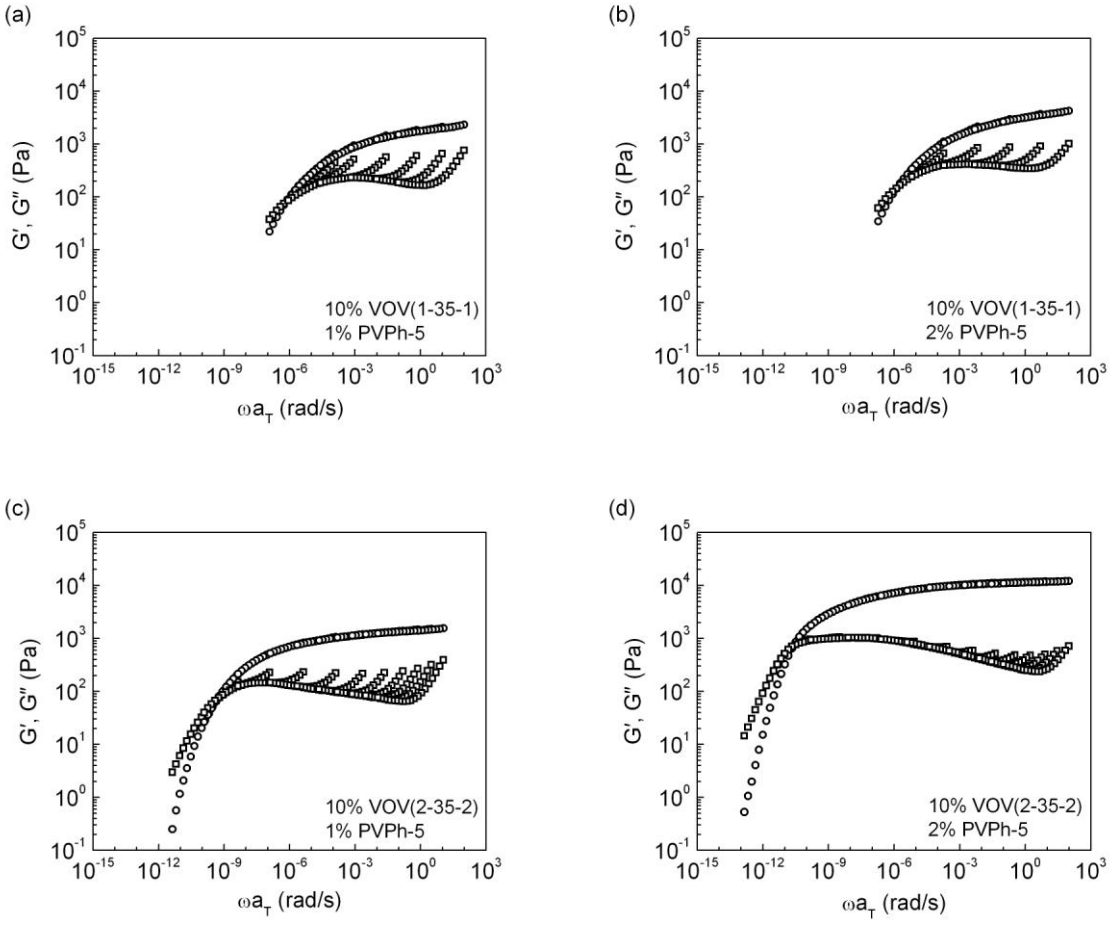

Figure 6.5 tTS master curves of G' (○) and G'' (□) versus reduced frequency. A uniform reference temperature of 30 ℃ was used. See the lower right-hand corner of each plot for identity details.

Dynamic frequency sweeps were performed every 10 ℃ at various temperatures. Time–temperature superposition (tTS) was satisfactorily applied to generate master curves for all gels, indicating that the governing relaxation processes have similar temperature dependence. The resulting shift factors are shown in Figure 6.6. The systematic deviations in G'' from tTS at the high-frequency end of low-temperature data was attributed to the relaxation of the PEO network strands.

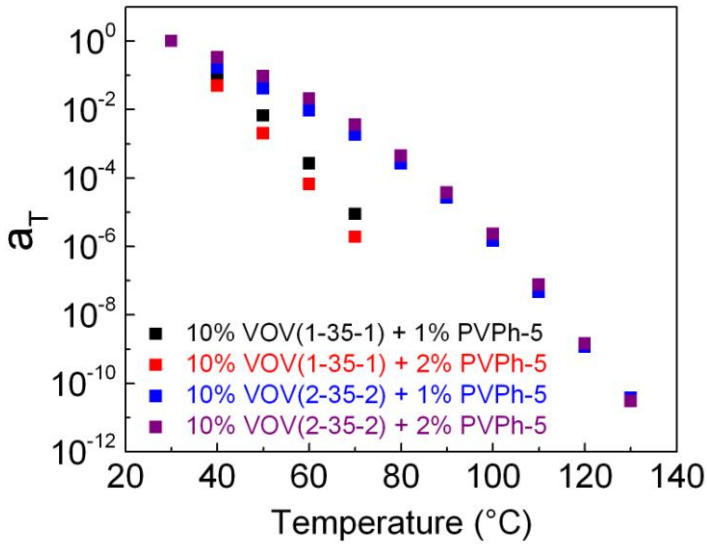

Figure 6.6 Temperature dependence of shift factors used in generating the master curves of Figure 6.5.

The most important observation is the rather low modulus of the VOV(1-35-1)-based gels (**1** and **2**). Since $n(T_{gel}) \approx 6$ at 30 ℃, at least 6 hydrogen bonds are required for a

given P2VP↔PVPh association to contribute to the equilibrium elasticity of the network. However, the fairly short P2VP blocks in VOV(1-35-1) render the formation of 6 hydrogen bonds per association rather difficult, due to steric hindrance. Therefore, the origin of the low modulus of the VOV(1-35-1)-based gels is attributed to the existence of a significant amount of dynamic chains (less than 6 hydrogen bonds per association), due to the limited number of pyridine units available on the P2VP blocks.

The low modulus of **3** was previously attributed to the existence of a significant amount of dangling ends,[14] due to inadequate cross-linker. However, there is an inherent defect in this interpretation. With the assumption that $n(T_{gel}) \approx 1$, it was estimated that 5 hydrogen bonds are formed on a given P2VP block. Nevertheless, it seems very unlikely that a certain fraction of P2VP blocks has 5 hydrogen bonds, whereas the remaining P2VP blocks are completely free with no hydrogen bonds at all. With the conclusion that $n(T_{gel}) \approx 6$ at 30 ℃, a more reasonable explanation is that while presumably every P2VP block is hydrogen-bonded with a PVPh cross-link, only those with at least 6 hydrogen bonds are elastically effective.

The absolute number of hydrogen bonds per P2VP↔PVPh association can be estimated from the temperature dependence of shift factors.

$$n(T) = n(T_{gel})\frac{T}{T_{gel}} + \frac{RT}{E}\ln\frac{a_T}{a_{T_{gel}}} \qquad (6.3)$$

The temperature dependence of $n(T)$ is shown in Figure 6.7. The saturation of $n(T)$ at low temperatures simply reflects the formation of the maximum number of hydrogen bonds, restricted by the limited number of pyridine or phenol units. Also, the absolute

number of hydrogen bonds is about one half of the degree of polymerization of the P2VP block, presumably due to steric hindrance. The solid line in Figure 6.7 represents $n(T)$ needed for gel point from Figure 6.3, where excellent agreement with the actual gel points is achieved.

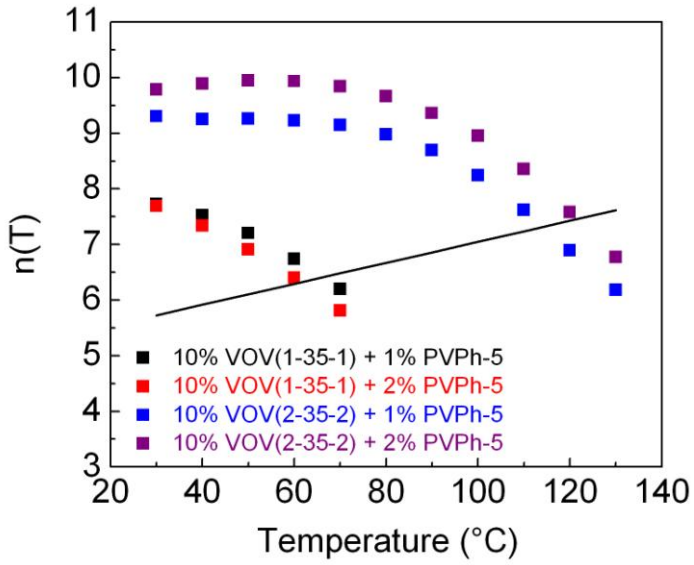

Figure 6.7 Temperature dependence of $n(T)$ calculated from equation 6.3. The solid line represents $n(T)$ needed for gel point from Figure 6.3.

6.2.4 Equilibrium Constant of Hydrogen Bond Formation

The equilibrium constant (K_{eq}) of hydrogen bond complex formation can be estimated from a straightforward analysis (K_{eq} = [complex]/[phenol][pyridine]). For example, the total concentrations of phenol and pyridine in **4** are 0.236 and 0.138 M, respectively. Since T_{gel} = 127 ℃, the number of hydrogen bonds per association at the gel point is *ca.* 8 from Figure 6.3. Therefore, the concentrations of hydrogen bond complex, free phenol, and free pyridine are estimated to be 0.0552, 0.181, and 0.0828 M, respectively, yielding $K_{eq} = 3.7\ M^{-1}$ at T_{gel}. The temperature dependence of K_{eq} is given by

$$\ln K_{eq} = -\frac{\Delta G^0}{RT} = -\frac{\Delta H^0}{RT} + \frac{\Delta S^0}{R} \qquad (6.4)$$

where ΔG^0, ΔH^0, and ΔS^0 are the standard Gibbs free energy, the enthalpy, and the entropy of complex formation, respectively. Assume ΔH^0 and ΔS^0 are temperature independent, $\Delta H^0 = -13$ kJ/mol

$$\Delta S^0 = R \ln K_{eq} + \frac{\Delta H^0}{T} \qquad (6.5)$$

$\Delta S^0 = -21.6\ J\ mol^{-1}\ K^{-1}$

K_{eq} at any given temperature is calculated from equation 6.4 and plotted in Figure 6.8.

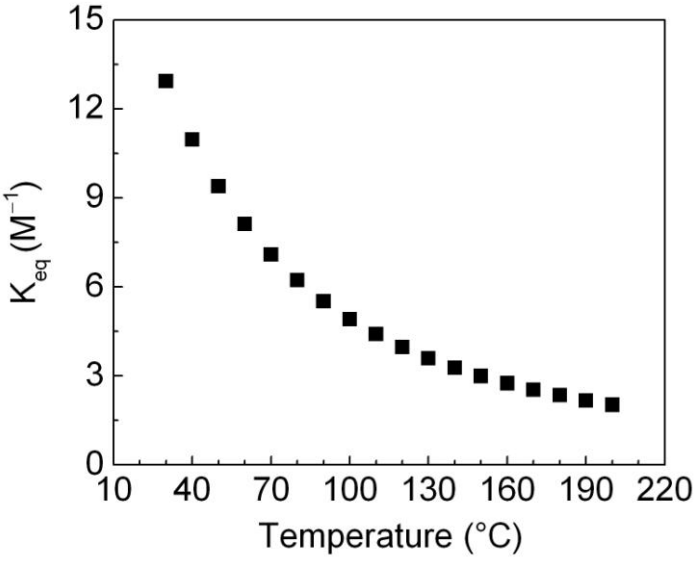

Figure 6.8 Temperature dependence of the equilibrium constant.

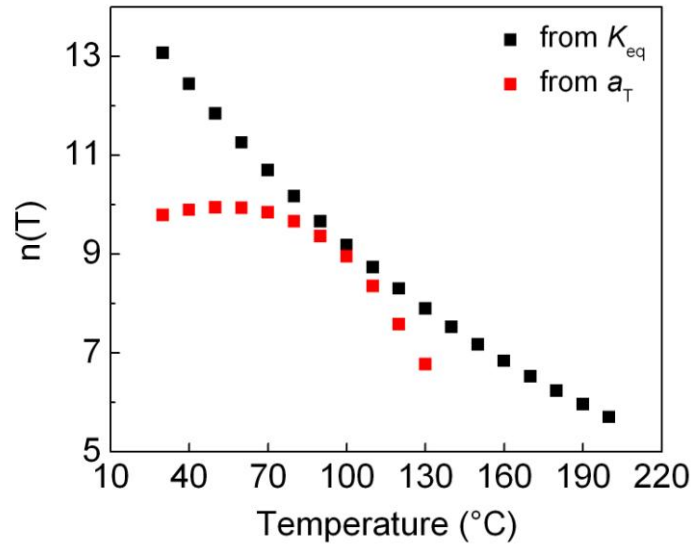

Figure 6.9 $n(T)$ calculated from equilibrium constant K_{eq} and shift factor a_T.

To push this analysis one step further, we can estimate the number of hydrogen bonds based on values of K_{eq}, which is plotted in Figure 6.9 and compared with those estimated from shift factors.

It can be seen that $n(T)$ calculated from a_T saturates at low temperatures, which simply reflects the formation of the maximum number of hydrogen bonds, due to the limited availability of either pyridine units on P2VP blocks or phenol units on PVPh cross-linkers. The deviation at high temperatures might come from the steric hindrance to form an actual hydrogen bond. This system is not therefore under equilibrium, especially at low temperatures.

6.2.5 Small-Angle X-ray Scattering

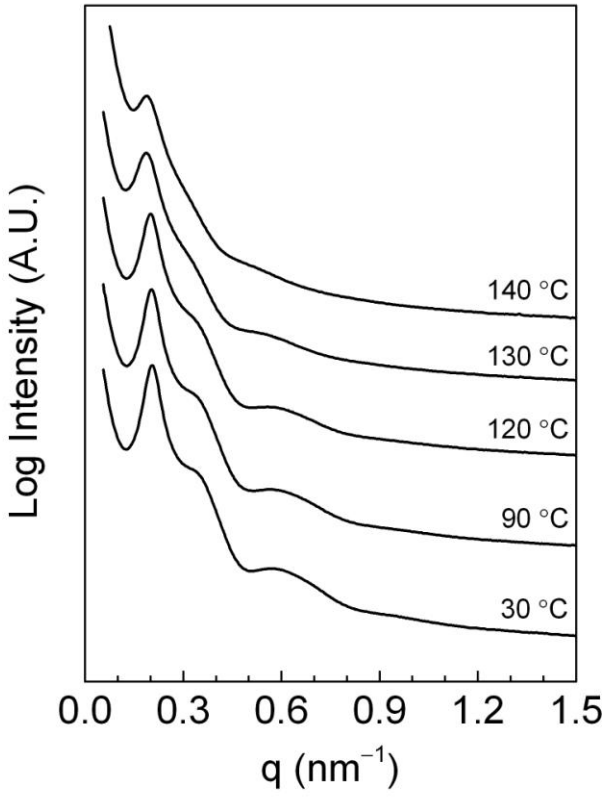

Figure 6.10 Variable temperature small-angle X-ray scattering (VT-SAXS) data from **4** recorded on heating.

Figure 6.10 shows VT-SAXS data from **4** recorded on heating, which has a gel point of 127 ℃. At temperatures higher than the gel point, the structure factor can still be seen, suggesting the existence of quite stable hydrogen-bonded phase. This observation also supports the conclusion that multiple hydrogen bonds per association are involved at the

gel point, because a single hydrogen bond would be expected to break up just above the gel point. Therefore, the polymer network would break down into free chains, and a homogeneous phase would be present. The complete dissociation of the hydrogen-bonded microdomains would result in the disappearance of the structure factor, since the X-ray contrast in the gel originates from the difference in electron density between the dense hydrogen-bonded P2VP/PVPh microdomains and the well-solvated PEO chains.

6.3 Conclusions

In this chapter, we have addressed an interesting and fundamental question as to how many hydrogen bonds per P2VP↔PVPh association are required at the gel point. The lifetime of a single phenol–pyridine hydrogen bond in [EMIM][TFSA] is estimated to be on the order of sub-nanoseconds, based on an empirical relationship from the literature. This ultrafast hydrogen bond dynamics implies that multiple hydrogen bonds per association are involved at the gel point, whereby the total activation energy is increased. While the lifetime of a single phenol–pyridine hydrogen bond varies by less than an order of magnitude over the temperature range of 30–180 ℃, the lifetime of an association changes by 15 orders of magnitude over the same temperature range. The most important conclusion is that multiple hydrogen bonds per P2VP↔PVPh association are required to generate a polymer network that is sufficiently stable over the timescale of seconds. In particular, at least 6 hydrogen bonds per association are required at room temperature and

this value slightly depends on the gel point itself, due to the weak temperature dependence of the lifetime of a single hydrogen bond.

6.4 References

(1) Jeffrey, G. A. *An Introduction to Hydrogen Bonding*; Oxford University Press, Inc.: New York, 1997.

(2) Desiraju, G. R.; Steiner, T. *The Weak Hydrogen Bond: in Structural Chemistry and Biology*; Oxford: New York, 1999.

(3) Woutersen, S.; Mu, Y.; Stock, G.; Hamm, P. *Chem. Phys.* **2001,** *266*, 137–147.

(4) Nibbering, E. T. J.; Elsaesser, T. *Chem. Rev.* **2004,** *104*, 1887–1914.

(5) Kim, Y. S.; Hochstrasser, R. M. *Proc. Natl. Acad. Sci. USA* **2005,** *102*, 11185–11190.

(6) Zheng, J.; Kwak, K.; Asbury, J.; Chen, X.; Piletic, I. R.; Fayer, M. D. *Science* **2005,** *309*, 1338–1343.

(7) Zheng, J.; Kwak, K.; Chen, X.; Asbury, J. B.; Fayer, M. D. *J. Am. Chem. Soc.* **2006,** *128*, 2977–2987.

(8) Zheng, J.; Kwak, K.; Fayer, M. D. *Acc. Chem. Res.* **2007,** *40*, 75–83.

(9) Zheng, J.; Fayer, M. D. *J. Am. Chem. Soc.* **2007,** *129*, 4328–4335.

(10) Zheng, J.; Fayer, M. D. *J. Phys. Chem. B* **2008,** *112*, 10221–10227.

(11) Sijbesma, R. P.; Beijer, F. H.; Brunsveld, L.; Folmer, B. J. B.; Hirschberg, J. H. K. K.; Lange, R. F. M.; Lowe, J. K. L.; Meijer, E. W. *Science* **1997,** *278*, 1601–1604.

(12) Söntjens, S. H. M.; Sijbesma, R. P.; van Genderen, M. H. P.; Meijer, E. W. *J. Am. Chem. Soc.* **2000,** *122*, 7487–7493.

(13) Noro, A.; Matsushita, Y.; Lodge, T. P. *Macromolecules* **2008,** *41*, 5839–5844.

(14) Noro, A.; Matsushita, Y.; Lodge, T. P. *Macromolecules* **2009,** *42*, 5802–5810.

Chapter 7

Summary and Outlook

7.1 Summary

The objective of this thesis research is to elucidate the underlying mechanisms that control the structure and dynamics in the supramolecular polymer networks formed by hydrogen bonding in ionic liquids. The substantially wide liquidus temperature range of the ionic liquid affords access to interesting and unprecedented rheological signatures of the resulting gels. For example, the longest relaxation time changes by 15 decades from the gel temperature down to room temperature; extremely wide temperature- and frequency-independent rubbery plateaus are pronounced, indicating the formation of a well-defined polymer network structure; the applicability of time–temperature superposition is striking, suggesting the invariance of the underlying relaxation mechanism. Furthermore, from a practical perspective, since ionic liquids have appealing electrochemical properties, such as high ionic conductivity and wide electrochemical windows, these ion gels are targeted for applications in various electrochemical devices, where two particular examples are organic transistors and electrochemical capacitors.[1,2]

The most impressive feature of this system is the strong temperature dependence of the viscoelastic properties, which was tentatively attributed to the formation of multiple hydrogen bonds on a single P2VP↔PVPh association, and therefore different activation energies are involved at different temperatures. It was further hypothesized that the

terminal relaxation time is determined by the average lifetime of a P2VP↔PVPh association, which is directly related to the number of hydrogen bonds involved. This hypothesis has been qualitatively tested by varying the P2VP block length. The terminal relaxation dynamics is dramatically retarded upon increasing the P2VP block length. The self-association of phenolic hydroxyl groups results in the aggregation of PVPh cross-linker chains in a cross-link. The size of a cross-link is essentially independent of the PVPh cross-linker length, as manifested by the minor effect on terminal relaxation time and gel temperature of cross-linker length.

The mechanical properties of this system are tunable over a significantly wide range. Low-viscosity solutions of the parent copolymer could be developed into elastic gels with tunable modulus (in the range of 2000–15000 Pa) simply by varying the concentration of the PVPh cross-linker added. Interestingly, the modulus goes through a maximum instead of increasing monotonically with the cross-linker concentration. This tunability essentially reflects significant changes in the microstructure of the hydrogen-bonded polymer networks. Therefore, matching the concentrations of the triblock and cross-linker such that the hydrogen bonding donors and acceptors are present under a certain stoichiometric balance is particularly important to achieve optimal mechanical properties.

The hydrogen-bonded phase can rearrange into a hexagonal morphology with long-range ordering after high-temperature annealing for a sufficient period of time. The thermodynamic stability of this hexagonal phase is limited at low temperature by chain exchange and at high temperature by the eventual dissolution of the hydrogen-bonded network microdomains. The slow kinetics of this structural development results in a

significant hysteresis at high temperatures in the rheological response during a cooling–heating cycle.

Because the dissociation energies of hydrogen bonds are on the order of a few $k_B T$, they continually dissociate and reform under thermal equilibrium with ultrafast dynamics. Estimating the lifetime of a single phenol–pyridine hydrogen bond in [EMIM][TFSA] based on an empirical relationship found in the literature yields values on the order of sub-nanoseconds. We therefore conclude that multiple hydrogen bonds per P2VP↔PVPh association are required to generate a polymer network that is sufficiently stable over a timescale of seconds. In particular, at least 6 hydrogen bonds per P2VP↔PVPh association are required at room temperature; this value slightly depends on the gel point itself, due to the weak temperature dependence of the lifetime of a single hydrogen bond.

7.2 Outlook

Nonlinear rheology is of particular interest for future research. The rheology presented in this thesis has been limited to the linear regime. However, nonlinear behavior is also interesting and very important, especially for processing considerations, where large strains and high strain rates are typically applied. Nonlinear rheological response, such as strain stiffening and shear thickening, often exhibits unexpectedly varied behavior from one system to another and is thus substantially more complicated than the linear response. As a result, complementary experimental and theoretical efforts have been devoted to understanding the underlying molecular mechanisms of nonlinear

rheological response.[3–8] When soft polymeric materials are subjected to nonlinear deformations, the corresponding rheological response is determined by the relationship between the structure of the material and the nature of the imposed deformation. In order to qualitatively compare the behavior of materials with strikingly different relaxation times, a reduced shear rate (Γ) is introduced, defined as the product of the characteristic relaxation time of the material (τ) and the applied shear rate ($\dot{\gamma}$).[3]

$$\Gamma = \tau\dot{\gamma} \tag{7.1}$$

The magnitude of Γ determines whether the material can structurally rearrange to accommodate the applied stress. Therefore, elastic and viscous behavior would be expected for $\Gamma >> 1$ and $\Gamma << 1$, respectively. In our thermoreversible supramolecular ion gels, the strongly temperature-dependent relaxation times afford access well into both the low-Γ and high-Γ regimes without changing the structural features of the system, making them ideal model systems for studying nonlinear rheological behavior in physically associating gels.

7.3 References

(1) Zhang, S. Ph.D. Dissertation, University of Minnesota, 2012.

(2) Lee, K. H. Ph.D. Dissertation, University of Minnesota, 2012.

(3) Berret, J.-F.; Séréro, Y.; Winkelman, B.; Calvet, D.; Collet, A.; Viguier, M. *J. Rheol.* **2001,** *45*, 477–492.

(4) Seitz, M. E.; Martina, D.; Baumberger, T.; Krishnan, V. R.; Hui, C.-Y.; Shull, K. R. *Soft Matter* **2009,** *5*, 447–456.

(5) Creton, C.; Hu, G.; Deplace, F.; Morgret, L.; Shull, K. R. *Macromolecules* **2009,** *42*, 7605–7615.

(6) Erk, K. A.; Henderson, K. J.; Shull, K. R. *Biomacromolecules* **2010,** *11*, 1358–1363.

(7) Erk, K. A.; Shull, K. R. *Macromolecules* **2011,** *44*, 932–939.

(8) Xu, D.; Craig, S. L. *Macromolecules* **2011,** *44*, 7478–7488.

Bibliography

Aboudzadeh, M. A.; Muñoz, M. E.; Santamaría, A.; Fernández-Berridi, M. J.; Irusta, L.; Mecerreyes, D. *Macromolecules* **2012,** *45*, 7599–7606.

Aida, T.; Meijer, E. W.; Stupp, S. I. *Science* **2012,** *335*, 813–817.

Almdal, K.; Dyre, J.; Hvidt, S.; Kramer, O. *Polym. Gels Networks* **1993,** *1*, 5–17.

Ambrožič, G.; Žigon, M. *Macromol. Rapid Commun.* **2000,** *21*, 53–56.

Andres, P. R.; Schubert, U. S. *Adv. Mater.* **2004,** *16*, 1043–1068.

Armand, M.; Endres, F.; MarFarlane, D. R.; Ohno, H.; Scrosati, B. *Nat. Mater.* **2009,** *8*, 621–629.

Bai, Z.; He, Y.; Lodge, T. P. *Langmuir* **2008,** *24*, 5284–5290.

Bai, Z.; He, Y.; Young, N. P.; Lodge, T. P. *Macromolecules* **2008,** *41*, 6615–6617.

Bai, Z.; Lodge, T. P. *J. Phys. Chem. B* **2009,** *113*, 14151–14157.

Bai, Z.; Lodge, T. P. *Langmuir* **2010,** *26*, 8887–8892.

Beck, J. B.; Rowan, S. J. *J. Am. Chem. Soc.* **2003,** *125*, 13922–13923.

Beijer, F. H.; Kooijman, H.; Spek, A. L.; Sijbesma, R. P.; Meijer, E. W. *Angew. Chem. Int. Ed.* **1998,** *37*, 75–78.

Beijer, F. H.; Sijbesma, R. P.; Kooijman, H.; Spek, A. L.; Meijer, E. W. *J. Am. Chem. Soc.* **1998,** *120*, 6761–6769.

Berl, V.; Schmutz, M.; Krische, M. J.; Khoury, R. G.; Lehn, J.-M. *Chem. Eur. J.* **2002,** *8*, 1227–1244.

Berret, J.-F.; Séréro, Y.; Winkelman, B.; Calvet, D.; Collet, A.; Viguier, M. *J. Rheol.* **2001,** *45*, 477–492.

Biedroń, T.; Bednarek, M.; Kubisa, P. *Macromol. Rapid Commun.* **2004,** *25*, 878–881.

Blaiszik, B. J.; Kramer, S. L. B.; Olugebefola, S. C.; Moore, J. S.; Sottos, N. R.; White, S. R. *Annu. Rev. Mater. Res.* **2010,** *40*, 179–211.

Bras, R. E.; Shull, K. R. *Macromolecules* **2009,** *42*, 8513–8520.

Bruce, P. G.; Vincent, C. A. *J. Chem. Soc., Faraday Trans.* **1993,** *89*, 3187–3203.

Brunsveld, L.; Folmer, B. J. B.; Meijer, E. W.; Sijbesma, R. P. *Chem. Rev.* **2001,** *101*, 4071–4097.

Burnworth, M.; Tang, L.; Kumpfer, J. R.; Duncan, A. J.; Beyer, F. L.; Fiore, G. L.; Rowan, S. J.; Weder, C. *Nature* **2011,** *472*, 334–337.

Cai, H.; Ait-Kadi, A.; Brisson, J. *Polymer* **2003,** *44*, 1481–1489.

Carmichael, A. J.; Haddleton, D. M.; Bon, S. A. F.; Seddon, K. R. *Chem. Commun.* **2000,** 1237–1238.

Cates, M. E. *Macromolecules* **1987,** *20*, 2289–2296.

Cavicchi, K. A.; Lodge, T. P. *Macromolecules* **2003,** *36*, 7158–7164.

Chantawansri, T. L.; Duncan, A. J.; Ilavsky, J.; Stokes, K. K.; Berg, M. C.; Mrozek, R. A.; Lenhart, J. L.; Beyer, F. L.; Andzelm, J. W. *J. Polym. Sci., Part B: Polym. Phys.* **2011,** *49*, 1479–1491.

Chiefari, J.; Chong, Y. K.; Ercole, F.; Kristina, J.; Jeffery, J.; Le, T. P. T.; Mayadunne, R. T. A.; Meijs, G. F.; Moad, C. L.; Moad, G.; Rizzardo, E.; Thang, S. H. *Macromolecules* **1998,** *31*, 5559−5562.

Cho, J. H.; Lee, J.; He, Y.; Kim, B. S.; Lodge, T. P.; Frisbie, C. D. *Adv. Mater.* **2008,** *20*, 686–690.

Cho, J. H.; Lee, J.; Xia, Y.; Kim, B.; He, Y.; Renn, M. J.; Lodge, T. P.; Frisbie, C. D. *Nat. Mater.* **2008,** *7*, 900–906.

Choi, S.-H.; Lodge, T. P.; Bates, F. S. *Macromolecules* **2011,** *44*, 3594–3604.

Choi, S.-H.; Lodge, T. P.; Bates, F. S. *Phys. Rev. Lett.* **2010,** *104*, 047802.

Cooke, G.; Rotello, V. M. *Chem. Soc. Rev.* **2002,** *31*, 275–286.

Cordier, P.; Tournilhac, F.; Souli é-Ziakovic, C.; Leibler, L. *Nature* **2008,** *451*, 977–980.

Creton, C.; Hu, G.; Deplace, F.; Morgret, L.; Shull, K. R. *Macromolecules* **2009,** *42*, 7605–7615.

Dai, J.; Goh, S. H.; Lee, S. Y.; Siow, K. S. *Polym. J.* **1994,** *26*, 905–911.

de Gennes, P. G. *J. Chem. Phys.* **1971,** *55*, 572–579.

de Greef, T. F. A.; Meijer, E. W. *Nature* **2008,** *453*, 171–173.

Desiraju, G. R.; Steiner, T. *The Weak Hydrogen Bond: in Structural Chemistry and Biology*; Oxford: New York, 1999.

Ding, J.; Zhou, D.; Spinks, G.; Wallace, G.; Forsyth, S.; Forsyth, M.; MacFarlane, D. *Chem. Mater.* **2003,** *15*, 2392−2398.

Drzal, P. L.; Shull, K. R. *Macromolecules* **2003,** *36*, 2000–2008.

Dupont, J.; de Souza, R. F.; Suarez, P. A. Z. *Chem. Rev.* **2002,** *102*, 3667–3692.

Earle, M. J.; Esperança, J. M. S. S.; Gilea, M. A.; Canongia Lopes, J. N.; Rebelo, L. P. N.; Magee, J. W.; Seddon, K. R.; Widegren, J. A. *Nature* **2006,** *439*, 831–834.

Erk, K. A.; Henderson, K. J.; Shull, K. R. *Biomacromolecules* **2010,** *11*, 1358–1363.

Erk, K. A.; Shull, K. R. *Macromolecules* **2011,** *44*, 932–939.

Faul, C. F. J.; Antonietti, M. *Adv. Mater.* **2003,** *15*, 673–683.

Feldman, K. E.; Kade, M. J.; de Greef, T. F. A.; Meijer, E. W.; Kramer, E. J.; Hawker, C. J. *Macromolecules* **2008,** *41*, 4694–4700.

Feldman, K. E.; Kade, M. J.; Meijer, E. W.; Hawker, C. J.; Kramer, E. J. *Macromolecules* **2009,** *42*, 9072–9081.

Fenton, D. E.; Parker, J. M.; Wright, P. V. *Polymer* **1973,** *14*, 589–589.

Ferry, J. D. *Viscoelastic Properties of Polymers*, 3rd ed.; John Wiley & Sons: New York, 1980.

Fetters, L. J.; Lohse, D. J.; Richter, D.; Witten, T. A.; Zirkel, A. *Macromolecules* **1994,** *27*, 4639–4647.

Flanigan, C. M.; Crosby, A. J.; Shull, K. R. *Macromolecules* **1999,** *32*, 7251–7262.

Folmer, B. J. B.; Sijbesma, R. P.; Versteegen, R. M.; van der Rijt, J. A. J.; Meijer, E. W. *Adv. Mater.* **2000,** *12*, 874–878.

Fustin, C.-A.; Guillet, P.; Schubert, U. S.; Gohy, J.-F. *Adv. Mater.* **2007,** *19*, 1665–1673.

Greaves, T. L.; Drummond, C. J. *Chem. Soc. Rev.* **2008,** *37*, 1709–1726.

Green, M. S.; Tobolsky, A. V. *J. Chem. Phys.* **1946,** *14*, 80–92.

Gu, Y.; Lodge, T. P. *Macromolecules* **2011,** *44*, 1732–1736.

Guan, Y.; Yu, S.-H.; Antonietti, M.; Böttcher, C.; Faul, C. F. J. *Chem. Eur. J.* **2005,** *11*, 1305–1311.

Hallett, J. P.; Welton, T. *Chem. Rev.* **2011,** *111*, 3508–3576.

Halperin, A.; Alexander, S. *Macromolecules* **1989,** *22*, 2403–2412.

Hamley, I. W. *Block Copolymers in Solution: Fundamentals and Applications*; John Wiley & Sons, Ltd.: Chichester, 2005.

Han, X.; Armstrong, D. W. *Acc. Chem. Res.* **2007,** *40*, 1079–1086.

Harrisson, S.; Mackenzie, S. R.; Haddleton, D. M. *Chem. Commun.* **2002,** 2850–2851.

Harrisson, S.; Mackenzie, S. R.; Haddleton, D. M. *Macromolecules* **2003,** *36*, 5072–5075.

He, Y.; Boswell, P. G.; Bühlmann, P.; Lodge, T. P. *J. Phys. Chem. B* **2007,** *111*, 4645–4652.

He, Y.; Li, Z.; Simone, P.; Lodge, T. P. *J. Am. Chem. Soc* **2006,** *128*, 2745–2750.

He, Y.; Lodge, T. P. *Chem. Commun.* **2007,** 2732–2734.

He, Y.; Lodge, T. P. *J. Am. Chem. Soc* **2006,** *128*, 12666–12667.

He, Y.; Lodge, T. P. *Macromolecules* **2008,** *41*, 167–174.

Hiemenz, P. C.; Lodge, T. P. *Polymer Chemistry,* 2nd ed.; CRC Press: New York, 2007.

Hirschberg, J. H. K. K.; Beijer, F. H.; van Aert, H. A.; Magusin, P. C. M. M.; Sijbesma, R. P.; Meijer, E. W. *Macromolecules* **1999,** *32*, 2696–2705.

Hirst, A. R.; Escuder, B.; Miravet, J. F.; Smith, D. K. *Angew. Chem. Int. Ed.* **2008,** *47*, 8002–8018.

Hofmeier, H.; Schubert, U. S. *Chem. Soc. Rev.* **2004,** *33*, 373–399.

Inomata, K.; Nakanishi, D.; Banno, A.; Nakanishi, E.; Abe, Y.; Kurihara, R.; Fujimoto, K.; Nose, T. *Polymer* **2003,** *44*, 5303–5310.

Jeffrey, G. A. *An Introduction to Hydrogen Bonding*; Oxford University Press, Inc.: New York, 1997.

Kim, Y. S.; Hochstrasser, R. M. *Proc. Natl. Acad. Sci. USA* **2005,** *102*, 11185–11190.

Kitazawa, Y.; Ueki, T.; Niitsuma, K.; Imaizumi, S.; Lodge, T. P.; Watanabe, M. *Soft Matter* **2012,** *8*, 8067–8074.

Kleppinger, R.; Mischenko, N.; Reynaers, H. L.; Koch, M. H. J. *J. Polym. Sci., Part A: Polym. Phys.* **1999,** *37*, 1833–1840.

Kleppinger, R.; Mischenko, N.; Theunissen, E.; Reynaers, H. L. *Macromolecules* **1997,** *30*, 7012–7014.

Kleppinger, R.; Reynders, K.; Mischenko, N.; Overbergh, N.; Koch, M. H. J.; Mortensen, K.; Reynaers, H. *Macromolecules* **1997,** *30*, 7008–7011.

Klingshirn, M. A.; Spear, S. K.; Subramanian, R.; Holbrey, J. D. Huddleston, J. G.; Rogers, R. D. *Chem. Mater.* **2004,** *16*, 3091–3097.

Kodama, K.; Nanashima, H.; Ueki, T.; Kokubo, H.; Watanabe, M. *Langmuir* **2009,** *25*, 3820–3824.

Kolomiets, E.; Buhler, E.; Candau, S. J.; Lehn, J.-M. *Macromolecules* **2006,** *39*, 1173–1181.

Kubisa, P. *Prog. Polym. Sci.* **2009,** *34*, 1333–1347.

Kuwabata, S.; Tsuda, T.; Torimoto, T. *J. Phys. Chem. Lett.* **2010,** *1*, 3177–3188.

Lai, J. T.; Filla, D.; Shea, R. *Macromolecules* **2002,** *35*, 6754−6756.

Lange, R. F. M.; van Gurp, M.; Meijer, E. W. *J. Polym. Sci., Part A: Polym. Chem.* **1999,** *37*, 3657−3670.

Larson, R. G. *The Structure and Rheology of Complex Fluids*; Oxford University Press: New York, 1999.

Laurer, J. H.; Bukovnik, R.; Spontak, R. J. *Macromolecules* **1996,** *29*, 5760–5762.

Laurer, J. H.; Khan, S. A.; Spontak, R. J.; Satkowski, M. M.; Grothaus, J. T.; Smith, S. D.; Lin, J. S. *Langmuir* **1999,** *15*, 7947–7955.

Laurer, J. H.; Mulling, J. F.; Khan, S. A.; Spontak, R. J.; Bukovnik, R. *J. Polym. Sci., Part B: Polym. Phys.* **1998,** *36*, 2379–2391.

Laurer, J. H.; Mulling, J. F.; Khan, S. A.; Spontak, R. J.; Lin, J. S.; Bukovnik, R. *J. Polym. Sci., Part B: Polym. Phys.* **1998,** *36*, 2513–2523.

Lee, H.-N.; Bai, Z.; Newell, N.; Lodge, T. P. *Macromolecules* **2010,** *43*, 9522–9528.

Lee, H.-N.; Lodge, T. P. *J. Phys. Chem. Lett.* **2010,** *1*, 1962–1966.

Lee, J.; Kaake, L. G.; Cho, J. H.; Zhu, X.-Y.; Lodge, T. P.; Frisbie, C. D. *J. Phys. Chem. C* **2009,** *113*, 8972–8981.

Lee, J.; Panzer, M. J.; He, Y.; Lodge, T. P.; Frisbie, C. D. *J. Am. Chem. Soc.* **2007,** *129*, 4532–4533.

Lee, K. H. Ph.D. Dissertation, University of Minnesota, 2012.

Lee, K. H.; Zhang, S.; Lodge, T. P.; Frisbie, C. D. *J. Phys. Chem. B* **2011,** *115*, 3315–3321.

Lee, L.-T.; Woo, E. M.; Hou, S. S.; Förster, S. *Polymer* **2006,** *47*, 8350–8359.

Lehn, J.-M. *Angew. Chem. Int. Ed. Engl.* **1990,** *29*, 1304–1319.

Lei, Y.; Lodge, T. P. *Soft Matter* **2012,** *8*, 2110–2120.

Leibler, L.; Rubinstein, M.; Colby, R. H. *Macromolecules* **1991,** *24*, 4701–4707.

Lewandowski, A.; Świderska, A. *Solid State Ionics* **2004,** *169*, 21–24.

Li, J.; Viveros, J. A.; Wrue, M. H.; Anthamatten, M. *Adv. Mater.* **2007,** *19*, 2851–2855.

Lodge, A. S. *Trans. Faraday Soc.* **1956,** *52*, 120–130.

Lodge, T. P. *Science* **2008,** *321*, 50–51.

Lu, J.; Yan, F.; Texter, J. *Prog. Polym. Sci.* **2009,** *34*, 431–448.

Lu, W.; Fadeev, A. G.; Qi, B.; Smela, E.; Mattes, B. R.; Ding, J.; Spinks, G. M.; Mazurkiewicz, J.; Zhou, D.; Wallace, G. G.; MacFarlane, D. R.; Forsyth, S. A.; Forsyth, M. *Science* **2002,** *297*, 983−987.

Ma, H.; Wan, X.; Chen, X.; Zhou, Q.-F. *J. Polym. Sci., Part A: Polym. Chem.* **2003,** *41*, 143–151.

Macosko, C. W. *Rheology: Principles, Measurements and Applications*; Wiley-VCH: New York, 1994.

Maddikeri, R. R.; Colak, S.; Gido, S. P.; Tew, G. N. *Biomacromolecules* **2011,** *12*, 3412–3417.

Meli, L.; Lodge, T. P. *Macromolecules* **2009,** *42*, 580–583.

Meli, L.; Santiago, J. M.; Lodge, T. P. *Macromolecules* **2010,** *43*, 2018–2027.

Meyer, W. H. *Adv. Mater.* **1998,** *10*, 439–448.

Mischenko, N.; Reynders, K.; Koch, M. H. J.; Mortensen, K.; Pedersen, J. S.; Fontaine, F.; Graulus, R.; Reynaers, H. *Macromolecules* **1995,** *28*, 2054–2062.

Moad, G.; Rizzardo, E.; Thang, S. H. *Aust. J. Chem.* **2005,** *58*, 379−410.

Montarnal, D.; Tournilhac, F.; Hidalgo, M.; Couturier, J.-L.; Leibler, L. *J. Am. Chem. Soc.* **2009,** *131*, 7966–7967.

Mortensen, K.; Theunissen, E.; Kleppinger, R.; Almdal, K.; Reynaers, H. *Macromolecules* **2002,** *35*, 7773–7781.

Müller, M.; Dardin, A.; Seidel, U.; Balsamo, V.; Iván, B.; Spiess, H. W.; Stadler, R. *Macromolecules* **1996,** *29*, 2577–2583.

Nair, K. P.; Breedveld, V.; Weck, M. *Macromolecules* **2008,** *41*, 3429–3438.

Nair, K. P.; Breedveld, V.; Weck, M. *Macromolecules* **2011,** *44*, 3346–3357.

Nair, K. P.; Breedveld, V.; Weck, M. *Soft Matter* **2011,** *7*, 553–559.

Nibbering, E. T. J.; Elsaesser, T. *Chem. Rev.* **2004,** *104*, 1887–1914.

Noro, A.; Hayashi, M.; Matsushita, Y. *Soft Matter* **2012,** *8*, 2416–2429.

Noro, A.; Hayashi, M.; Ohshika, A.; Matsushita, Y. *Soft Matter* **2011,** *7*, 1667–1670.

Noro, A.; Matsushita, Y.; Lodge, T. P. *Macromolecules* **2008,** *41*, 5839–5844.

Noro, A.; Matsushita, Y.; Lodge, T. P. *Macromolecules* **2009,** *42*, 5802–5810.

Noro, A.; Yamagishi, H.; Matsushita, Y. *Macromolecules* **2009,** *42*, 6335–6338.

Obert, E.; Bellot, M.; Bouteiller, L.; Andrioletti, F.; Lehen-Ferrenbach, C.; Boué, F. *J. Am. Chem. Soc.* **2007,** *129*, 15601–15605.

Ohno, H.; Yoshizawa, M.; Ogihara, W. *Electrochim. Acta* **2004,** *50*, 255–261.

Ozair, S. N. Ph.D. Dissertation, University of Minnesota, 2009.

Pârvulescu, V. I.; Hardacre, C. *Chem. Rev.* **2007,** *107*, 2615–2665.

Perrier, S.; Davis, T. P.; Carmichael, A. J.; Haddleton, D. M. *Chem. Commun.* **2002,** 2226–2227.

Pham, T. P. T.; Cho, C.-W.; Yun, Y.-S. *Water Res.* **2010,** *44*, 352–372.

Piepenbrock, M.-O. M.; Lloyd, G. O.; Clarke, N.; Steed, J. W. *Chem. Rev.* **2010,** *110*, 1960–2004.

Pinkert, A.; Marsh, K. N.; Pang, S.; Staiger, M. P. *Chem. Rev.* **2009,** *109*, 6712–6728.

Puigmartí-Luis, J.; Laukhin, V.; Pérez del Pino, Á.; Vidal-Gancedo, J.; Rovira, C.; Laukhina, E.; Amabilino, D. B. *Angew. Chem. Int. Ed.* **2007,** *46*, 238−241.

Raspaud, E.; Lairez, D.; Adam, M.; Carton, J.-P. *Macromolecules* **1994,** *27*, 2956–2964.

Raspaud, E.; Lairez, D.; Adam, M.; Carton, J.-P. *Macromolecules* **1996,** *29*, 1269–1277.

Reynders, K.; Mischenko, N.; Kleppinger, R.; Reynaers, H.; Koch, M. H. J.; Mortensen, K. *J. Appl. Cryst.* **1997,** *30*, 684–689.

Robitaille, C. D.; Fauteux, D. *J. Electrochem. Soc.* **1986,** *133*, 315–325.

Rodríguez-Llansola, F.; Miravet, J. F.; Escuder, B. *Chem. Commun.* **2011,** *47*, 4706−4708.

Roe, R. J. *Methods of X-ray and Neutron Scattering in Polymer Science*; Oxford University Press: New York, 2000.

Rogers, R. D.; Seddon, K. R. *Science* **2003,** *302*, 792–793.

Rubinstein, M.; Semenov, A. N. *Macromolecules* **1998,** *31*, 1386–1397.

Ryan, J.; Aldabbagh, F.; Zetterlund, P. B.; Yamada, B. *Macromol. Rapid Commun.* **2004,** *25*, 930–934.

Salim, N. V.; Hameed, N.; Guo, Q. *J. Polym. Sci., Part B: Polym. Phys.* **2009,** *47*, 1894–1905.

Schild, H. G. *Prog. Polym. Sci.* **1992,** *17*, 163–249.

Seiffert, S.; Sprakel, J. *Chem. Soc. Rev.* **2012,** *41*, 909–930.

Seitz, M. E.; Burghardt, W. R.; Faber, K. T.; Shull, K. R. *Macromolecules* **2007,** *40*, 1218–1226.

Seitz, M. E.; Burghardt, W. R.; Shull, K. R. *Macromolecules* **2009,** *42*, 9133–9140.

Seitz, M. E.; Martina, D.; Baumberger, T.; Krishnan, V. R.; Hui, C.-Y.; Shull, K. R. *Soft Matter* **2009,** *5*, 447–456.

Semenov, A. N.; Rubinstein, M. *Macromolecules* **1998,** *31*, 1373–1385.

Shin, J.-H.; Henderson, W. A.; Passerini, S. *Electrochem. Commun.* **2003,** *5*, 1016–1020.

Shin, J.-H.; Henderson, W. A.; Passerini, S. *J. Electrochem. Soc.* **2005,** *152*, A978–A983.

Sijbesma, R. P.; Beijer, F. H.; Brunsveld, L.; Folmer, B. J. B.; Hirschberg, J. H. K. K.; Lange, R. F. M.; Lowe, J. K. L.; Meijer, E. W. *Science* **1997,** *278*, 1601–1604.

Simone, P. M.; Lodge, T. P. *Macromol. Chem. Phys.* **2007,** *208*, 339–348.

Singh, B.; Sekhon, S. S. *J. Phys. Chem. B* **2005,** *109*, 16539–16543.

Sivakova, S.; Bohnsack, D. A.; Mackay, M. E.; Suwanmala, P.; Rowan, S. J. *J. Am. Chem. Soc.* **2005,** *127*, 18202–18211.

Smith, D. K. *Nat. Chem.* **2010,** *2*, 162–163.

Smitha, B.; Sridhar, S.; Khan, A. A. *J. Membr. Sci.* **2005,** *259*, 10–26.

Snedden, P.; Cooper, A. I.; Scott, K.; Winterton, N. *Macromolecules* **2003,** *36*, 4549–4556.

Soenen, H.; Berghmans, H.; Winter, H. H.; Overbergh, N. *Polymer* **1997,** *38*, 5653–5660.

Soenen, H.; Liskova, A.; Reynders, K.; Berghmans, H.; Winter, H. H.; Overbergh, N. *Polymer* **1997,** *38*, 5661–5665.

Söntjens, S. H. M.; Sijbesma, R. P.; van Genderen, M. H. P.; Meijer, E. W. *J. Am. Chem. Soc.* **2000,** *122*, 7487–7493.

Susan, M. A. B. H.; Kaneko, T.; Noda, A.; Watanabe, M. *J. Am. Chem. Soc.* **2005,** *127*, 4976–4983.

Suzuki, T.; Shinkai, S.; Sada, K. *Adv. Mater.* **2006,** *18*, 1043–1046.

Swatloski, R. P.; Spear, S. K.; Holbrey, J. D.; Rogers, R. D. *J. Am. Chem. Soc* **2002,** *124*, 4974–4975.

Tanaka, F.; Edwards, S. F. *Macromolecules* **1992,** *25*, 1516–1523.

Tang, C.; Lennon, E. M.; Fredrickson, G. H.; Kramer, E. J.; Hawker, C. J. *Science* **2008,** *322*, 429–432.

Tang, H.; Tang, J.; Ding, S.; Radosz, M.; Shen, Y. *J. Polym. Sci., Part A: Polym. Chem.* **2005,** *43*, 1432–1443.

Tokuda, H.; Hayamizu, K.; Ishii, K.; Susan, M. A. B. H.; Watanabe, M. *J. Phys. Chem. B* **2004,** *108*, 16593–16600.

Tokuda, H.; Hayamizu, K.; Ishii, K.; Susan, M. A. B. H.; Watanabe, M. *J. Phys. Chem. B* **2005,** *109*, 6103–6110.

Tokuda, H.; Ishii, K.; Susan, M. A. B. H.; Tsuzuki, S.; Hayamizu, K.; Watanabe, M. *J. Phys. Chem. B* **2006,** *110*, 2833–2839.

Tsuda, R.; Kodama, K.; Ueki, T.; Kokubo, H.; Imabayashi, S.; Watanabe, M. *Chem. Commun.* **2008,** 4939–4941.

Ueki, T.; Arai, A. A.; Kodama, K.; Kaino, S.; Takada, N.; Morita, T.; Nishikawa, K.; Watanabe, M. *Pure Appl. Chem.* **2009,** *81*, 1829–1841.

Ueki, T.; Nakamura, Y.; Yamaguchi, A.; Niitsuma, K.; Lodge, T. P.; Watanabe, M. *Macromolecules* **2011,** *44*, 6908–6914.

Ueki, T.; Watanabe, M. *Chem. Lett.* **2006,** *35*, 964–965.

Ueki, T.; Watanabe, M. *Langmuir* **2007,** *23*, 988–990.

Ueki, T.; Watanabe, M. *Macromolecules* **2008,** *41*, 3739–3749.

Ueki, T.; Watanabe, M.; Lodge, T. P. *Macromolecules* **2009,** *42*, 1315–1320.

Ueki, T.; Yamaguchi, A.; Ito, N.; Kodama, K.; Sakamoto, J.; Ueno, K.; Kokubo, H.; Watanabe, M. *Langmuir* **2009,** *25*, 8845–8848.

Ustinov, A.; Weissman, H.; Shirman, E.; Pinkas, I.; Zuo, X.; Rybtchinski, B. *J. Am. Chem. Soc.* **2011,** *133*, 16201–16211.

van Gemert, G. M. L.; Peeters, J. W.; Söntjens, S. H. M.; Janssen, H. M.; Bosman, A. W. *Macromol. Chem. Phys.* **2012,** *213*, 234–242.

van Rantwijk, F.; Sheldon, R. A. *Chem. Rev.* **2007,** *107*, 2757–2785.

Vega, D. A.; Sebastian, J. M.; Loo, Y.-L.; Register, R. A. *J. Polym. Sci., Part B: Polym. Phys.* **2001,** *39*, 2183–2197.

Vijayakrishna, K.; Jewrajka, S. K.; Ruiz, A.; Marcilla, R.; Pomposo, J. A.; Mecerreyes, D.; Taton, D.; Gnanou, Y. *Macromolecules* **2008,** *41*, 6299–6308.

Vijayaraghavan, R.; MacFarlane, D. R. *Chem. Commun.* **2004,** 700–701.

Vijayaraghavan, R.; MacFarlane, D. R. *Chem. Commun.* **2005,** 1149–1151.

Vygodskii, Y. S.; Lozinskaya, E. I.; Shaplov, A. S. *Macromol. Rapid Commun.* **2002,** *23*, 676–680.

Walden, P. *Bull. Acad. Impér. Sci. St. Pétersbourg* **1914,** *8*, 405–422.

Wang, X.; Dormidontova, E. E.; Lodge, T. P. *Macromolecules* **2002,** *35*, 9687–9697.

Wathier, M.; Grinstaff, M. W. *Macromolecules* **2010,** *43*, 9529–9533.

Welton, T. *Chem. Rev.* **1999,** *99*, 2071–2083.

Wilkes, J. S. *Green Chem.* **2002,** *4*, 73–80.

Wilkes, J. S.; Levisky, J. A.; Wilson, R. A.; Hussey, C. L. *Inorg. Chem.* **1982,** *21*, 1263–1264.

Wilkes, J. S.; Zaworotko, M. J. *J. Chem. Soc., Chem. Commun.* **1992,** 965–967.

Winterton, N. *J. Mater. Chem.* **2006,** *16*, 4281–4293.

Wool, R. P. *Soft Matter* **2008,** *4*, 400–418.

Woutersen, S.; Mu, Y.; Stock, G.; Hamm, P. *Chem. Phys.* **2001,** *266*, 137–147.

Xu, D.; Craig, S. L. *Macromolecules* **2011,** *44*, 7478–7488.

Yamauchi, K.; Lizotte, J. R.; Long, T. E. *Macromolecules* **2003,** *36*, 1083−1088.

Yang, Z.; Xu, K.; Wang, L.; Gu, H.; Wei, H.; Zhang, M.; Xu, B. *Chem. Commun.* **2005,** 4414−4416.

Yokoyama, H.; Kramer, E. J. *Macromolecules* **1998,** *31*, 7871–7876.

Yount, W. C.; Loveless, D. M.; Craig, S. L. *J. Am. Chem. Soc.* **2005,** *127*, 14488–14496.

Yuan, J.; Antonietti, M. *Polymer* **2011,** *52*, 1469–1482.

Zeng, X.-M.; Chan, C.-M.; Weng, L.-T.; Li, L. *Polymer* **2000,** *41*, 8321–8329.

Zeroni, I.; Ozair, S.; Lodge, T. P. *Macromolecules* **2008,** *41*, 5033–5041.

Zhang, S. Ph.D. Dissertation, University of Minnesota, 2012.

Zhang, S.; Lee, K. H.; Frisbie, C. D.; Lodge, T. P. *Macromolecules* **2011,** *44*, 940–949.

Zhang, S.; Lee, K. H.; Sun, J.; Frisbie, C. D.; Lodge, T. P. *Macromolecules* **2011,** *44*, 8981–8989.

Zheng, J.; Fayer, M. D. *J. Am. Chem. Soc.* **2007,** *129*, 4328–4335.

Zheng, J.; Fayer, M. D. *J. Phys. Chem. B* **2008,** *112*, 10221–10227.

Zheng, J.; Kwak, K.; Asbury, J.; Chen, X.; Piletic, I. R.; Fayer, M. D. *Science* **2005,** *309,* 1338–1343.

Zheng, J.; Kwak, K.; Chen, X.; Asbury, J. B.; Fayer, M. D. *J. Am. Chem. Soc.* **2006,** *128,* 2977–2987.

Zheng, J.; Kwak, K.; Fayer, M. D. *Acc. Chem. Res.* **2007,** *40*, 75–83.

Zhong, S.; Pochan, D. J. *Polym. Rev.* **2010,** *50*, 287–320.

Appendix

Small-Angle Neutron Scattering

Small-angle neutron scattering (SANS) measurements were performed on the CG-2 General Purpose SANS instrument at the High Flux Isotope Reactor (HFIR) facility at Oak Ridge National Laboratory (ORNL). The neutron wavelength was 4.75 Å and the sample-to-detector distance was 14 m. Temperature was calibrated using a thermocouple immersed in oil in a quartz cell. Samples were sandwiched between two quartz disks separated by an aluminum spacer and sealed by high-temperature adhesives. Data reduction was performed using the Igor package provided by ORNL. Scattering data were corrected for sample transmission, empty cell, background scattering, and detector sensitivity. Absolute intensity curves $I(q)$ were obtained using the direct beam method, followed by azimuthal averaging.

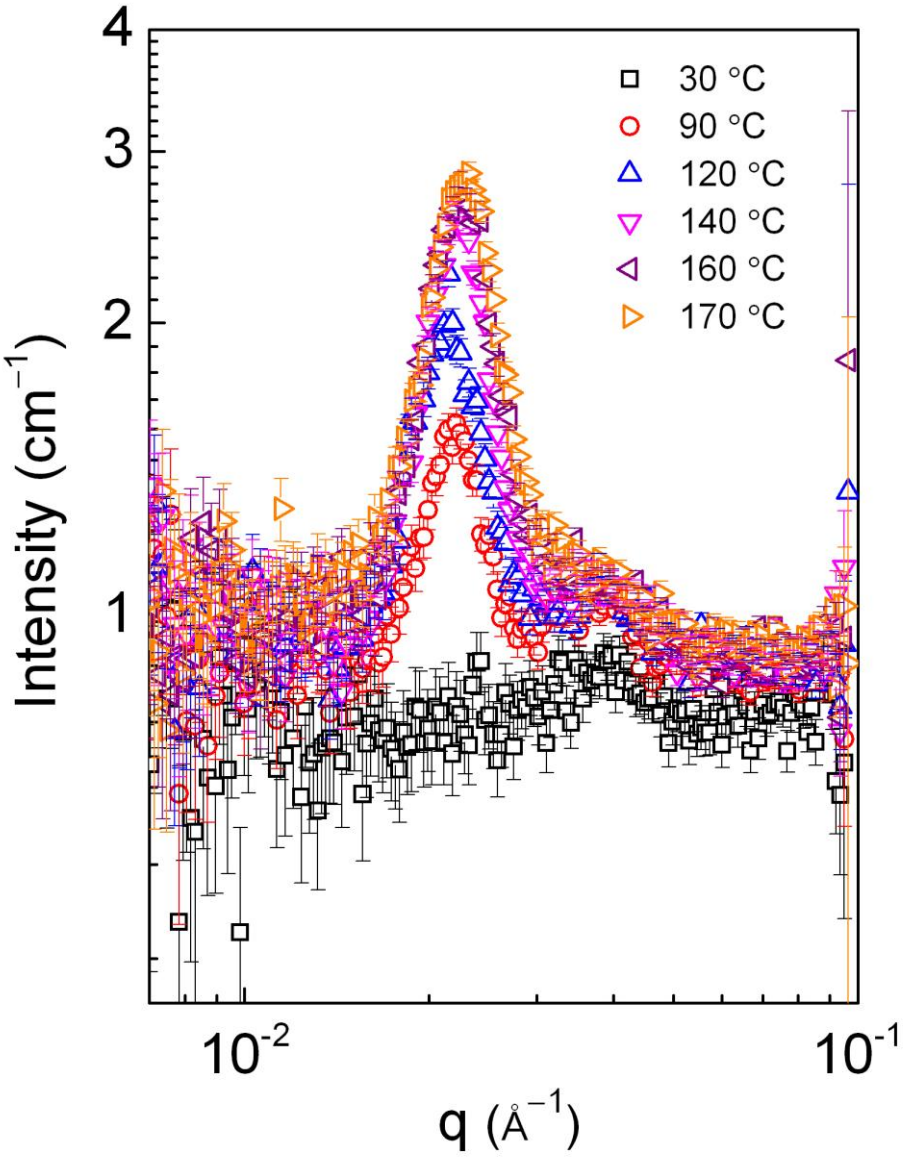

Figure A.1 Variable temperature SANS patterns taken on heating for a supramolecular ion gel comprised of 30 wt% VOV(3-35-3) and 9 wt% PVPh-5.

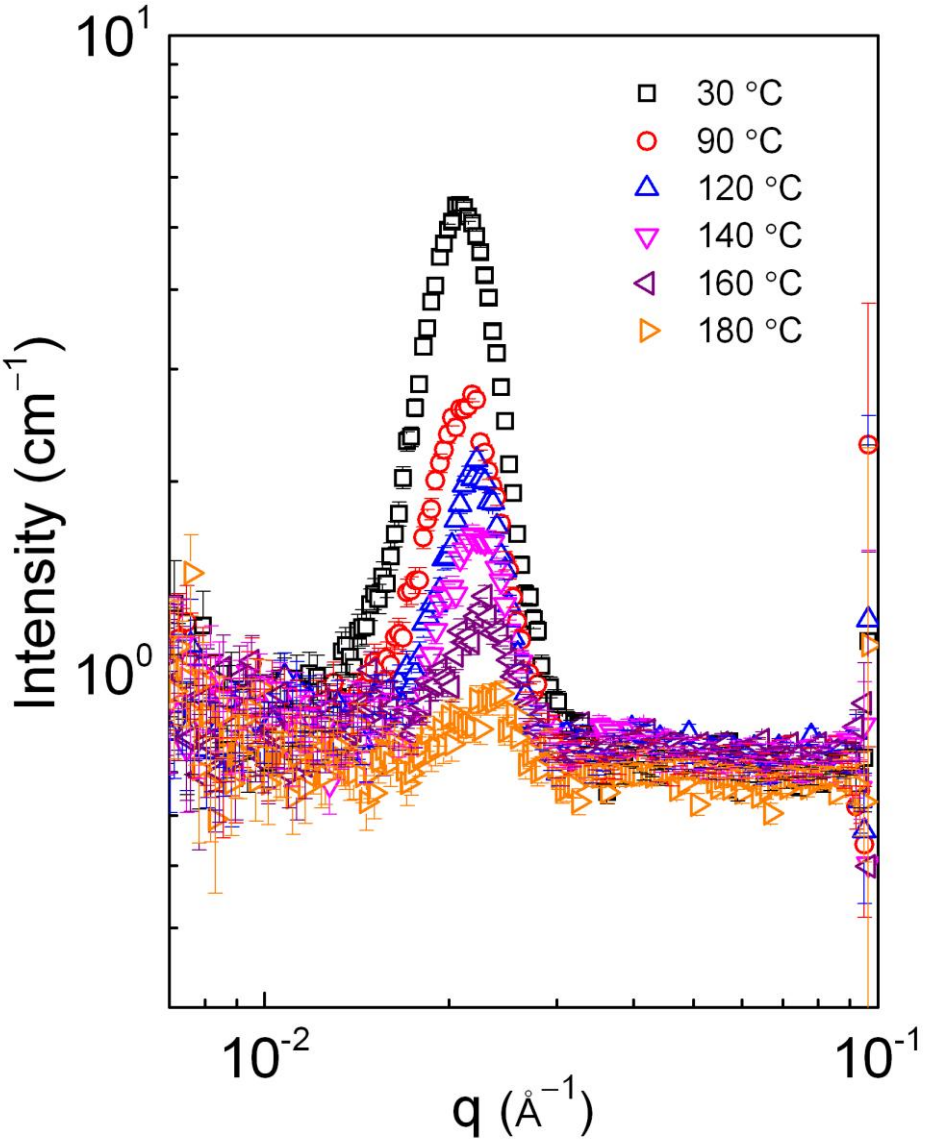

Figure A.2 Variable temperature SANS patterns taken on heating for a supramolecular ion gel comprised of 20 wt% VOV(3-35-3) and 6 wt% PVPh-5.

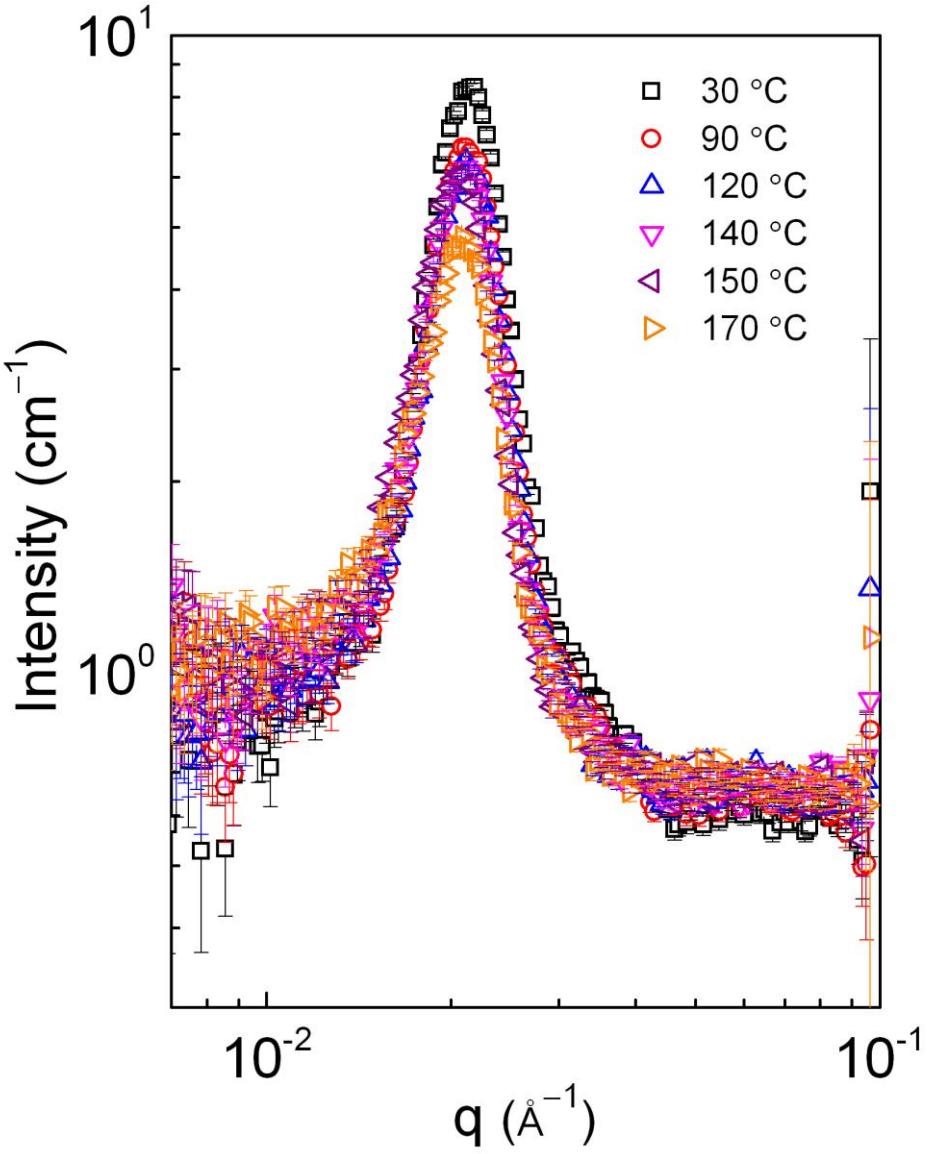

Figure A.3 Variable temperature SANS patterns taken on heating for a supramolecular ion gel comprised of 10 wt% VOV(3-35-3) and 3 wt% PVPh-5.

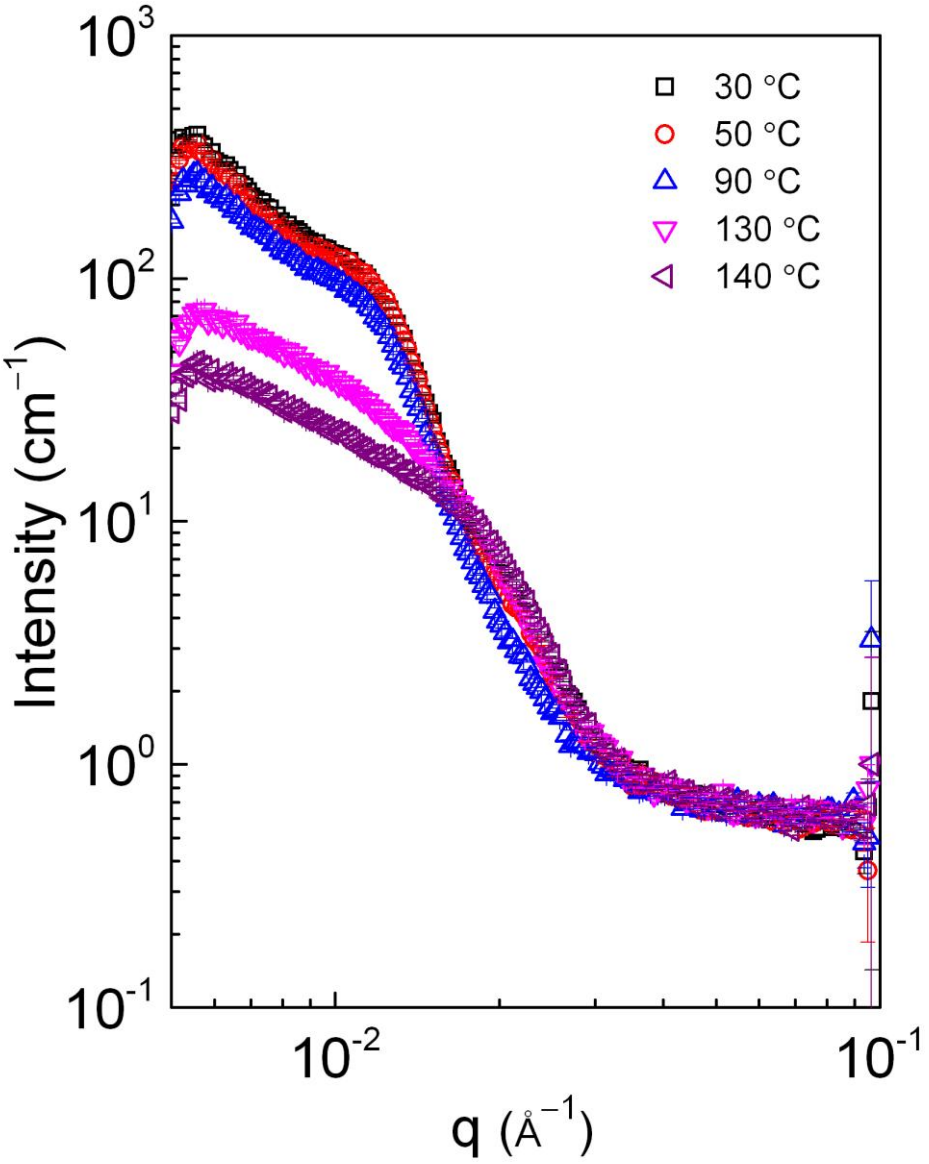

Figure A.4 Variable temperature SANS patterns taken on heating for a supramolecular ion gel comprised of 10 wt% VOV(3-35-3) and 10 wt% PVPh-5.

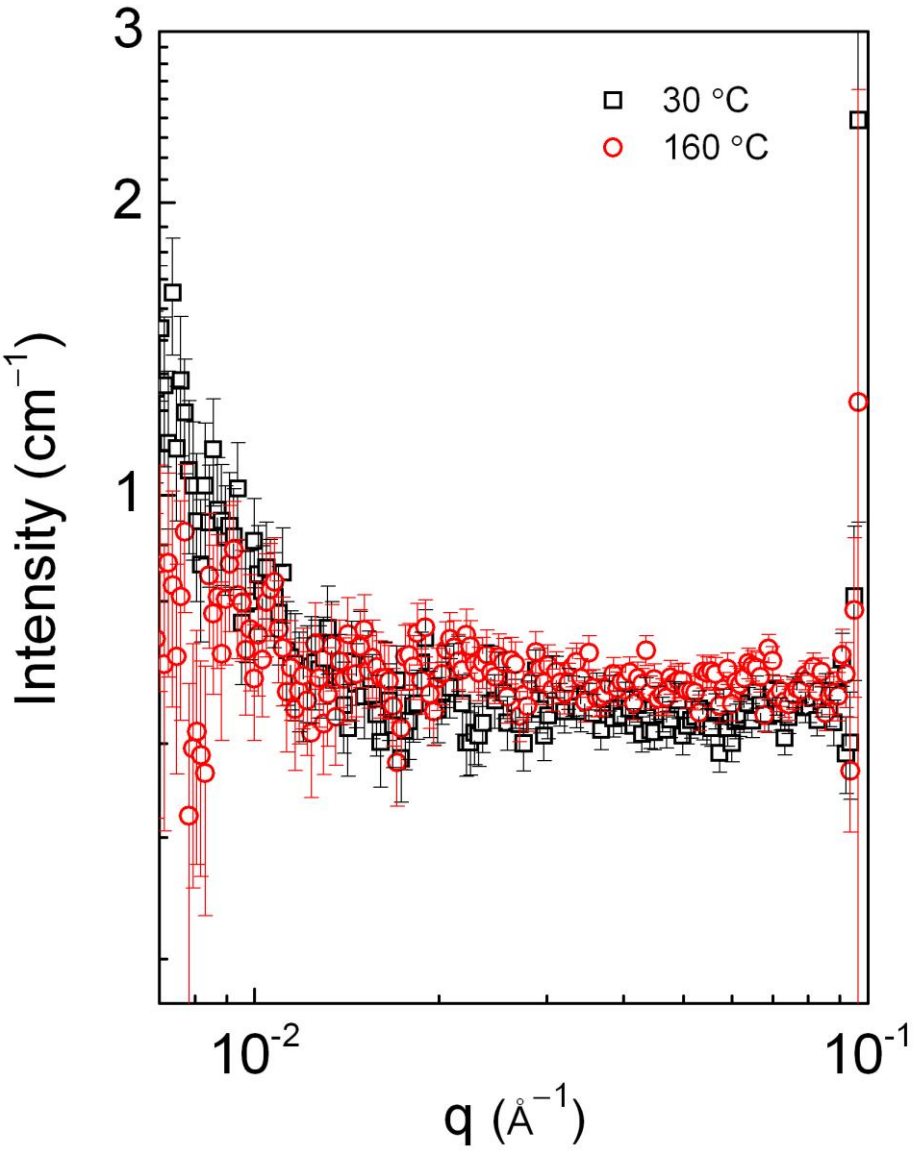

Figure A.5 Variable temperature SANS patterns recorded on heating for a solution comprised of 30 wt% VOV(3-35-3) in [EMIM][TFSA].

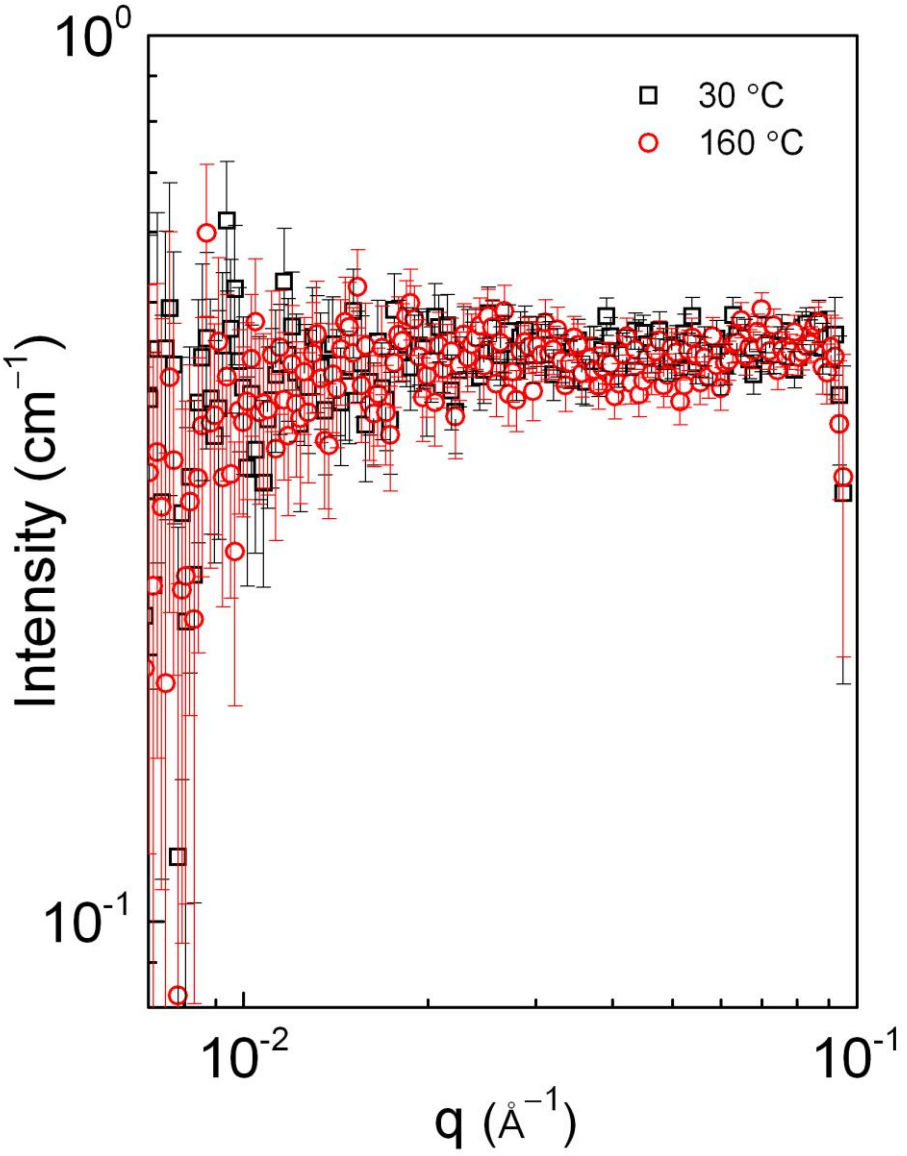

Figure A.6 Variable temperature SANS patterns recorded on heating for a solution comprised of 9 wt% PVPh-5 in [EMIM][TFSA].